Assessment of Power System Equipment Insulation Based on Distorted Excitation Voltage

Author:
Muntakim, Pratic A

Publication Date:
2023

DOI:
https://doi.org/10.26190/unsworks/24850

THE UNIVERSITY OF NEW SOUTH WALES

School of Electrical Engineering and Telecommunications

Assessment of Power System Equipment Insulation Based on Distorted Excitation Voltage

Faculty name: Engineering

Pratic A Muntakim

Supervisor: A/Prof. Dr Toan Phung

Co-supervisor: Dr Daming Zhang

Date submitted: 26th June 2022

The University of New South Wales Thesis/Dissertation Sheet	
Surname or Family name:	**Muntakim**
First name: **Pratic A**	Other name/s:
Abbreviation for degree as given in the University calendar: **MPhil**	
School: Electrical Engineering and Telecommunications	Faculty: Engineering
Title: Assessment of Power System Equipment Insulation Based on Distorted Excitation Voltage	

Abstract 350 words maximum:

Electrical insulation plays a critical role in high voltage power system equipment. The presence of electrical, thermal, and mechanical stresses imposed when they are in operation for a long time cause gradual degradation of the insulation. Therefore, regular condition monitoring and diagnostic testing of power system equipment are of paramount importance for the reliable operation of electricity supply networks and systems.

The dielectric dissipation factor (DDF) measurement is one of the most common techniques for insulation assessment. From a traditional perspective, a pure sinusoidal voltage is used for excitation in the testing. However, the grid voltage nowadays in reality is often distorted with a waveform having multiple harmonic components. Generally, there are distorted voltages and currents generated due to the presence of non-linear equipment or components in the system. Thus, testing under distorted voltage with harmonics provides a more realistic diagnostic measurement as compared to traditional AC sinusoidal high voltage testing.

This dissertation investigates the impact of harmonically distorted excitation on the dielectric dissipation factor of high voltage power equipment. A practical measurement method based on distorted excitation is proposed and tested on a reference capacitor-resistor test object. A theoretical and mathematical model is developed to quantify the impact of distortion on the DDF measured in contrast to the case of non-distorted excitation. It is established that for the same total RMS magnitude of the applied excitation, the DDF decreases with the increasing harmonic proportion in the applied voltage waveform. For validation, laboratory experiments and computer simulations were carried out, and data obtained were compared with the analytical results.

The proposed technique is then tested on some real high voltage components (33kV dry-type current transformers). The results confirm the monotonically decreasing trend, but the pattern is more complex. The dielectric dissipation factor mathematical and electrical circuit model is implemented based on the polarisation loss. The theoretical formulation is implemented in a computer simulation using MATLAB Simulink to validate the results. In summary, the thesis provides useful diagnostic insights on the characteristics of the dielectric dissipation factor measurement under distorted excitation.

Declaration relating to disposition of project thesis/dissertation

I hereby grant to the University of New South Wales or its agents the right to archive and to make available my thesis or dissertation in whole or in part in the University libraries in all forms of media, now or here after known, subject to the provisions of the Copyright Act 1968. I retain all property rights, such as patent rights. I also retain the right to use in future works (such as articles or books) all or part of this thesis or dissertation.

I also authorise University Microfilms to use the 350 word abstract of my thesis in Dissertation Abstracts International (this is applicable to doctoral theses only).

……………………………………………………………

Signature

…………………………………………………….

The University recognises that there may be exceptional circumstances requiring restrictions on copying or conditions on use. Requests for restriction for a period of up to 2 years must be made in writing. Requests for a longer period of restriction may be considered in exceptional circumstances and require the approval of the Dean of Graduate Research.

FOR OFFICE USE ONLY

Date of completion of requirements for Award:

THIS SHEET IS TO BE GLUED TO THE INSIDE FRONT COVER OF THE THESIS

ORIGINALITY STATEMENT

☑ I hereby declare that this submission is my own work and to the best of my knowledge it contains no materials previously published or written by another person, or substantial proportions of material which have been accepted for the award of any other degree or diploma at UNSW or any other educational institution, except where due acknowledgement is made in the thesis. Any contribution made to the research by others, with whom I have worked at UNSW or elsewhere, is explicitly acknowledged in the thesis. I also declare that the intellectual content of this thesis is the product of my own work, except to the extent that assistance from others in the project's design and conception or in style, presentation and linguistic expression is acknowledged.

COPYRIGHT STATEMENT

AUTHENTICITY STATEMENT

☑ I certify that the Library deposit digital copy is a direct equivalent of the final officially approved version of my thesis.

# ACKNOWLEDGEMENT

The adventurous trajectory of my MPhil has lots of bumps along the way. It has not been achieved overnight. The results obtained are due to dreams and aspirations backed by determination, passion, focus and lots of sacrifice.

The dissertation would not be possible without the invaluable support from many fantastic people along the path. My foremost and heartfelt gratitude is to my supervisor Associate Professor Dr Toan Phung because he had faith in me from the start of the journey. His constant constructive feedback, guidance and support like a parent in every step of this research paved the way to the achievement. I also acknowledge the time he has provided me regarding the reviews of the dissertation drafts and research paper which has been published. My journey would not be complete without his sincere support, valuable comments, suggestions and constructive discussion. He is my mentor and a fantastic incredible person.

I would love to acknowledge all the professional and technical staff at UNSW School of Electrical Engineering And Telecommunications, explicitly Mr Zhenyu Liu whose constant support for the experimental works in the High Voltage Laboratory and technical feedback shaped the research. I would also love to acknowledge Dr Sayidul Morsalin whose constant feedback, teaching the technical laboratory experiments and support helped me throughout the journey and also Dr Apu Banik for his valuable insights. Shubin Zhang and Junyang Zhang for their cooperation and support along the journey.

I also express my heartfelt gratitude to Dr Jayashri Ravishankar, Dr Daming Zhang, Dr Guo Chen, Dr Faz Rahman, Dr Matthew Priestley, Dr Inmaculada Tomeo-Reyes and Dr Arash Khatamianfar from UNSW School of Electrical Engineering and Telecommunications for their invaluable support through the journey.

I am very grateful to all of my friends in Sydney who shared their time with me. Thank you Abu Mohammad Safat-Ee Huq, Mushita Masud Munia, Dr S M Showybul Islam Shakib, Shahriyar Safat Dipta, Hossein Rahimpour, Ahmed Musleh, Kuthsav Thattai, Swapneel Thite, Abdur Rahman, Dr Arifur Rahim, Dr Rajib Rahman, Dr Thomas Dixon, Dr Kate Jackson, Dr Yu-Ling Hsueh, Dr Edyta Osika, Dr Animesh Sahoo, Awais Ahmed, Reuben Hackett, Dr Muhammad Ali, Hua Chai, Dr Miao Li, Dr Rundong Li, Boyu Liu and Dr Clay Chu.

Last but not the least, there are hardly any words in expressing my immense gratitude to my parents and my brother Prottoy. Thank you Ammu(Mother) for giving me this beautiful life

and bringing me into this world. Thank you, Abbu(father) for your support and for always being with me during difficulties. Thank you, brother Prottoy, to be with me during my challenging times and for inspiring me. To Zunhai Osman, the love of my life, my fiancée for being my support, loving me, motivating me, and teaching me how to dream and think. I express my heartfelt apology to you for not spending enough time with you due to my research commitment. Thank you all as I am surrounded by such an amazing group of people.

Abstract

Electrical insulation plays a critical role in high voltage power system equipment. The presence of electrical, thermal, and mechanical stresses imposed when they are in operation for a long time cause gradual degradation of the insulation. Therefore, regular condition monitoring and diagnostic testing of power system equipment are of paramount importance for the reliable operation of electricity supply networks and systems.

The dielectric dissipation factor (DDF) measurement is one of the most common techniques for insulation assessment. From a traditional perspective, a pure sinusoidal voltage is used for excitation in the testing. However, the grid voltage nowadays in reality is often distorted with a waveform having multiple harmonic components. Generally, there are distorted voltages and currents generated due to the presence of non-linear equipment or components in the system. Thus, testing under distorted voltage with harmonics provides a more realistic diagnostic measurement as compared to traditional AC sinusoidal high voltage testing.

This dissertation investigates the impact of harmonically distorted excitation on the dielectric dissipation factor of high voltage power equipment. A practical measurement method based on distorted excitation is proposed and tested on a reference capacitor-resistor test object. A theoretical and mathematical model is developed to quantify the impact of distortion on the DDF measured in contrast to the case of non-distorted excitation. It is established that for the same total RMS magnitude of the applied excitation, the DDF decreases with the increasing harmonic proportion in the applied voltage waveform. For validation, laboratory experiments and computer simulations were carried out, and data obtained were compared with the analytical results.

The proposed technique is then tested on some real high voltage components (33kV dry-type current transformers). The results confirm the monotonically decreasing trend, but the pattern is more complex. The dielectric dissipation factor mathematical and electrical circuit model is implemented based on the polarisation loss. The theoretical formulation is implemented in a computer simulation using MATLAB Simulink to validate the results. In summary, the thesis provides useful diagnostic insights on the characteristics of the dielectric dissipation factor measurement under distorted excitation.

Inclusion Of Publications Statement

Thesis Title and Abstract	Declarations	Inclusion of Publications Statement	Corrected Thesis and Responses

UNSW is supportive of candidates publishing their research results during their candidature as detailed in the UNSW Thesis Examination Procedure.

Publications can be used in the candidate's thesis in lieu of a Chapter provided:

- The candidate contributed **greater than 50%** of the content in the publication and are the "primary author", i.e. they were responsible primarily for the planning, execution and preparation of the work for publication.
- The candidate has obtained approval to include the publication in their thesis in lieu of a Chapter from their Supervisor and Postgraduate Coordinator.
- The publication is not subject to any obligations or contractual agreements with a third party that would constrain its inclusion in the thesis.

☑ The candidate has declared that **some of the work described in their thesis has been published and has been documented in the relevant Chapters with acknowledgement**.

A short statement on where this work appears in the thesis and how this work is acknowledged within chapter/s:

Journal Papers
1. Pratic A Muntakim, B.T. Phung, "A Review of Dielectric Dissipation Factor Interpretation and Measurement under Distorted Excitation Voltage" (To be submitted)
Conference Papers
1. Pratic A Muntakim, Junyang Zhang, Shubin Zhang, B.T. Phung," Dielectric Dissipation Factor Measurement of Power Equipment under Distorted Excitation Voltage", 2021 International Conference on Smart-Green Technology in Electrical and Information Systems (ICSGTEIS), Bali, Indonesia, 28th - 30th October 2021 (oral presentation)
2. Pratic A Muntakim, Shubin Zhang, Junyang Zhang, B.T. Phung, "Insulation Assessment Based on Dielectric Dissipation Factor Measurement under Non-sinusoidal Excitation", 2021 IEEE 5th International Conference on Condition Assessment Techniques in Electrical Systems (CATCON), Kerala, India, 3rd - 5th December 2021 (oral presentation)?

(a) Some of the works from chapter 2 is going to be submitted as a Review Journal paper.
(a) Some of the works in the second conference paper have been published in chapter 3.
(b) Some of the works in the second conference paper have been published in chapter 4.
(c) Some of the works in the first conference paper have been published in chapter 5.

Candidate's Declaration

I declare that I have complied with the Thesis Examination Procedure.

<table>
<tr><td colspan="3">CANDIDATE'S DECLARATION
I declare that:
I have complied with the Thesis Examination Procedure
where I have used a publication in lieu of a Chapter, the listed publication(s) below meet(s) the requirements to be included in the thesis.</td></tr>
<tr><td>Name</td><td>Signature</td><td>Date</td></tr>
</table>

Pratic A Muntakim		

Postgraduate Coordinator's Declaration

I declare that:

- the information below is accurate
- where listed publication(s) have been used in lieu of Chapter(s), their use complies with the Thesis Examination Procedure
- the minimum requirements for the format of the thesis have been met.

PGC's Name	PGC's Signature	Date
Dr Rukmi Dutta		

List of Publications

Journal Papers

1. **Pratic A Muntakim,** B.T. Phung, "A Review of Dielectric Dissipation Factor Interpretation and Measurement under Distorted Excitation Voltage*", to be submitted to the Journal of Engineering Science and Technology Review (JESTR)*

Conference Papers

1. **Pratic A Muntakim,** Junyang Zhang, Shubin Zhang, B.T. Phung," Dielectric Dissipation Factor Measurement of Power Equipment under Distorted Excitation Voltage*", 2021 International Conference on Smart-Green Technology in Electrical and Information Systems (ICSGTEIS),* Bali, Indonesia, 28^{th} - 30^{th} October 2021 (oral presentation)

2. **Pratic A Muntakim,** Shubin Zhang, Junyang Zhang, B.T. Phung, "Insulation Assessment Based on Dielectric Dissipation Factor Measurement under Non-sinusoidal Excitation"*, 2021 IEEE* 5^{th} *International Conference on Condition Assessment Techniques in Electrical Systems (CATCON),* Kerala, India, 3^{rd} - 5^{th} December 2021 (oral presentation)

Table of Contents

Chapter 1

Chapter 2

Chapter 3

Chapter 4

Chapter 5

Chapter 6

Abbreviations

DDF	Dielectric Dissipation Factor
AC	Alternating current
RMS	Root Mean Square
kV	Kilo Volt
PD	Partial Discharge
DDF$_h$	Dielectric Dissipation Factor under distorted excitation
VLF	Very low frequency
HV	High voltage
XLPE	Cross-Linked Polyethylene
RHS	Right Hand Side
PDIV	Partial Discharge Inception Voltage
THD	Total Harmonic Distortion
MV	Medium Voltage
UHV	Ultra High Voltage
LV	Low Voltage
DSP	Digital Signal Processing
FFT	Fast Fourier Transform
DSO	Digital Storage Oscilloscope
AWG	Arbitrary Waveform Generator
SG	Signal Generator
TO	Test Object
DR	Dielectric Response
CT	Current Transformer
FDS	Frequency Domain Spectroscopy
DUT	Device under test
HVT	High Voltage Transformer

List of Figures

List of Tables

Nomenclature

tanδ	Dielectric Dissipation factor
DDF	Dielectric Dissipation factor
V_{RMS}	Root mean square voltage
I_{RMS}	Root mean square current
P_{avg}	Average power
THD_h	Total Harmonic Distortion
ω	Angular Frequency
R_d	Channel Resistance
C_d	Gap Capacitance
R_c	Charging Resistance
C_c	Charging Capacitance
R_o	Conduction Resistance
C_o	Bulk Capacitance
R_{pol}	Polarisation Resistance modelled
C_{pol}	Polarisation Capacitance modelled
P_t	Total Power loss
P_{PD}	Partial Discharge Power loss
P_c	Conduction Power loss
P_{pol}	Polarisation power loss
$E(t)$	Time-dependent electrical field
E_o	Initial electrical field
σ	Non-linear conductivity
σ_o	DC conductivity
γ, ζ	Coefficients of non-linearity
$J(E,t)$	Time and electric field dependent current density
f	Frequency
$J(t)$	Time-dependent current density
J_n	Peak value of current density

n	Harmonic number
φ_n	Phase angle of current density
α_i	Phase angle of voltage
ℓ_i	Amplitude of the i-th harmonic as a fraction of the fundamental
v(t)	Time varying voltage
i(t)	Time varying voltage
δ	Loss angle
$cos\theta$	Power factor
I_R	Current through the resistor
I_C	Current through the capacitor
C	Capacitance
R	Resistance
P_R	Resistive power
ε_r^*	Complex permittivity
ε_r'	Real permittivity
ε_r''	Imaginary permittivity
Y	Admittance
G	Conductance
P	Active power
Q	Reactive power
ε_{dc}	Permittivity under DC voltage excitation
ε_∞	Permittivity at the optical frequency
τ	Time constant
Z_1	High voltage Schering bridge branch impedance
Z_4	Low voltage Schering bridge branch impedance
Z_3	First Parallel branch of the Schering bridge
Z_2	Second Parallel branch of the Schering bridge
N	Turns ratio of coil
C_G	Gas capacitance
C_M	Low voltage capacitance

C_R	Reference Capacitance
P_1	Dielectric power loss
P	Total dissipated power
R_s	Shunt Resistance
$V_{d.c}$	Constant DC voltage
V_n	Amplitude of voltage
α_n	Phase angle
ψ_k	Added phase shift
DDF_h	Dielectric Dissipation Factor for harmonically distorted excitation
k	Correction factor or Distortion factor
R_s	Polarisation series resistive branch
C_s	Polarisation series capacitive branch
R_p	Polarisation parallel resistive branch
C_p	Polarisation parallel capacitive branch
R_{eq}	Equivalent resistance
C_{eq}	Equivalent capacitance
$I_{R_{eq}}$	Peak Current through the equivalent resistor
$I_{C_{eq}}$	Peak Current through the equivalent capacitor
$i_{Ceq}(t)$	Time-varying current through the equivalent resistor
$i_{R_{eq}}(t)$	Time-varying current through the equivalent capacitance

Chapter 1
Introduction

1.1 Background

In modern times, the application of non-linear loads in commercial and industrial environments has caused voltage/current distortions in the electricity supply networks, resulting in increased power losses [1]. These losses are due to the high-frequency harmonics present in the waveform, which is of great concern for grid-connected power system equipment, electrical components and devices [2], [3]. Ageing of the insulation in high voltage equipment is often related to the dielectric losses and partial discharges and these are also influenced by the distorted voltage waveform [4],[5]. Harmonic distortion also causes overloading of neutrals, overheating of transformers, nuisance tripping of circuit breakers and overstressing of power factor correction capacitors [6], [7].

One of the main effects of harmonics on high voltage equipment like transformers is aging [8]. The insulation system in equipment is a determinant of the age [9]. The ageing of insulation is significantly affected and accelerated when harmonics are present in the system [10-12]. Harmonics cause overloading resulting in overheating, which in turn affects the insulation. Moreover, the reliability of electrical plant components is greatly affected by harmonics. For a fixed voltage, high-frequency harmonics can cause an increase in the peak value causing dielectric loss and thermal stress. The harmonic current plays a significant role in the degradation of the insulation since it causes power loss.

The dielectric dissipation factor (DDF) or $\tan\delta$ is an important parameter of the insulation as it is used as a measure of the insulation power loss. The dissipation factor is also known as the insulation factor [13]. Previous work has investigated the $\tan\delta$ characteristics in the very low frequency (VLF) range well below the power frequency [14]. However, there is hardly any research as to how the DDF varies when the power frequency voltage mixed with some higher-order harmonics are applied. Thus, the motivation for this research and it will involve the study of mathematical and theoretical modelling, experimentation and simulation of the dielectric dissipation factor, and its measurement. Figure 1.1 describes the measurement process and the challenges involved.

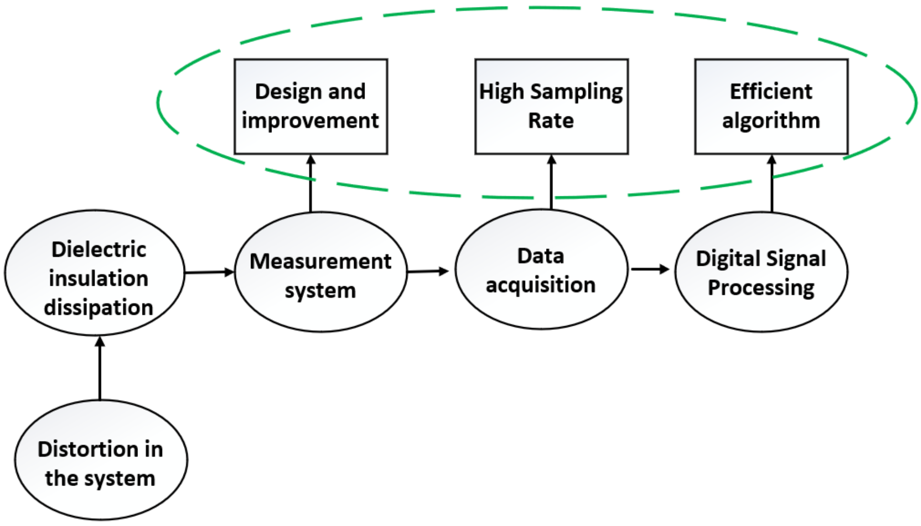

Fig 1.1 DDF measurement challenges

1.2 Motivation

The diagnosis process of the electrical insulation quality can be understood through the application of high voltage excitation [15], [16]. The dielectric dissipation factor (DDF) measurement is one of the most important parts of the dielectric response measurement. This method is widely used for evaluating the bulk insulation condition of high voltage power system equipment [17]. Since the dielectric loss is a function of the dissipation factor, a high value indicates that the insulation health is not up to the mark. Studies show that with time, the growth of electrical treeing and the dielectric losses are more significant in the insulation [18]. Factors found to be influencing the impact of very low frequency in the dielectric dissipation factor measurement have been explored in several studies [19],[20].

At present, commercially available test equipment specifically designed for DDF measurement operates on the basis that the high-voltage excitation waveform is purely sinusoidal. The working principle relies on measuring the phase shift between the purely capacitive current (through a reference capacitor) and the actual load current (through the test object) to determine the dielectric loss angle and hence the tan-delta. When the tester performs the DDF test, they simply measure the DDF at a certain voltage level, i.e., the rms value (no consideration whether the voltage is distorted). The test voltage is the mains 230V supply voltage fed to an auto-transformer and stepped up to high voltage via another transformer. In reality, this mains supply voltage nowadays is polluted with harmonics due to the significant presence of non-linear loads connected to the supply network.

Thus, the motivation of this research is to bring to attention this problem. When traditional DDF measurement instruments are used with a distorted supply voltage, the working principle based on phase shift measurement is no longer valid because it does not take into account if multiple frequency components are present in the system, and how the DDF will behave. The simplistic model of the dielectric dissipation factor is inadequate in explaining the dielectric behaviour in such situations. In addition, the dipole movement in dielectrics varies at different individual frequencies. Thus, there is a need for developing dielectric dissipation factor measurement techniques under distorted excitation, adjusting the model of the $\tan\delta$ when distorted excitation is taken into perspective. To this end, one needs to perform adequate experimental measurements, analyse test results, and develop a circuit model and mathematical expression for the DDF [21]. The problems to solve of the DDF measurement under distorted excitation are briefly stated below:

1. The defects due to insulation aging are not observable with the naked eye nor the equipment can be removed away from operation for insulation assessment. So, practical methods are required to evaluate the insulation condition based on the equipment's output waveform characteristics.

2. Only sinusoidal excitation is considered when the DDF measurement is done using commercial testing equipment. Though some of the products can operate over a range of different frequencies, multiple-frequency excitations are not available. Therefore, a proper measurement system needed to be developed.

3. According to current research, the DDF is measured based on the phase shift between the waveforms of the test object relative to the reference test object. Such a methodology is problematic in situations of simultaneous multiple-frequency excitation and thus a different approach is required.

1.3 Objectives

The main objectives addressed in this research take into consideration the practical issues that the AC grid supply nowadays is polluted with harmonics affecting the operation of grid-connected equipment and their condition monitoring. This thesis aims to investigate the dielectric dissipation factor measurement and characteristics under distorted excitation voltage. Specifically:

1. Develop a theoretical model of DDF based on distorted excitation voltage. The ratio of the active power loss to the reactive power loss is the main basis of the theoretical modelling.
   - Mathematically derive the DDF considering the harmonically distorted excitation voltage and the corresponding current.
   - Develop a computer simulation model of the insulation.
2. Develop and construct a DDF measurement system under distorted excitation. The system is also implemented in MATLAB Simulink. Different harmonic combinations are implemented, and simulation results are compared with the actual experiment.
   - Develop arbitrary waveform to generate the non-sinusoidal excitation.
   - Construct a reference test object to validate the measurement system.
   - Apply mathematical calculations to verify experimental results.
3. Apply the measurement system for testing real high voltage test objects under distorted excitation voltage.

1.4 Methodology

Figure 1.2 is a pictorial representation of the whole research. The work is divided into 3 stages.

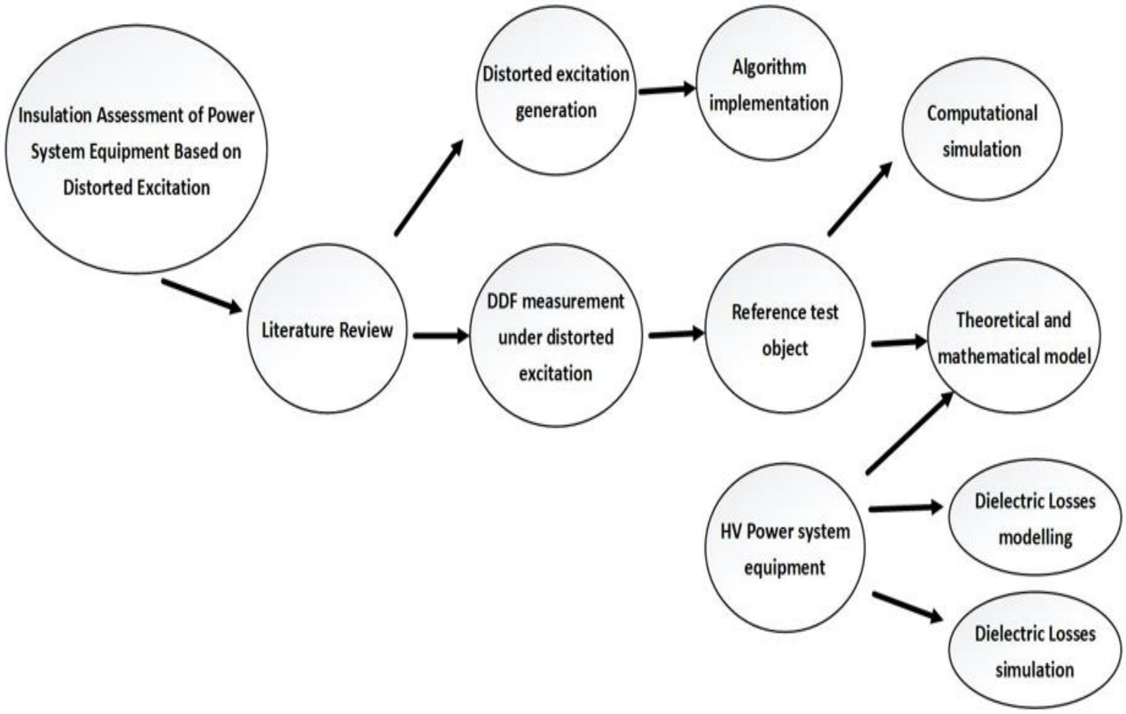

Fig 1.2 Methodology flow chart

1.4.1 Distorted voltage waveform generation

The objective of this stage is to generate the distorted voltage waveforms based on IEEE and IET standards to simulate the real power grid. For the experiments, the desired waveforms are generated by coding their mathematical formulas using the Keysight BenchLink Waveform Builder software. The software is specifically designed for synthesizing any combinations of excitation. The codes are then loaded to the waveform generator which produces the actual output voltage. For computer simulations work, similar waveforms are synthesized in MATLAB Simulink using voltage source blocks.

1.4.2 Development of the DDF measurement technique

Commercial instruments used for DDF measurement are based on pure sinusoidal excitation voltage [19]. It is necessary to develop a practical scheme to enable such a measurement under distorted sinusoidal excitation. Before constructing the actual measurement system, a computer simulation of the system will be implemented and tested on a reference RC load of known values (hence known DDF) to prove the working of the technique. Following the simulations, the actual physical setup of the measurement circuit, excitation voltage source, and reference RC test objects will be constructed for experiments. The results obtained from laboratory experiments will be compared with the results from computer simulations to demonstrate the viability of the proposed technique for practical applications.

1.4.3 Implementation of the measurement method on real test objects

The next step of the research is to apply the developed system for measuring the DDF of some real high voltage components. Three 33kV resin-impregnated dry-type current transformers of similar design are used as the test objects. Their measurement results are analysed and compared. The reference test object results will also be used for comparison, any deviation in the DDF trend will be of interest as it reveals the more complex nature of real dielectrics that influences the dielectric losses.

1.5 Research Contributions

From the perspective of condition monitoring and diagnostic testing, it is important to know the implications of distorted (non-sinusoidal) excitation on the dielectric dissipation factor measurement. Research on the subject has been mostly restricted to pure sinusoidal excitation. In spite of advances in computer-based instrumentation, there is still a research gap for development of practical DDF measurement systems that can operate under distorted excitation waveforms from the supply voltage [22]. The contributions from this research in improving the existing literature are:

- Theoretical and mathematical modelling of the DDF from a non-sinusoidal excitation perspective.
- Simulation model of DDF measurement under distorted excitation.
- Development of the DDF measurement technique based on the ratio of the real power versus reactive power. This is a more universal approach as it covers both pure and harmonically distorted sine waves.
- Experimental study of the DDF characteristics of real high voltage components under distorted excitation.

1.6 Dissertation Outline

The thesis consists of six chapters:

1. Following the Introduction chapter, the second chapter provides the literature review of the physical properties of dielectric materials and the dielectric dissipation factor measurement as a means to assess the insulation condition.
2. The third chapter presents the computer simulation of DDF measurement circuits, non-sinusoidal excitation generation and dielectric modelling.
3. The fourth chapter discusses the simulation and experimentation of the DDF measurement under distorted excitation. The test object is a reference resistor and capacitor with known values and almost ideal properties.
4. In the fifth chapter, DDF measurements are carried out with some real high voltage components (33kV dry-type current transformers). The dielectric losses in real insulation are taken into consideration and modelled.
5. In the sixth chapter, important findings are summarised, and future research opportunities are discussed.

Chapter 2
Literature Review

2.1 Introduction

In the history of the electrical engineering sector's development, a viable electricity supply infrastructure (transformers, power cables, circuit breakers, etc) plays a key role in the functioning of power utilities and societies as a whole [23]. Here, insulation plays the most important role as it must sustain the electrical stresses imposed by the electrical system [24]. Previous studies reported that operating HV electrical equipment, in the long run, will cause ageing, and change the physical micro composition and various dielectric losses [25]. The risk is that the breakdown of the electrical insulation of any HV component may lead to the catastrophic failure of other equipment tied to the system [26].

Power utilities are constantly in a trade-off between whether to refurbish, repair or completely replace their valuable assets. Assessing the equipment and its condition is an important task that should be performed regularly [22], [27]. When AC electric stress is applied to a dielectric material, polarisation occurs as dipoles start to move collectively – known as the dielectric response (DR) [28]. The electric stress can also cause localised breakdown is known as partial discharge (PD) [29]. The dielectric response and partial discharge under sinusoidal power frequency (50/60Hz) excitation have been well studied. However, far too little research has been paid to the case of distorted (non-sinusoidal) excitations [30]; the results may not be comparable with those obtained at the power frequency.

The AC grid voltage is often not a pure sinusoidal waveform – they also contain harmonics. Figure 2.1 shows an example of the presence of harmonic distortion in a medium voltage busbar, and in this particular case, the harmonic component contributing the most is the fifth harmonic [15]. Consequently, the insulation of grid-connected equipment/components is exposed to electrical stress not only at 50/60Hz power frequency but also experiences higher-order harmonics from the distorted excitation. The insulation efficacy is often evaluated based on the measurement of the dielectric dissipation factor (DDF) or $\tan\delta$. The power loss dissipated in the insulation is correlated to the $\tan\delta$ measurement [31]. A lower DDF value signifies a better condition of the insulation. Various testing standards for assessing the insulation condition have been established over the years based on operational experience and the $\tan\delta$ threshold limits have been established accordingly [32].

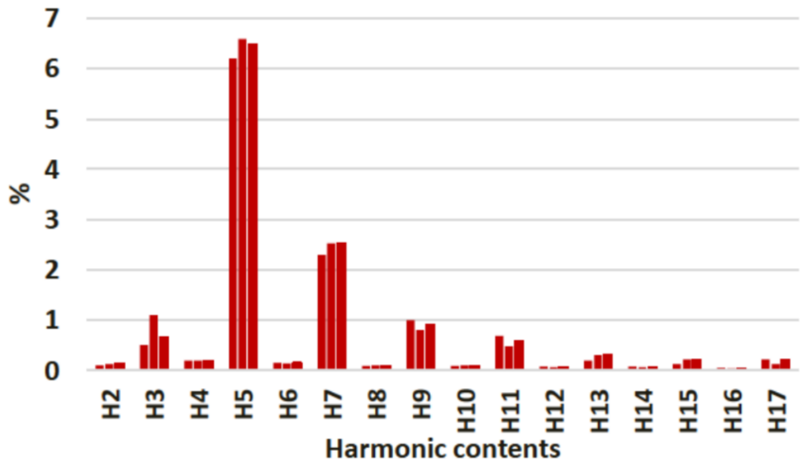

Fig 2.1 Harmonic distortion in a medium voltage busbar [15]

This chapter provides an overview of the characteristics and properties of dielectrics including losses, non-linearity, excitation voltage waveforms for diagnostics testing, the dielectric dissipation factor and its measurement.

2.2 Properties of dielectrics

Recently, researchers have shown an increased interest in DDF diagnostics based on polarisation because it is a physical phenomenon that requires understanding. In the time-domain or the frequency-domain measurements, dielectric properties play a significant role [24], [25].

There have been various studies regarding the dielectric polarisation phenomenon when it is subject to electric stress [33]. Figure 2.2 (a) illustrates the spatial geometry of dielectric, and (b) shows the polarisation and depolarisation curve.

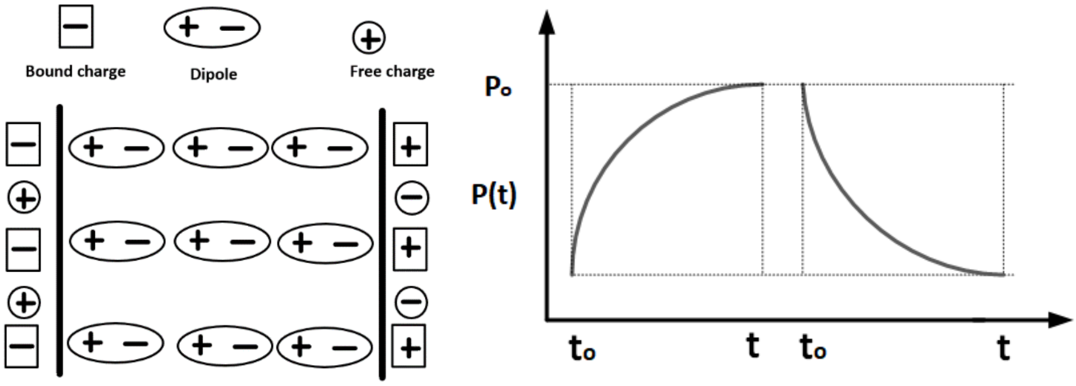

Fig 2.2 (a) Spatial geometry, (b) Polarisation and depolarisation curve

When excitation voltage is applied, the dipoles of random orientation start to align with the resulting electric field. Dipoles can be considered as a pair of positively and negatively charged particles. The dipoles under excitation contribute to electronic, atomic and orientation polarisation if the permanent dipoles are not taken to account at the macroscopic levels. Considering the external phenomenon dipoles are also divided into tunnelling polarisation, bulk polarisation and interfacial polarisation [34]. Figure 2.3 summarises the different polarisations in dielectric materials, and they are explained briefly in the following.

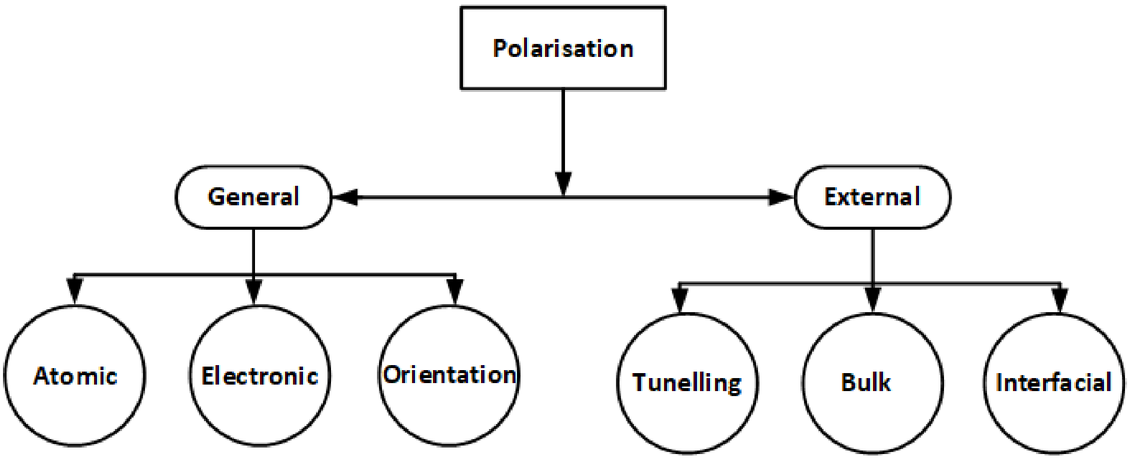

Fig 2.3 Different types of polarisations in dielectrics

2.2.1 Ionic polarisation

Ionic polarisation has a similarity with electronic polarisation, though it is dependent on the frequency and its harmonics. When an electric field is applied the oppositely charged ions in a molecule move away from each other forming an ionic dipole. When the electric field is removed, the ions return to equilibrium [35].

2.2.2 Electronic polarisation

According to Bohr's atomic model, the nucleus at the centre consists of positively charged protons. Electrons are very small compared to the size of the nucleus and revolve around fixed orbits of different energy levels. According to the model, the atom is thought of as a uniform sphere as it is the most stable structure. When an external field is applied, the orbiting electrons around the nucleus tend to cluster together forming one negative end of a dipole and a positive charge at the opposite end. The dipole moment depends on the applied electric field which varies inversely with distance. At a distance from the field, the electron cloud returns to the equilibrium position and the stable state is eventually restored. It is a spontaneous process and occurs within a very short time [36].

2.2.3 Orientation polarisation

It is a physical process in space and can be described as the release of an ionic molecule having a slightly higher electro-positivity relative to the other. Permanent dipoles are formed in the absence of an electric field. Considering the experimental evidence, the dipole moment can be stated as the charge transferred between atoms [37]. When symmetry is considered the vector-sum is null. When external electric stress is applied, the dipoles align with the field direction [38].

2.2.4 Tunnelling polarisation

This polarisation can be attributed to the tunnelling effect. It is a quantum mechanical phenomenon that contributes to the accumulation of polarized charges. It occurs naturally even when there is no electric stress. The reversal of potential polarity causes inversion of the space charges and results in delocalised charges moving around. Some charges are able to tunnel through the potential barrier even though they do not have enough energy to overcome the barrier [90].

2.2.5 Interfacial polarisation

When multi-dielectrics are composed of materials having different conductivities, interfacial polarisation will occur if boundaries are considered mostly inhomogeneous. This phenomenon is most dominant in the frequency spectrum of 0.1Hz-10kHz known as the

Maxwell-Wagner effect [39]. Space charges accumulate at the interfacial zone of boundaries. The accumulated charges influence the resistivity and dielectric properties of the material.

2.2.6 Bulk polarisation

It occurs due to the charge carriers hopping in amorphous and non-conductive insulating materials. It contributes to current conduction. The localized sites play a vital role and it occurs due to the random distribution of molecules and spaced structure [40]. The localized spaces resist the charge conduction, and this space enables electrons to hop from one side to the other. The time spent at the localized site is higher if the travelling distance is shorter for the vibration frequency [41].

2.3 Dielectric losses

The impact of losses on the insulation efficacy is of the highest concern. The insulation is an indispensable part of a power apparatus and requires regular maintenance. In order to have a safe operation, the insulation must be able to tolerate high electrical stress [42], [43]. If there is an overstressing of AC voltage, there is a high possibility of permanently damaging the equipment. Diagnostic testing is very important because it provides a proactive view and earlier fault detection. Considering the existing literature, dielectric losses can be broadly categorized into three categories as represented in Figure 2.4.

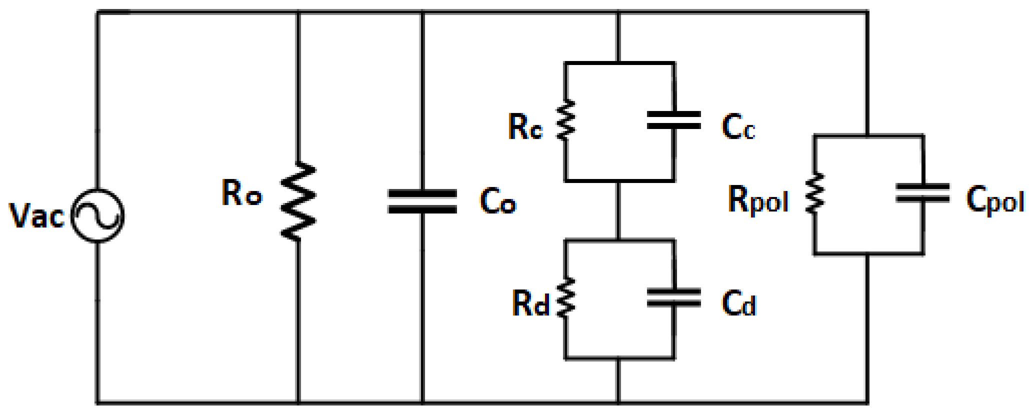

Fig 2.4 Different dielectric losses

2.3.1 Partial Discharge loss

This is generally associated with the ionization inside the voids and cracks. These voids and cracks are present due to aging or manufacturing defects in the insulation. If the external applied voltage results in a voltage developed across the void that exceeds its breakdown strength, there is ionization in the void and localised breakdown (partial discharge) occurs. [44]. The total phenomenon can be modelled as an electric circuit. One block can be formed by a channel resistance R_d and gap capacitance C_d which represents the discharging phenomenon. The other block is formed by a charging resistance R_c and capacitance C_c.

2.3.2 Conduction loss

The conduction loss is modelled by a resistor R_o in parallel with the bulk capacitance C_o . This loss is present due to the imperfection of the dielectric materials [46]. After the application of an electric field, the conduction is caused by the movement of the charges in the dielectric materials. When the electric field is low, the charge movement is dominant and contributes to dielectric loss [47], [48]. With the increase in the electric field, ionic conduction increases. When the electric field is increased, the charge velocity increases. It is explained by the potential-energy well model of conduction. When the electric stress is high, the electron clouds are drifted in such a way that they are aligned towards the high potential [49]. Above a certain temperature, the ionic movement increases significantly. Electron mobility is also influenced by humidity and water content. Conductivity is generally measured at a DC voltage.

2.3.3 Polarisation loss

Polarisation is a phenomenon when the electron cloud in the molecule of the dielectric shifts causing a concentrated positive and negative charge. The phenomenon is caused by external electric fields and also due by the internal structure of the material. The process generates an induced dipole moment. The dipoles along with the presence of trapped charges at the boundary or unusual formation of material cause a displacement current, hence polarisation loss [52]. This phenomenon can be modelled as a circuit presentation of a combination of Polarisation resistance R_{pol} and capacitor C_{pol}, either in series or equivalent parallel. There are various polarisation phenomena, and they can be accounted for by adding more similar branches in the circuit.

Mathematically, the total dielectric losses can be summed up as

$$P_t = P_{PD} + P_C + P_{pol} \quad (2.1).$$

Here, P_t denotes the total power loss, P_{PD} is the partial discharge power loss, P_c is the conduction power loss, and P_{pol} is the polarisation power loss.

2.4 Non-linear dielectrics

The insulation of high voltage cables, bushings and rotating machines are non-linear in nature because of their complex insulation. The non-linear insulation material differs from linear insulation material and the dielectric parameters vary with the nature of excitation applied, i.e., change in voltage, frequency, and structure of non-linear materials. The behaviour of non-linear dielectric is complicated and a general explanation between the measured material properties and the behaviour of the material in an insulating system is not always straightforward. The nonlinear behaviour refers to the non-linear current response under a sinusoidal excitation. The complex dielectric material has non-linear properties, and their relative permittivity varies as non-linear function of the frequency.

Study was carried out on a composite sheet to investigate the non-linear behaviour of the dielectric material [56], [57]. The surface leakage current was found to compose of harmonic contents besides the fundamental component. This phenomenon was also observed in other studies on outdoor insulators, especially when the insulator is aged and has pollution [58], [59]. The equivalent circuit model derived considering the non-sinusoidal nature of leakage current under sinusoidal voltage provides a framework for the nonlinear behaviour of dielectric material as depicted in Figure 2.5 [60]. However, the model is based on the experimental analysis of a flat sheet insulator to avoid any geometrical complexity. In recent times, very few equivalent circuit models of practical insulators are considered for experimental tests [61]. Under distorted voltage, the modelling of the equivalent circuit will change [15].

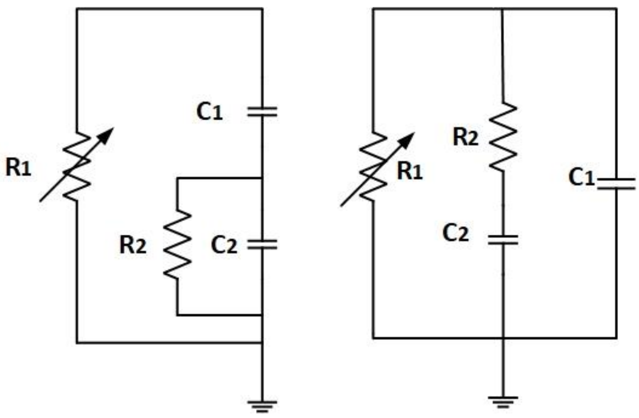

Fig 2.5 Non-linear dielectrics with field-dependent conductivity

The insulation of high-voltage power equipment is often assumed to be linear for simplicity. However, with the increase in voltage beyond a certain threshold, the insulation system behaviour becomes complicated, mostly for transformers [62]. Commercial instruments like Omicron DIRANA and Megger IDAX are limited to a fixed test voltage to avoid this problem [63]. Insulations are generally complex due to the physical structures and mechanisms producing polarisation. The explanation of these properties is complicated. Factors such as insulation geometry, impurities, aging, temperature and moisture make it non-linear [64]. The dielectric response of insulation, particularly for power transformers, is mainly due to electric field dependent conductivity and polarization [65]. To describe the phenomenon, various research groups have proposed different approaches based on impedance and dielectric spectroscopy.

2.4.1 Non-linear dielectrics under linear excitation

Non-linear dielectric materials are defined as materials having properties such as electrical conductivity and polarisation etc as a non-linear function of electric field and temperature [66], [67]. As a consequence, the power loss properties are more complicated than linear dielectrics. When a sinusoidal waveform at a single frequency is applied, the resultant current waveform is distorted (non-sinusoidal) because of the presence of non-linear electrical conduction. The distortion is manifested in the harmonics in the current.

Consider the case where the dielectric is under a uniform electric field. Assume the dielectric constant is electric field-independent, and a uniform electric field from a sinusoidal voltage is used. The circuit model is proposed as having a parallel combination of non-linear resistance and linear capacitance. Let the electric field be $E(t) = E_o e^{j\omega t}$, the non-linear electrical conductivity can be expressed as [62]

$$\sigma = \sigma_o + \left(\gamma E + \zeta E^2 + \ldots\right) \quad (2.2).$$

Here, σ_o is the DC conductance and γ, ζ are the coefficients of non-linearity. The current density J can be written as

$$J(E,t) = \sigma(E,t) \cdot E(t) \quad (2.3).$$

The field-dependent conductivity causes the current to distort resulting in the presence of additional harmonic components, i.e., higher harmonics or "super-harmonics". Upon the application of a sinusoidal voltage of frequency $f = \omega/2\pi$, where ω is the angular frequency, the resulting current generated can be represented as a sum of the Fourier series:

$$J(t) = \sum_{n=1} J_n \sin(n\omega t + \varphi_n) \quad (2.4).$$

Here, J_n is the peak of the n-th component of the current density $J(t)$, φ_n is the phase angle and n is the harmonic number.

The parallel equivalent circuit model of insulation is limited to a single frequency and voltage simultaneously [68]. On the other hand, when the insulation is non-linear, particularly at high voltage, the loss current behaves non-linearly and it is represented by the parallel combination of a voltage-dependent resistor and capacitor [69]. If the environmental conditions are stable, the non-linear loss current is a function of supply voltage and conductivity as a function of the electric field.

2.4.2 Non-linear dielectrics under distorted excitation

Although there has been some research on the implications of non-linear dielectrics when sinusoidal excitations are applied, very little has been done regarding non-linear dielectrics under distorted excitations. In general, the non-linear behaviour of a dielectric is associated with the non-linearity of response current, i.e., the presence of multiple harmonic frequency components [70]. The study of dielectric response under non-sinusoidal voltage is complicated. There are very few works of literature explaining the electrical characterisation of different non-linear dielectric materials, where most explanations are concerning nonlinear impedance spectroscopy [68], [71].

The non-sinusoidal voltage can be represented as an equation using the Fourier series, with the harmonic components added to the fundamental component. And the current response to each of these itself can be expressed as a Fourier series. Mathematical equations and formulas have been developed for some limited cases where the non-linear current generated contains similar harmonic components to the distorted excitation voltage. But for other cases, it becomes very difficult to mathematically characterise the non-linearity.

Though the superposition theorem can be applied for modelling non-linear resistance, when capacitive and inductive elements are present this process becomes invalid [72], [73]. As a consequence, when a non-linear dielectric is considered, a capacitive element is presently making it challenging to model using superposition.

2.5 Different waveforms in diagnostic testing

2.5.1 Sinusoidal waveform

For insulation diagnostic measurements such as partial discharge, dielectric dissipation factor etc, the sinusoidal waveform is used extensively. Traditionally, a low-voltage AC supply with a step-up transformer is used for generating high voltage at power frequency for testing. With the evolution of modern technologies, power electronics are used extensively to provide lightweight portable high voltage AC supply, especially for very low frequencies with a higher testing capacity [70]. In order to generate a sinusoidal waveform, the approach is based on the AC-DC-AC converter as shown in Figure 2.6.

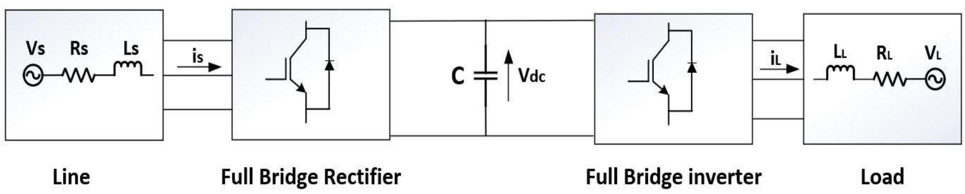

Fig 2.6 AC DC AC converter

2.5.2 Non-sinusoidal waveform

Non-sinusoidal excitation waveforms are also used in high-voltage testing. An example is the rectangular cosine (cos-rect) waveform. In order to generate this waveshape, an inductance and a high-value capacitor is controlled by an automated thyristor switch. Based on resonance, the method is able to reduce power consumption and increase the load capacity at the output terminal [74]. The rectangular shape helps in the measurement of the leakage current. The polarity change of cos-rect takes a cosine shape and contains an oscillation frequency close to 50Hz [75].

A non-sinusoidal periodic voltage can be represented as a trigonometric series known as the Fourier series [76], [77]. It is an algebraic summation of individual sinusoidal functions at different harmonic frequency:

$$v(t) = V_1 \sin(\omega t + \alpha_1) + \sum_{i=2}^{n} \ell_i V_1 \sin(i\omega t + \alpha_i) \qquad (2.5).$$

Here, $\omega = 2\pi f$, and f represents the fundamental frequency which is 50Hz or 60Hz for power frequency. The first term on the RHS of Equation 2.5 represents the fundamental frequency component, its amplitude is V_1 and phase angle is α_1. The second term contains higher-order harmonic components which cause the distorted voltage. ℓ_i denotes the amplitude of the *i*-th harmonic as a fraction of the fundamental component, n is the total harmonic number.

The extent of waveform distortion can be quantified in terms of the total harmonic distortion (THD) parameter:

$$THD_h = \sqrt{\sum_{i=2}^{n} \ell_i^2} \qquad (2.6).$$

This parameter compares the amount of harmonic content relative to its fundamental component [78], [51]. Table 2.1 provides the different standards covering voltage distortion in the power system.

Table 2.1 A brief description of different standards for voltage distortion

Standard	Description
IEC 61000- 3-6	The standard is based on the voltage quality, the total harmonic distortions are set from 6.5% to 3% for MV and HV/EHV. In general, the distribution from supply to the load is distributed to distorting installations [79].
IEEE 519	This standard deals with the injection limit of the harmonic current in the power system [80].
STC	This standard deals with the technical requirements met by the Transmission Licensee and Power System Operations [81].
EN 50160	A guide for the limits for power quality for general public MV and LV electricity distribution systems [82].
ER G5/4-1	For non-linear equipment, this is the set planning level for the THD of voltage [83].
IEC 61000-2-4	These standards are set for compatibility levels for industrial and non-public power distribution [84].

2.6 Dielectric dissipation factor

The dielectric dissipation factor (DDF) is also known as the loss factor or insulation factor. Insulation deterioration can be attributed to how the DDF behaves. Power utilities usually carry out regular condition monitoring of the DDF of high-voltage equipment to assess the insulation efficacy. Dielectrics are modelled in terms of equivalent electrical circuits from which the DDF can be inferred.

2.6.1 Simple RC circuit model

No insulation is ideal, there is a finite resistance. Furthermore, the polarizability will result in heat generation when an AC voltage is applied due to dipole movement to align with the changing electric field. As a consequence, the capacitance from the dielectric insulation cannot be free of losses [38]. There will always be real power losses in the insulation. The presence of moisture and temperature change also influence dielectric losses and measurement. The theoretical and mathematical model of the tan-delta under pure-sinusoidal excitation is given below.

An ideal dielectric can be considered as a capacitor, *C*. In practice, it is lossy, i.e., consumes real (active) power. The dielectric loss comprises three components: ohmic or conduction loss, polarization loss and partial discharge loss. The ideal capacitance is modelled as a capacitor, the losses are modelled as resistor R in parallel and the DDF is the phasor angle between the capacitive current and the total current [85]. It is illustrated in Figure 2.7.

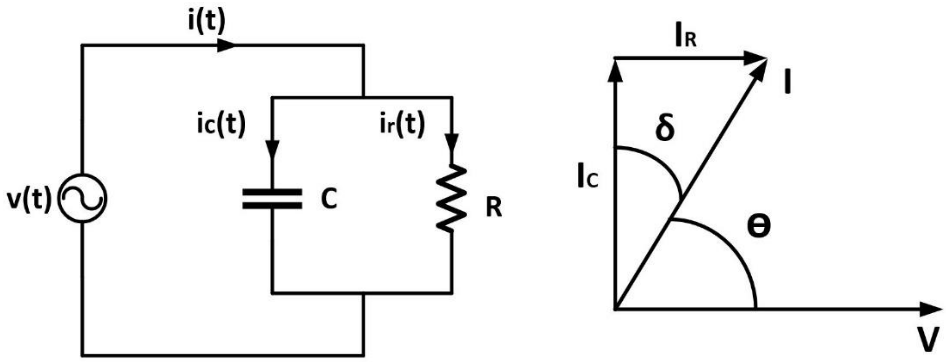

Fig 2.7 (a) Dielectric Insulation (b) Phasor representation DDF for sinusoidal excitation

One definition of DDF can be inferred from the phasor diagram which is the tangent of dissipation loss angle δ when a pure sinusoidal excitation is considered:

$$DDF \triangleq \tan\delta = \frac{I_R}{I_C} = \frac{1}{\omega RC} \qquad (2.7).$$

Here, I_R and I_C represents the current through the resistor and capacitor respectively. The voltage and current phasors in Figure 2.7(b) rotate circularly with a constant angular frequency. From Figure 2.7 (a), the resistance R represents the power loss and *C* is the capacitance. This resistance cannot be measured with a traditional ohmmeter; it is a notional parameter representing the total dielectric losses in the system, not just the conduction loss. From Figure 2.7(b), note that the power factor is $\cos\theta$ which is the same as $\tan\delta$ for small δ angle value. This is because $tan\delta \approx sin\delta = cos\theta$.

$\tan\delta$ is an indicator of the dielectric loss and hence the insulation quality, the lower the value the better the insulation. For insulation in high-voltage equipment, the low value of DDF is important and good insulation typically has a milli-radian value of DDF or less. Making use of Equation 2.7, the dielectric power loss P_R is

$$P_R = I_R^2 \times R = \frac{V^2}{R} = \omega C V^2 \tan\delta \qquad (2.8).$$

It is also important to measure DDF as a function of the applied voltage [86]. A sudden increase (tip-up) of the DDF at some voltage is indicative of the onset of partial discharge activity.

The traditional definition of the DDF via Equation 2.7 has limitations when multiple harmonic components are present in the system. Alternatively, the dielectric dissipation factor can be explained in terms of energy or power in the dielectric. The dielectric permittivity can be written as

$$\varepsilon_r^* = \varepsilon_r^{'} - j\varepsilon_r^{''} \qquad (2.9).$$

Here, ε_r^* denotes the complex relative dielectric permittivity. The real part $\varepsilon_r^{'}$ is related to the stored energy (reactive power Q) in the dielectric whereas the imaginary part $\varepsilon_r^{''}$ is related to the dissipation of energy (active power P). The complex admittance for the dielectric under a single-frequency excitation can be written as

$$Y = G + j\omega C = \frac{1}{R} + j\omega C \qquad (2.10).$$

Here, Y is the admittance and G is the conductance of the dielectric when expressed in terms of circuit parameters. The complex power S delivered to the dielectric can be expressed in terms of the active power P and reactive power Q [122]:

$$S = P + jQ = YV^2 = \left(G + j\omega C\right)V^2 = GV^2 + j\omega CV^2 \qquad (2.11).$$

Here, V is the excitation voltage, and the magnitude of S is called the apparent power. Combining Equations 2.7 − 2.11, the dielectric dissipation factor can be written as

$$DDF \equiv \tan\delta = \frac{\varepsilon_r^{''}}{\varepsilon_r^{'}} = \frac{P}{Q} = \frac{GV^2}{\omega CV^2} = \frac{VI_R}{VI_C} = \frac{I_R}{I_C} = \frac{1}{\omega RC} \qquad (2.12).$$

Equation 2.12 compiles all the equations of the dielectric dissipation factor, both the traditional along with the modern definition. The following section describes the dielectric circuits with different models taking into consideration all the losses.

2.6.2 Complex RC circuit

The dielectric materials in real insulation exhibit polarization phenomena. The polarization and the conduction loss are the major losses in the insulation. The molecules in the dielectric material are not perfectly spherical, and the movement of the molecules with the application of an external electric field is not always uniform, i.e., different relaxation times. Various researchers have tried to model the dielectric circuit based on the Debye model, Davidson-Cole (D-C) model, Cole-Cole (C-C) model, etc [120]. The D-C and C-C model are modified versions of the Debye model. These models are widely used in the modelling of insulation.

The equivalent electrical circuit for the Debye model is shown in Figure 2.8, having multiple *RC* relaxation branches. The complex permittivity of the dielectric can be expressed as

$$\varepsilon^*(\omega) = \varepsilon' - j\varepsilon'' = \varepsilon_\infty + \sum_{k=1}^{n} \frac{\varepsilon_{dc} - \varepsilon_\infty}{1 + j\omega\tau_k} \quad (2.13).$$

Here, $\varepsilon_{dc}, \varepsilon_\infty$ are the permittivity under DC voltage excitation and at the optical frequency respectively [120]. The model is explained in terms of the RC relaxation branch which is denoted by the τ. When an electric field is present in the system, the non-identical response of the different branches is expressed by the time constant $\tau = RC$. The geometric capacitance is denoted by C_o and the fundamental DC resistance is denoted by R_o.

The simplified equivalent circuit can be derived from the corresponding arrangements of lumped capacitance C and loss component σ. These parameters can be expressed as the summation of individual components:

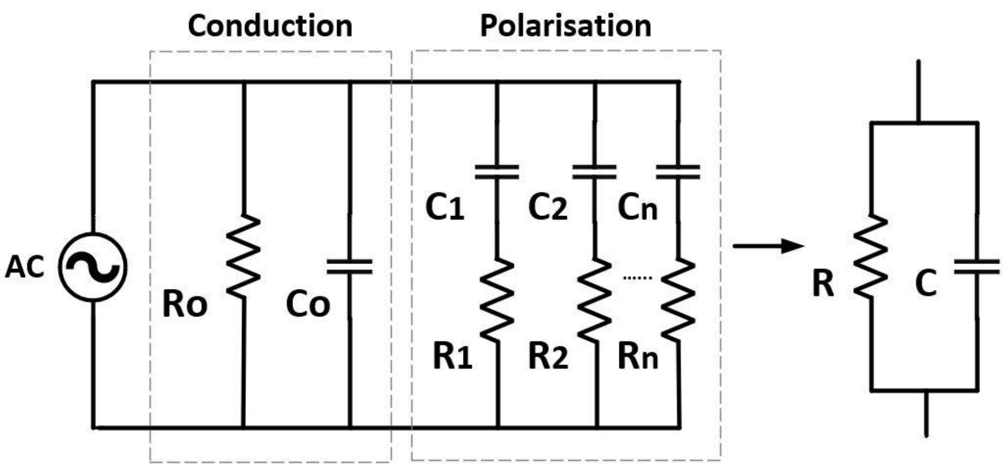

Fig 2.8 Debye circuit of dielectric (left) and the simplified equivalent circuit (right)

$$C = C_o + \sum_{k=1}^{n} C_k^{'} = C_o + \sum_{k=1}^{n} \frac{C_k}{1+(\omega\tau_k)^2} \quad (2.14),$$

and the conductivity is given by

$$\sigma = \sigma_o + \sum_{k=1}^{n} \sigma_k^{'} = \frac{1}{R_o} + \omega\sum_{k=1}^{n} \frac{C_k\omega\tau_k}{1+(\omega\tau_k)^2} \quad (2.15)$$

[53]. Here, n and σ denotes the number of parallel *RC* branches and the conductivity respectively. The dielectric dissipation factor can be expressed from the Equations 2.14 and 2.15 [53]:

$$\tan\delta = \frac{\sigma}{\omega C} = \frac{\frac{1}{R_o} + \omega\sum_{k=1}^{n} \frac{C_k\omega\tau_k}{1+(\omega\tau_k)^2}}{\omega\left(C_o + \sum_{k=1}^{n} \frac{C_k}{1+(\omega\tau_k)^2}\right)} \quad (2.16).$$

Note that when the polarisation part of the circuit is ignored, the DDF as given by Equation 2.16 becomes

$$\tan\delta = \frac{1}{\omega R_o C_o} \quad (2.17).$$

2.7 Dielectric dissipation factor measurement

The properties of dielectrics can be studied through their response over a wide range of frequencies. From a diagnostic point of view, the properties measured are mostly in the dielectric dissipation factor measurement. The measurement procedures are specified in standards or guidelines, e.g., IEEE 400 [87]. Nowadays, commercial DDF test equipment is mostly microcontroller-based automated systems, operational functions are controlled accurately with software.

2.7.1 Traditional measurement

The traditional measurement system is based on pure sinusoidal excitation voltage. The DDF is measured against an almost ideal reference capacitor of known capacitance value and having negligible dielectric loss [26].

(i) HV Schering Bridge

The Schering Bridge is one of the most traditional $\tan\delta$ measurement techniques. The circuit is shown in Figure 2.9. The bridge is composed of two branches - a measuring and a reference branch [88], [89]. One branch has the test object $Z_1(C_1 \text{ and } R_1)$ connected to the high voltage and in series with Z_4 at the earth end. The reference branch Z_2 is composed of a standard (reference) capacitor C_2. A parallel combination completes the low voltage Z_3. *G* is the galvanometer; its deflection indicates current flow when the bridge is not balanced.

The resistors have a low inductance so there is minimal measurement error. Under balanced conditions, no current flows through *G* [91] and it can be shown that:

$$\frac{Z_1}{Z_2} = \frac{Z_4}{Z_3} \quad \Rightarrow \quad \tan\delta = \omega R_3 C_3 \tag{2.18}$$

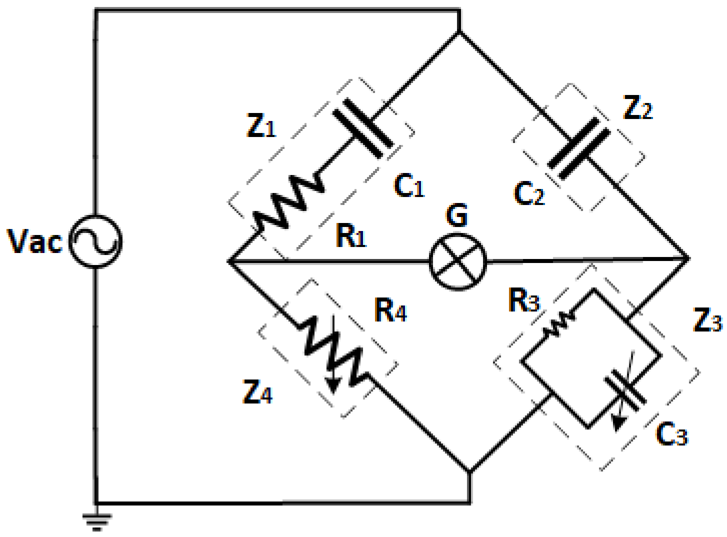

Fig 2.9 Schering bridge [90]

(ii) Transformer Ratio Arm Bridge

The effect of temperature and component aging can change the circuit parameters on the resistive arms. Such limitations led to the search for an alternative circuit. The transformer ratio arm bridge is based on the transformer coupling or turns-ratio. The voltage and current across the test object and standard capacitor are compared by having two uniformly distributed coils with different turns ratio [92]. This type of bridge is divided into two categories based on voltage and current ratio.

The transformer current ratio arm bridge uses a current comparator. The circuit is shown in Figure 2.10. The windings are carefully shielded to eliminate the effect of mechanical vibrations and stray capacitances. Considering a lossless environment, when a balanced condition is achieved, there is a null magnetomotive force developed in the current windings. Under this condition, the DDF is measured [93].

The transformer voltage ratio arm bridge is able to measure the DDF of low-capacitance test objects in low-voltage high-frequency conditions. The circuit is shown in Figure 2.11. The bridge is based on the winding ratio and good stability over time is expected. The accuracy of the capacitance and DDF measurement is up to 0.01-0.001%. The system is limited to materials having high permeability [94].

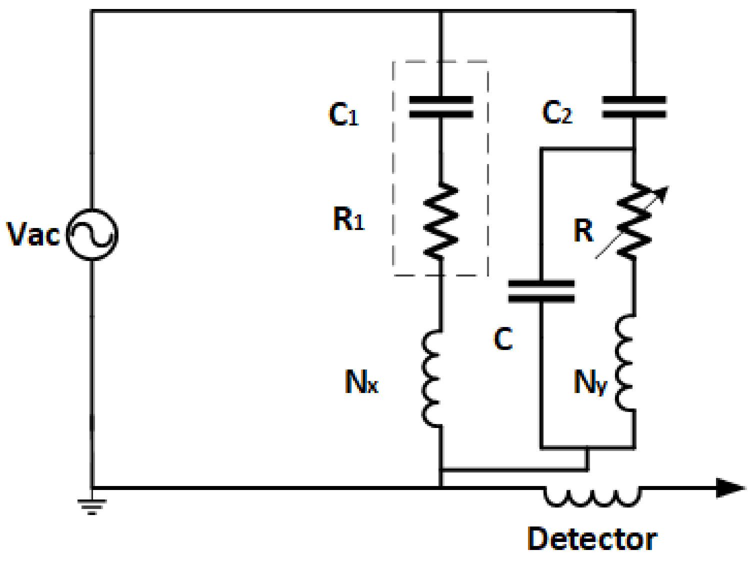

Fig 2.10 Current Ratio arm bridge [90]

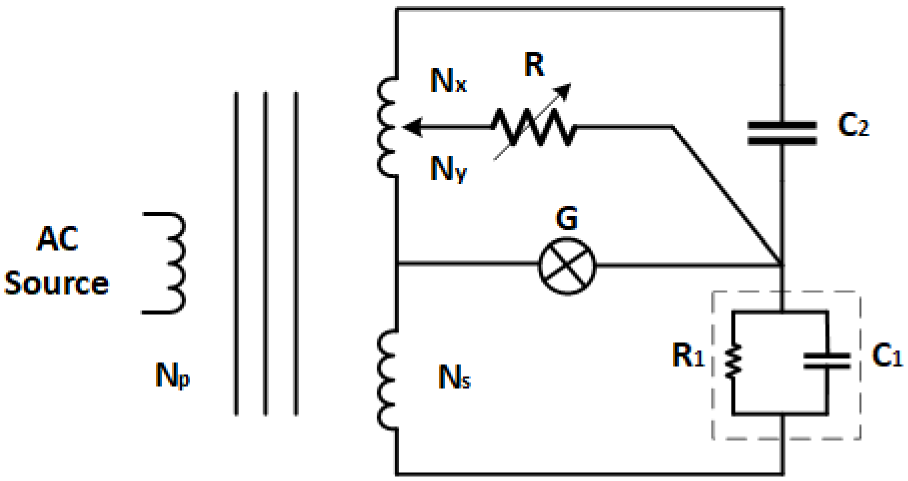

Fig 2.11 Voltage Ratio arm bridge [90]

2.7.2 DDF digital measurement

Over time, alternative techniques have emerged with the advancement of electronic devices. These offer much improved versions of measurement techniques as compared to classical measurement techniques.

(a) DDF bridge relay-based

A relay based DDF measurement circuit is shown in Figure 2.12. In this design, fine balancing is implemented with relays and electronic circuits. The circuit control operation is carried out by a microcontroller. The test object is compensated by the current flowing from the reference capacitor. The current is controlled using the microcontroller. The secondary coils compensate for flux in the differential transformer and enable the bridge to reach the balanced point [97].

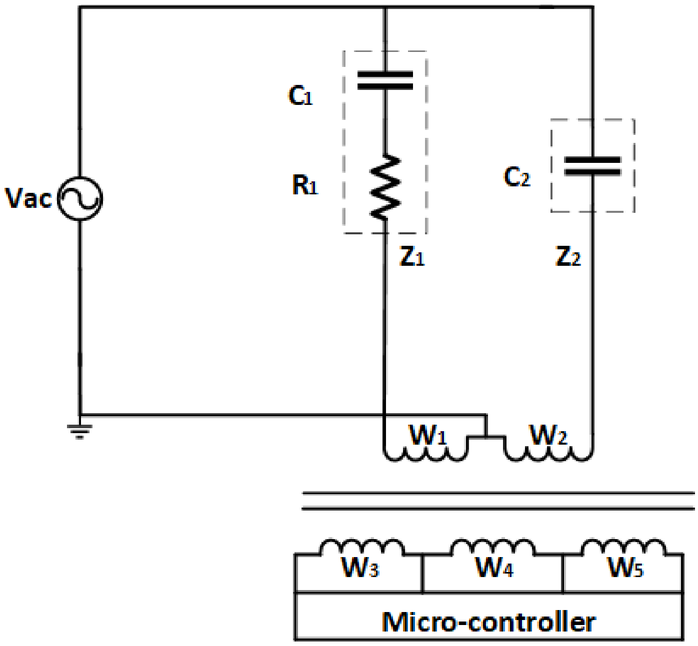

Fig 2.12 Relay based c-DDF measurement circuit [90]

(b) DDF bridge DSP-based

This method uses the signals obtained from the test sample and the reference capacitor to compare their relative position. The bridge-based measurement is an improvement over the previous method as it is relatively faster in the measurement of the dielectric response. Under the rated condition, the capacitance value of the dielectric is stable, but with the increase of voltage around the partial discharge inception voltage the capacitance value changes relatively.

The accuracy of the capacitance measurement is crucial for the assessment of the dielectric. The digital DSP-based method is efficient in the measurement of capacitance. It is a computer-based digital method that is significantly more powerful. The signals are processed using modern digital signal processing (DSP) methods replacing the conventional relay-based system. The advantage of the measurement system is that there is no need for balancing and compensation. DSP based measurement systems can be further classified into three categories based on the measurement procedure. An example of a DSP-based system is the Omicron C-tanδ MI 600 [99], shown in Figure 2.13.

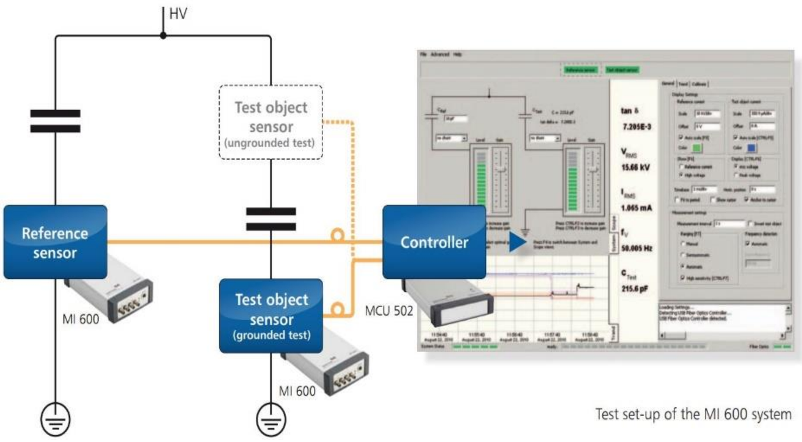

(a)

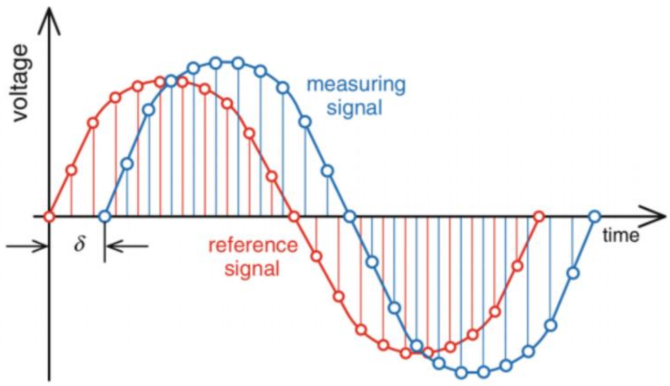

(b)

Fig 2.13 (a) DSP-based C-tanδ Bridge OMICRON MI 600 system (b) Phase shift diagram for tanδ measurement [101]

The circuit is divided into two branches: (i) the reference branch comprising a standard (reference) capacitor and a sensor unit, (ii) the measurement branch comprising the test object and a sensor unit. The sensor signals are digitised, converted to an optical signal and sent to the computer via optical fibre for further processing. The system also includes a computer with Mtronix software and an MCU 502 USB controller.

The DDF is measured by the phase angle change between the reference object current and the test object current. The system can measure the DDF in the frequency range from 5Hz up to 50kHz. The software provides a real-time oscilloscope-like display of the DDF, voltage, current, frequency, capacitance, and trend display of quantities.

Table 2.2 summarises the salient features of various commercially available DDF measuring systems discussed above.

Table 2.2 Comparison of DDF measurement techniques based on pure sinusoidal excitation

Discussed Topics	Measurement sensitivity	Capacitive load range	Frequency range	VI range	Data processing	Stray capacitance	Error
c-DDF bridge DSP	Highly sensitive [95]	Measure up to any value	0.01-500 Hz (low to medium)	10kV or higher, milli to micro amp	Real-time data processing	N/A	Minimum error
c-DDF relay	Comparatively higher	Below 1pF	0.01-500Hz (low to medium)	10kV or higher, milli to micro amp	Real-time data processing	N/A	Slightly higher [96]
Voltage ratio arm bridge	Higher than the Schering bridge	Between 100pF - 100μF	50 Hz ~ 1kHz	Up to 25 kV, 1 - 250 [92]	N/A	Present	Load error and ratio error
Current ratio arm bridge	Relatively lower than voltage ratio arm bridge	Between 100pF - 100μF	0.1-100kHz (High Frequency)	Up to 25 kV, 1 - 250 mA	N/A	Shielding present	Load error and ratio error
Schering Bridge	Lowest [91]	Between 100pF to higher values	0.1 ~ 100kHz (High Frequency)	10 kV, 1 - 100 mA	N/A	Shielding present	Load Error

2.8 DDF measurement under distorted excitation

Nowadays, the significant presence of non-linear loads causes increased power quality issues for the electricity grid [102]. The resultant current harmonics generated impact the shape of the voltage waveform observed in the network. The harmonic distortion in transmission and distribution line voltage may exceed the IEEE Std 519-2014 limits [103]. The American Electric Power System reported that the harmonic component of the 5th order dominated over other components [104]. Another report states that other odd harmonic components (3rd, 7th and 9th) also show some extensive measure of variation and it is present in a higher quantity [105]. In Australia, a similar experience is reported in a survey [106]. Therefore, from the available research survey, we can infer that supply voltage can hardly be purely sinusoidal in real life and can frequently exceed the standards limit quite significantly.

The DDF measurement under pure sinusoidal excitation has been well established and commercialised. In contrast, its measurement in the presence of distortion in the excitation voltage is still in the research stage. The phase-shift method and the null point method become invalid for excitation containing multiple frequencies [101].

Three different approaches can be adapted to determine the dielectric losses under distorted excitation voltage [48]. For pure sinusoidal excitation voltage, the dielectric power loss given by Equation 2.8 can be expressed as

$$P_1 = \omega C V^2 \tan\delta = \omega \varepsilon_r C_o V^2 \tan\delta \tag{2.19}$$

Here, P_1 is the first harmonic component of dielectric power loss, C_o denotes the geometric capacitance and ε_r is the relative permittivity. Under a distorted excitation voltage as given by Equation 2.5, the total dissipated power can be found by summation of the power loss at each frequency component, i.e.,

$$P = P_1 + \sum_{i=2}^{n} i\omega \varepsilon_{r(i)} C_o V_i^2 \left(\tan\delta\right)_i \tag{2.20}$$

Here, P is the total dissipated power. One approach is by extrapolation where the $\left(\tan\delta\right)_i$ and $\varepsilon_{r(i)}$ are measured at each frequency component $(i\omega)$ at low voltage using Frequency Domain Spectroscopy (FDS) instrument such as the Omicron DIRANA. Then the losses in Equation 2.20 can be calculated by upscaling the voltage to the actual test voltage level.

The second method is by superposition where the actual excitation voltage is applied to the test object but only one frequency component at each time and then the $\tan\delta$ and power loss can be measured using commercial measurement systems. The total power loss is then the summation of the individual power losses.

The third approach is to measure the total voltage and current directly then from which the real power P and reactive power Q can be determined. The DDF can be calculated using Equation 2.12.

Experimental work was carried out to measure the dielectric loss on dielectric test samples (cast resin) under harmonic distorted voltages [48]. The measurement setup is shown in Figure 2.14.

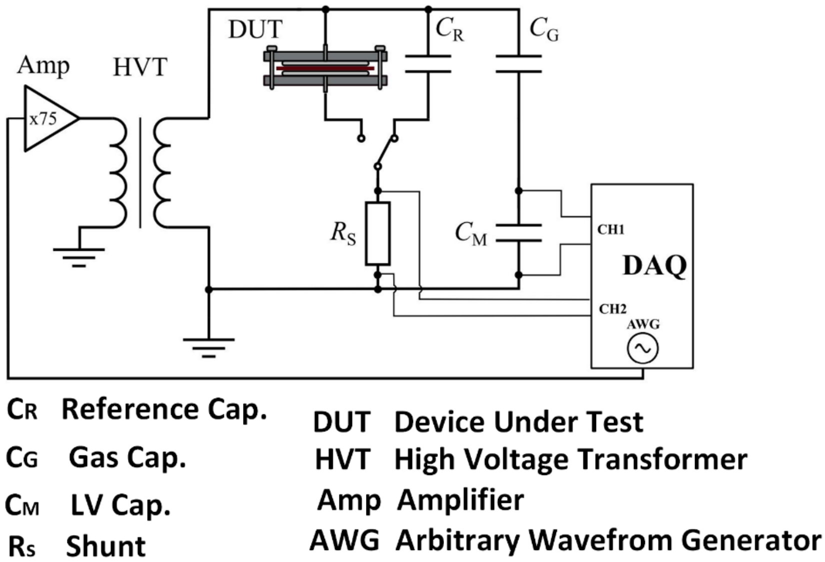

Fig 2.14 DDF measurement circuit under distorted excitation [48]

The harmonically distorted excitation is generated using a signal generator (AWG). The signal is amplified and fed to a step-up transformer to get high voltage output. The voltage signal can be measured using the capacitive voltage divider (C_G and C_M) and the current signal can be obtained by measuring the voltage across the shunt resistor R_S. The DDF is then calculated using the third approach. To obtain accuracy in the measurement, the extra branch with the lossless reference capacitor C_R is for measuring the dielectric loss in the capacitors of the voltage divider. This is done at the beginning to measure the intrinsic power loss of the setup which is later subtracted from the power loss measurement of the test object (DUT) to obtain its actual power loss.

2.9 Chapter summary

The chapter reviews the dielectric properties of insulation materials, their complex nature, circuit models for the dielectric loss, mathematical representation for the dielectric dissipation factor, and existing measurement techniques under pure sinusoidal and distorted excitation voltage. The important aspects covered are summarised below:

- The properties of dielectric materials, various polarisation mechanisms and how they impact the dielectric.
- Dielectric losses (conduction loss, polarisation loss, and partial discharge loss) and dielectric circuit models
- Linear and non-linear dielectrics, how the material behaves when subjected to the electric field from sinusoidal and non-sinusoidal applied voltage.
- The waveforms in the diagnostic testing of high voltage equipment and various standards or guidelines concerning voltage distortion.
- The dielectric power loss under pure sinusoidal and distorted excitation is reviewed.
- The principle of DDF measurement and existing techniques for measurements

Chapter 3

Computer Simulations

The main question addressed in this chapter is the modelling and computer simulation of the proposed DDF measurement technique. MATLAB-Simulink is used to construct a reference dielectric model and then apply different types of distorted excitation voltage to obtain the circuit signal numerical data from which the DDF is computed. The process is summarised in Figure 3.1. The results of the study show that voltage distortion will cause changes to the DDF relative to the pure sinusoidal excitation. The findings paved the way for laboratory experiments using real measurement setups and test objects which will be reported in the following two chapters.

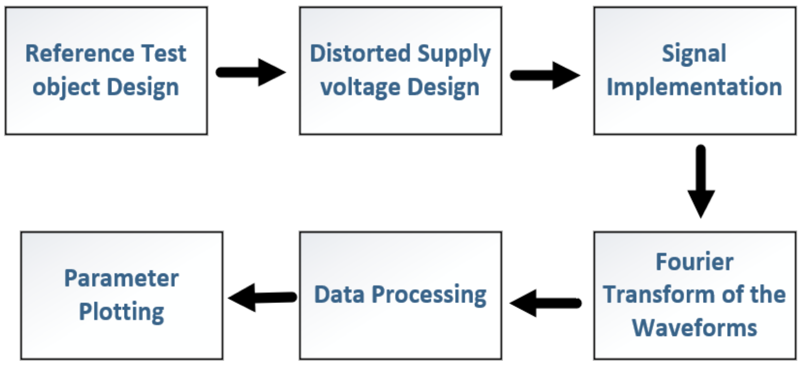

Fig 3.1 Simulation process

3.1 Simulation model development

The MATLAB-Simulink-based Dielectric Dissipation Factor Measurement is developed to study the impact of distorted excitation on the DDF. The simulation circuit consists of the test object represented by an ideal parallel RC model. The harmonically distorted signal is implemented by a combination of multiple AC voltage signal generators, one at the fundamental power frequency (50Hz) and the others at the higher-order harmonic frequency. Different distorted waveforms of some Total Harmonic Distortion (THD) are produced by changing the voltage amplitude and phase of these generators. A capacitor and 3 resistors of known fixed values are used to form 3 different reference test objects. The model simulates the entire system setup in the laboratory.

The complete circuit is illustrated in Figure 3.2 which consists of T_o as the reference test object and R_s as the resistance for current measurement. For the excitation, a pure sinusoidal 50Hz voltage is used, and a distorted excitation block is added in series with it. The voltage measurement and the current measurement blocks capture the test object's voltage and current respectively for display and subsequent data analysis.

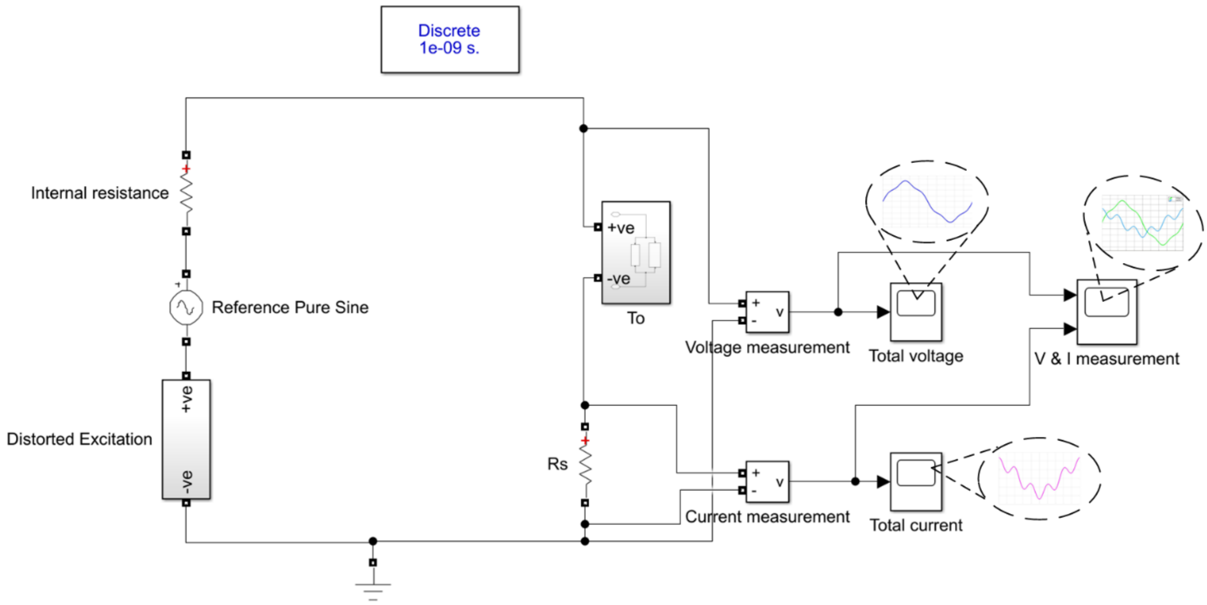

Fig 3.2 Simulation-based DDF measurement circuit model

3.2 Theoretical modelling

The theoretical modelling of the DDF measurement under distorted excitation is based on the observation that under a distorted test voltage containing multiple harmonic components, the traditional approach of DDF measurement based on pure sinusoidal voltage excitation encounters difficulty. The pure sinusoid model relies on the unambiguous phase angle between the voltage and the corresponding response current phasors, but when an excitation with multiple frequencies is present, the harmonic phasors have different angular velocities.

Consider a voltage source applied to a parallel RC network as shown in Figure 3.3. This RC combination represents a simple model for a lossy dielectric as discussed in Section 2.6.1.

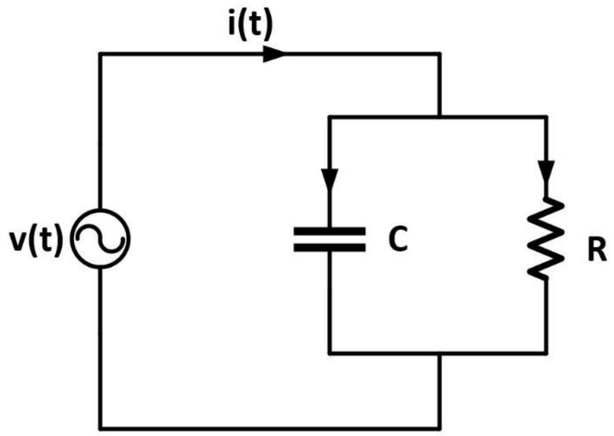

Fig 3.3 Distorted excitation applied to a parallel RC branch

If the source is a periodic harmonically distorted excitation voltage, it can be expressed in terms of the Fourier series [111]:

$$v(t) = V_{d.c.} + V_1 \sin(\omega t + \alpha_1) + V_2 \sin(2\omega t + \alpha_2) + \ldots + V_n \sin(n\omega t + \alpha_n) \qquad (3.1).$$

Here, $V_{d.c}$ is the DC voltage component. For the n-th harmonic voltage component, its amplitude is V_n, the corresponding RMS value is $V_n/\sqrt{2}$ and α_n denotes the phase angle. $\omega = 2\pi f$ denotes the angular frequency. For AC, the DC component can be discarded. All the remaining terms are orthogonal functions, and the RMS of the total voltage can be expressed as [112]:

$$V_{RMS} = \sqrt{V_{1_{RMS}}^2 + V_{2_{RMS}}^2 + \ldots + V_{n_{RMS}}^2} \qquad (3.2).$$

The corresponding response current in the system is:

$$i(t) = I_1 \sin(\omega t + \alpha_1 + \psi_1) + I_2 \sin(2\omega t + \alpha_2 + \psi_2) + \ldots + I_n \sin(n\omega t + \alpha_n + \psi_n) \qquad (3.3).$$

Here, ψ is added phase shift in the current, and I_n is the n-th harmonic amplitude. Similarly, the RMS current can be written as:

$$I_{RMS} = \sqrt{I_{1_{RMS}}^2 + I_{2_{RMS}}^2 + \ldots + I_{n_{RMS}}^2} \qquad (3.4).$$

The real power dissipated P is:

$$P = \frac{V_{RMS}^2}{R} = \frac{1}{T}\int v(t) \times i(t)\,dt \qquad (3.5),$$

where $T = 1/f$ is the period of the fundamental component. The apparent power S can be written as:

$$S^2 = V_{RMS}^2 I_{RMS}^2 \qquad (3.6),$$

and the reactive power Q is:

$$Q = \sqrt{S^2 - P^2} \qquad (3.7).$$

A more general approach for DDF measurement is based on the ratio of the real power P (dielectric loss) and the reactive power Q [112]:

$$DDF = \frac{\text{Real Power}}{\text{Reactive Power}} = \frac{P}{Q} \qquad (3.8).$$

It can be shown through the mathematical derivations detailed in Appendix A that:

$$DDF = k \times \frac{1}{\omega RC} \qquad (3.9),$$

where k is the correction factor [113]:

$$k = \sqrt{\frac{1 + THD_h^2}{1 + \sum_{i=2}^{n} \left(i\ell_i\right)^2}} \qquad (3.10),$$

and THD_h denotes the total harmonic distortion which is defined as:

$$THD_h = \sqrt{\sum_{i=2}^{n} \ell_i^2} \qquad (3.11),$$

where $\ell_i = V_i / V_1$ denotes the amplitude of harmonic *i* as a fraction of the fundamental component. The following assumptions are made:

a) Dielectric loss is modelled as a resistor of a fixed value.

b) Capacitor is a loss-free ideal capacitor.

c) The harmonic contents are percentage multiple of fundamental voltage simulating the grid distortion and no inter harmonics.

d) Non-linear *RC* behaviour is not taken into consideration.

e) The equivalent parallel RC model is considered.

3.3 System design

The entire measurement system consists of different circuit parameters. These parameters are modelled as though the entire experiment is conducted in an ideal laboratory condition. The circuit components are selected in such a way that can be practically implemented for a laboratory experiment.

(a) Reference test object

The reference test object replicates a dielectric. It consists of a parallel *RC* branch to simulate the ideal laboratory conditions. The circuit is shown in Figure 3.4. The parameters shown in Table 3.1 correspond to the actual reference test objects in the laboratory experiment.

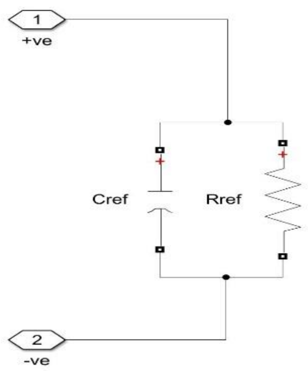

Fig 3.4 Reference test object

Table 3.1 Reference test object parameters

Test object	Capacitance (nF)	Resistance (MΩ)
S-1	1.05	93.83
S-2	1.05	42.66
S-3	1.05	29.77

(b) Distorted excitation

The distorted excitation block in Figure 3.5 consists of harmonically distorted excitations with respect to the fundamental. The harmonic distortion considered for the simulated experiment consists of the 3rd, 5th and 7th harmonics. They are connected in series. The parameters in the excitation block can be adjusted according to the THD requirements. The block can be easily modified to implement any harmonic combination of the Fourier series.

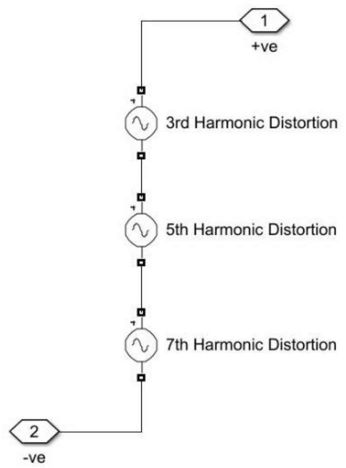

Fig 3.5 Harmonic distortion block

3.4 Results

(a) Distorted excitation:

The generated distorted excitation consists of harmonic components in addition to the 50Hz sinusoidal excitation. In all excitation cases tested, the RMS value of the total voltage, as calculated by using Equation 3.2, is kept the same at 10 kV. Also, all the phase angles in Equation 3.1 are zero.

An example is shown in Figure 3.6. The test object is S-1. Figure 3.6(a) portrays a distorted excitation voltage with 10% 5th harmonic and its corresponding distorted current. Only one harmonic is considered in this case. In order to keep the total RMS values to 10kV, $V_{1_{RMS}} = 9.95\ kV$, its peak value is $V_{1_{peak}} = \sqrt{2} * V_{1_{RMS}} = 14.072\ kV$, and $V_{5_{RMS}} = 10\%\ V_{1_{RMS}}$.

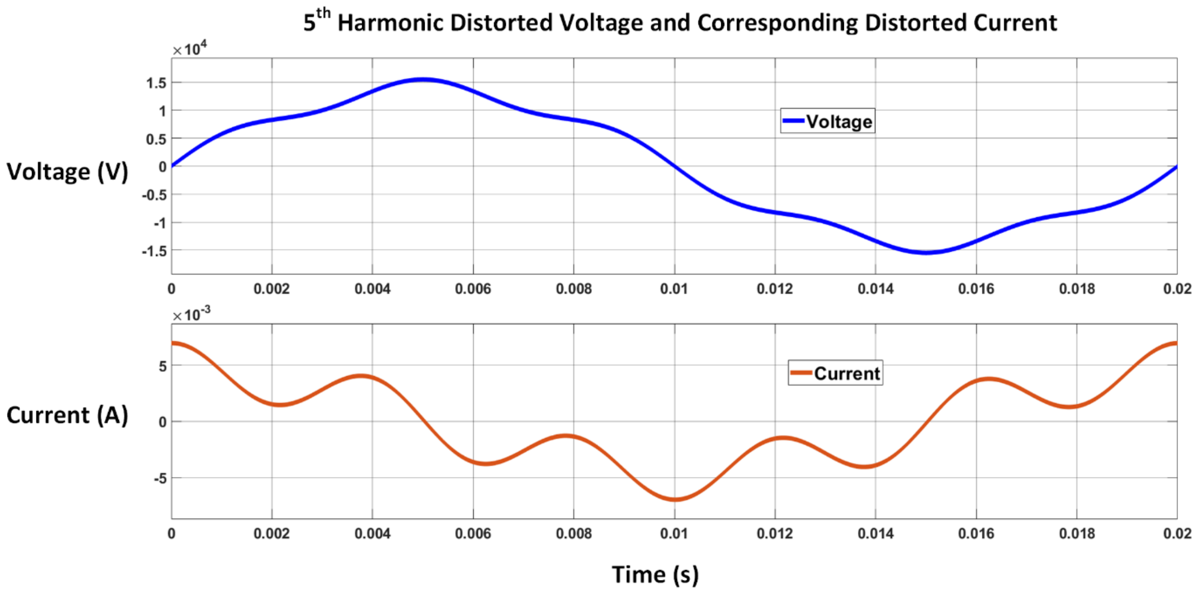

(a)

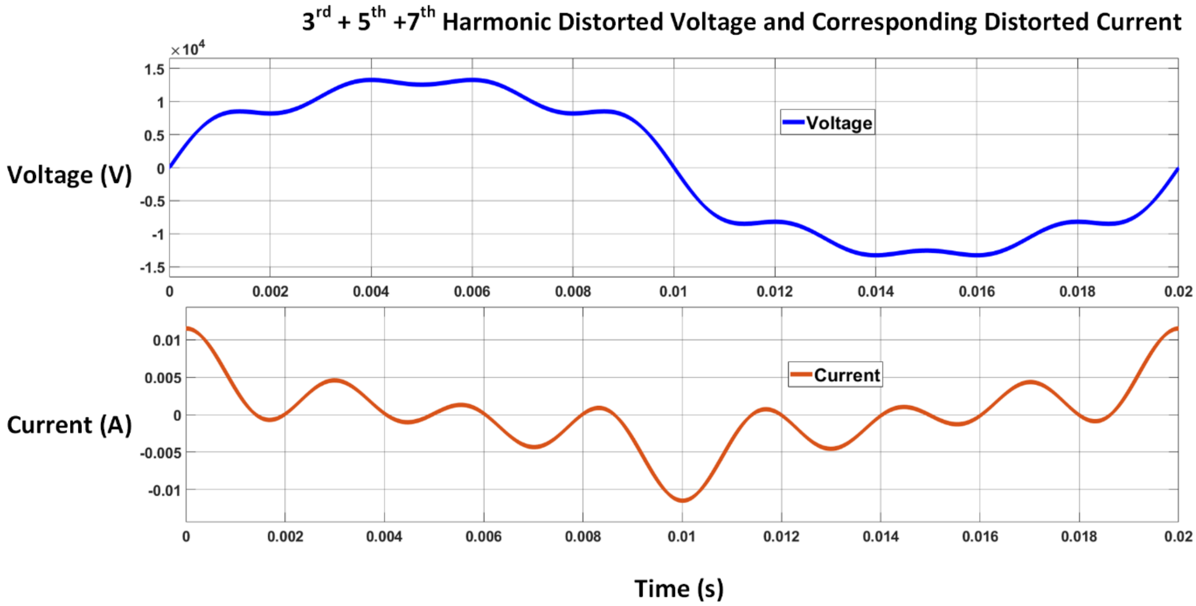

(b)

Fig 3.6 Harmonic distorted voltage and current vs time: (a) 10% 5th harmonic, (b) 3rd, 5th and 7th harmonics of 10% each

On the other hand, Figure 3.6(b) portrays a distorted excitation voltage with 3 harmonic components (10% 3rd, 10% 5th and 10% 7th harmonics) and the corresponding distorted current. To achieve 10kV RMS total voltage, $V_{1_{RMS}} = 9.8533\ kV$, its peak value is $V_{1_{peak}} = \sqrt{2} * V_{1_{RMS}} = 13.935\ kV$, and $V_{3_{RMS}} = V_{5_{RMS}} = V_{7_{RMS}} = 10\%\ V_{1_{RMS}}$. Note that in this case (b), the fundamental and the fifth harmonic components are smaller relative to their counterparts in case (a) above. This is expected (to accommodate additional third and seventh harmonics) in order to achieve the same total RMS voltage of 10kV in both cases.

Figure 3.6 shows the resultant voltage and current waveforms in the time domain. It can be seen that the distorted excitation voltage results in a severely distorted current. Although they are stationary relative to each other, defining the phase shift between them is ambiguous. For the case of Figure 3.6(a), both waveforms cross the zero once every half AC cycle (10ms). However, in Figure 3.6(b), the current waveform crosses the zero 7 times.

(b) Corresponding Fourier transform:

MATLAB Simulink provides a Fast Fourier Transform (FFT) toolbox which can be used to analyse the voltages and currents in the frequency domain and also the total harmonic distortion (THD). The results are shown in Figure 3.7 for the same distorted excitation voltages considered in Figure 3.6.

We can infer that the presence of harmonics in the system has a significant impact on the distorted current. From the discrete Fourier transform of the signals in Figure 3.7(a), it can be clearly observed that the relative magnitude of the (fifth) harmonic with respect to its fundamental component has increased for the current. Whilst the THD of the excitation voltage is 10%, the THD of the resultant current almost reaches 50%. Although both the voltage and current waveforms share the same harmonic composition (i.e., both comprising the fundamental and the fifth harmonic), they are different in terms of the magnitudes. The distortion in the voltage gives rise to a different distortion in the current which is interesting for noting.

To understand the impact of harmonics further, multiple harmonic components were introduced into the system. Figure 3.7(b) depicts the FFTs of an excitation voltage having multiple harmonics and the corresponding distorted current. Whilst the THD of the voltage is 17.32%, it has resulted in a significant increase in the THD of the current to 91.06%. Although all the voltage harmonics (third, fifth, and seventh) have the same magnitude, the change in the current harmonics is different, increasing with the harmonic order. The presence of multiple harmonics in the excitation voltage causes significant distortion to the resultant current in a non-linear manner. Thus, it can be inferred that the harmonic distortion will cause a significant impact on the dielectric dissipation factor measurement.

Although not considered in this simulation study, the voltage-current relationship will be much more complicated when non-linear test objects are involved. Fourier analysis of signals in the frequency domain is even more useful for such situations to reveal new harmonic and inter-harmonic components. And it will be very challenging to determine the DDF.

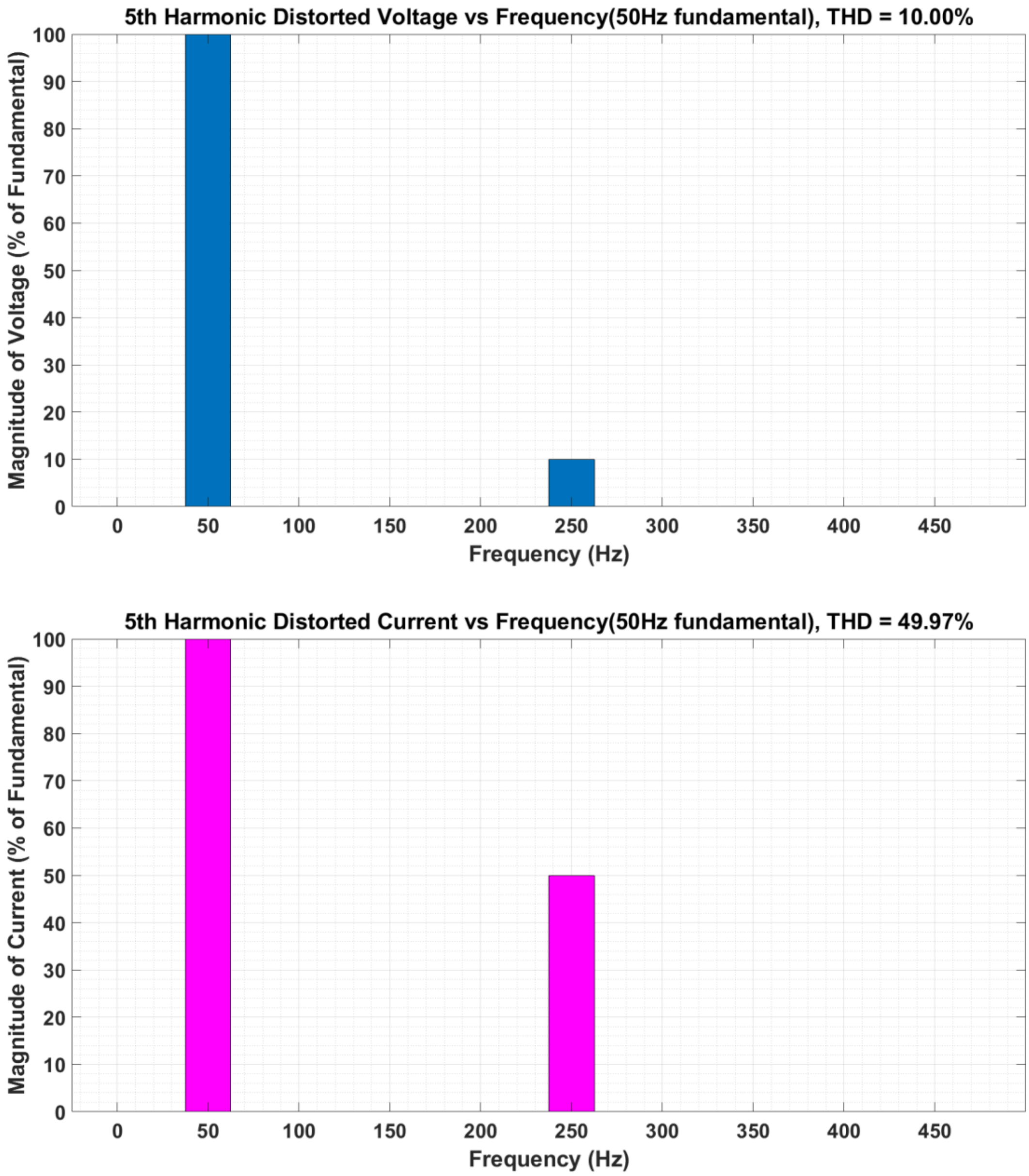

(a)

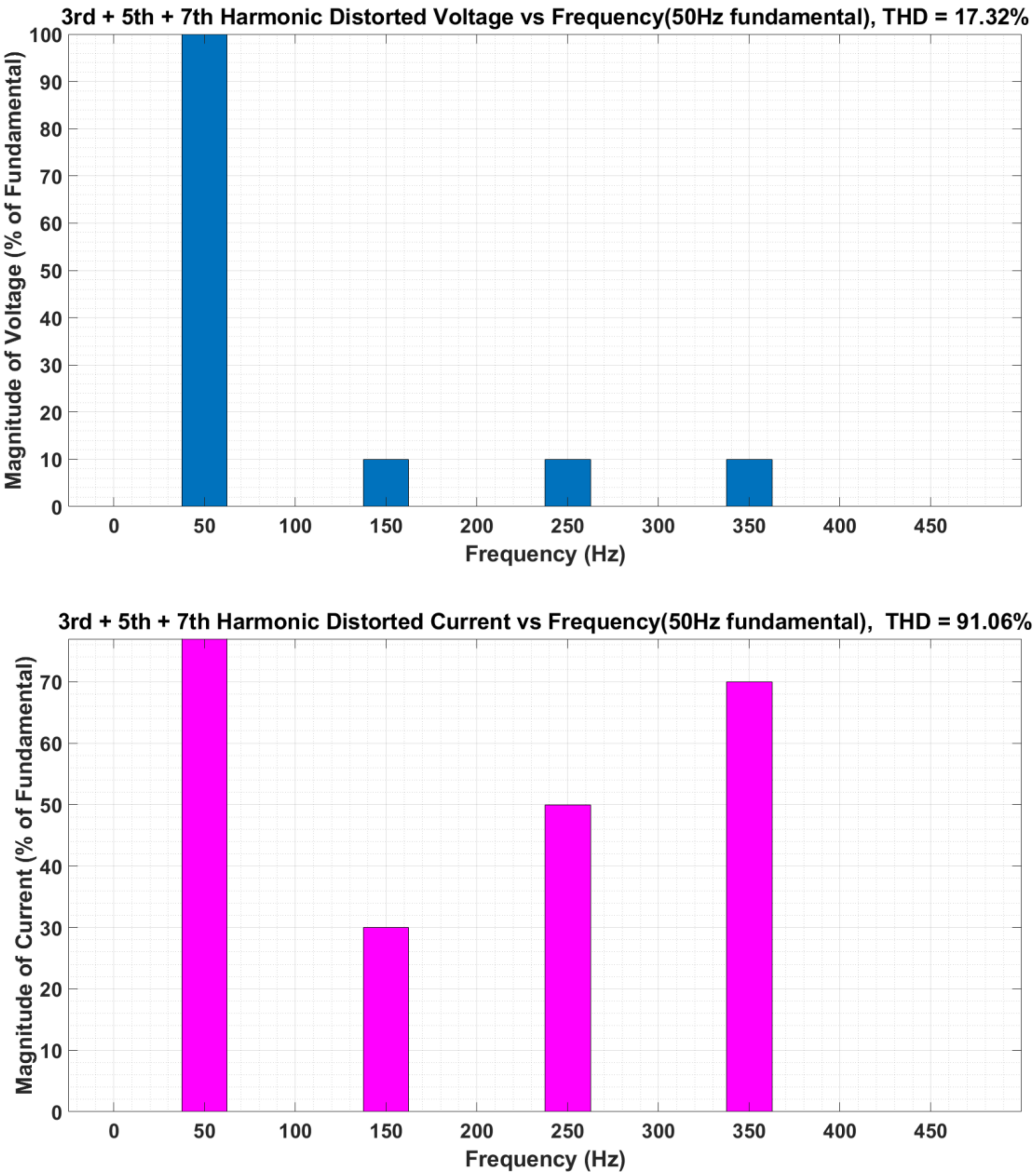

(b)

Fig 3.7 FFT of harmonic distorted voltage and current: (a) 10% 5th harmonic, (b) 3rd, 5th and 7th harmonics of 10% each

(c) Correction Factor:

The correction factor or the distortion factor is defined as the ratio between the dielectric dissipation factor for harmonically distorted excitation DDF_h to that when it is a pure sine wave DDF. From Equations 3.9 - 3.10, we get:

$$k = \frac{DDF_h}{DDF} = \sqrt{\frac{1+THD_h^2}{1+\sum_{i=2}^{n}(i\ell_i)^2}} = \sqrt{\frac{1+\sum_{i=2}^{n}\ell_i^2}{1+\sum_{i=2}^{n}(i\ell_i)^2}} \qquad (3.12).$$

From this equation, it can be inferred that $0 < k \leq 1$. In the case of pure sinusoidal excitation $k = 1$. With the increase in the harmonic percentage and the number of harmonics, the total harmonic distortion will increase whereas the value of *k* will decrease.

For the simulation purpose to observe the trend of the correction factor, only one test object is selected. The correction factor can be considered independent of the dielectric dissipation factor. The correction factor changes with the change in the harmonic distortion. The plots in Figure 3.8 show how the correction factor behaves.

Figure 3.8(a) plots the correction factor versus the total harmonic distortion for a fixed harmonic order. From the plot, when the harmonic order is known, the correction factor can be obtained for any THD content. The k1, k2 and k3 are three different correction factors vs THD plots for reference test object S-1. The plots are for different harmonic orders (but one harmonic only in each plot). When the THD is 0% it is the pure sinusoidal case, and $k = 1$. It can be seen from the plot that, for a given harmonic, the distortion factor decreases with an increase in the THD. A similar pattern of the plot is observed but the value is decreased when the harmonic order is increased. The rate of change (slope of the curve) increases with increasing THD value.

Figure 3.8(b) plots the correction factor versus the harmonic order for a fixed total harmonic distortion. From the plot, when the THD is known, the correction factor can be obtained for any harmonic. The k1, k2 and k3 are three correction factors vs harmonic order plots for different THD for reference test object S-1. When the harmonic order is 1, then THD=0% and $k = 1$. All the plots start from 1 and decrease in value with an increase in the harmonic order. This signifies that the higher the harmonic order, the more impact it has on the dielectric dissipation factor measurement. With the increase in the THD value the graph shifts downward which signifies that when the waveform contains more harmonic distortion the measurement of DDF will be inaccurate as compared to pure sinusoidal excitation.

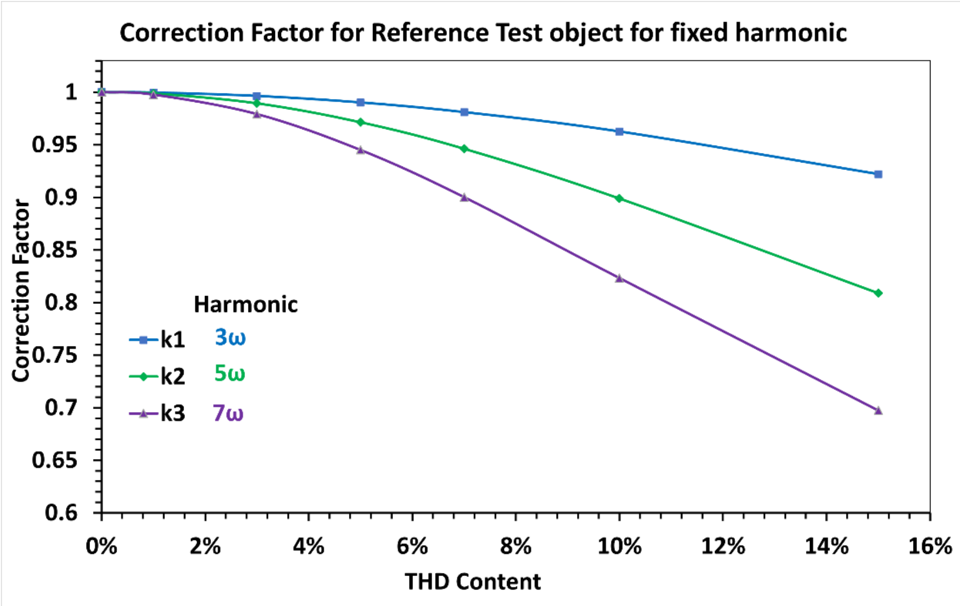

(a)

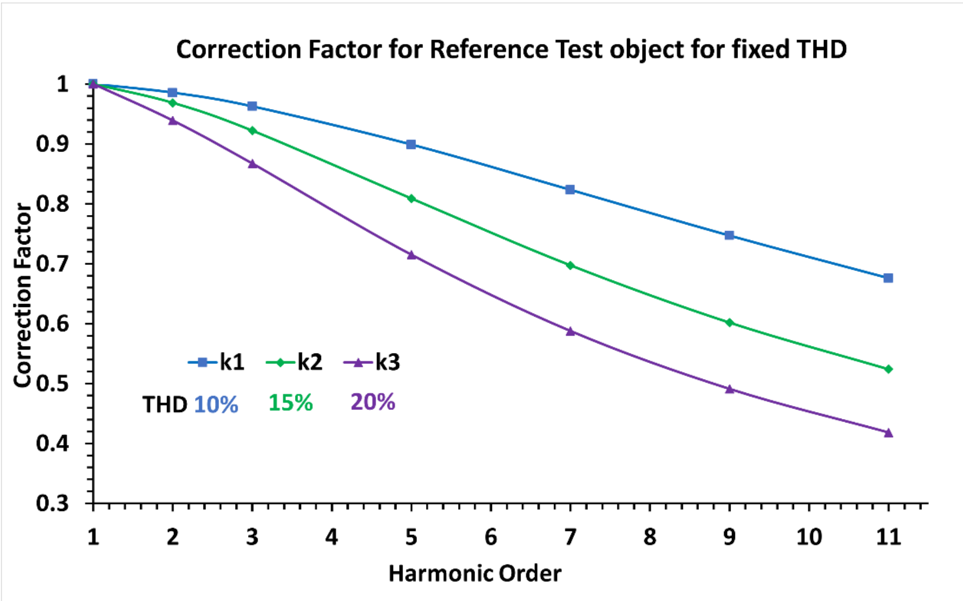

(b)

Fig 3.8 (a) Correction factor vs THD plot for fixed harmonic order, (b) Correction factor vs harmonic order plot for fixed THD

(d) DDF for distorted excitation:

The dielectric dissipation factor for the three reference test objects in Table 3.1 follows a similar trend as shown in Figure 3.9. With the increase in the harmonic order and the total harmonic distortion, the value of DDF_h decreases.

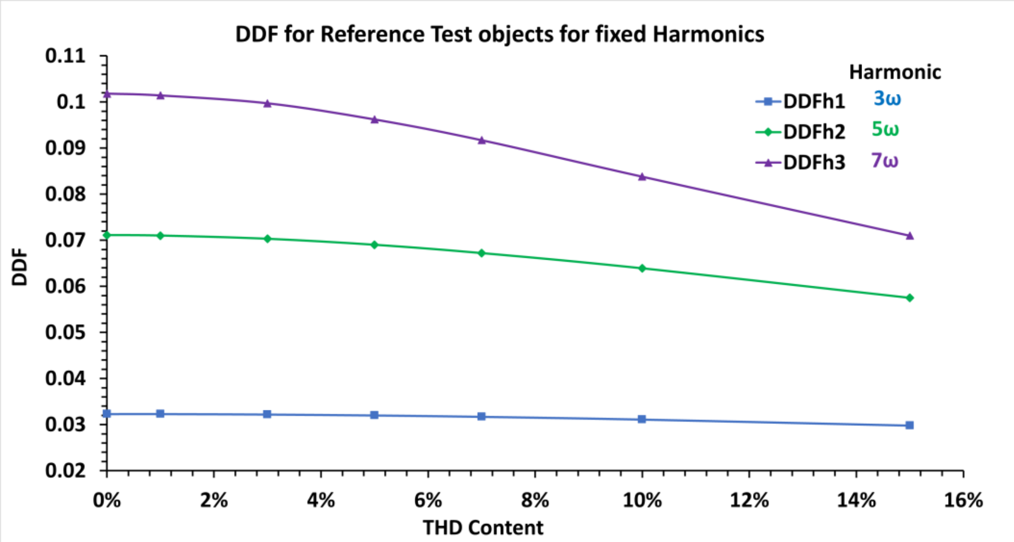

(a)

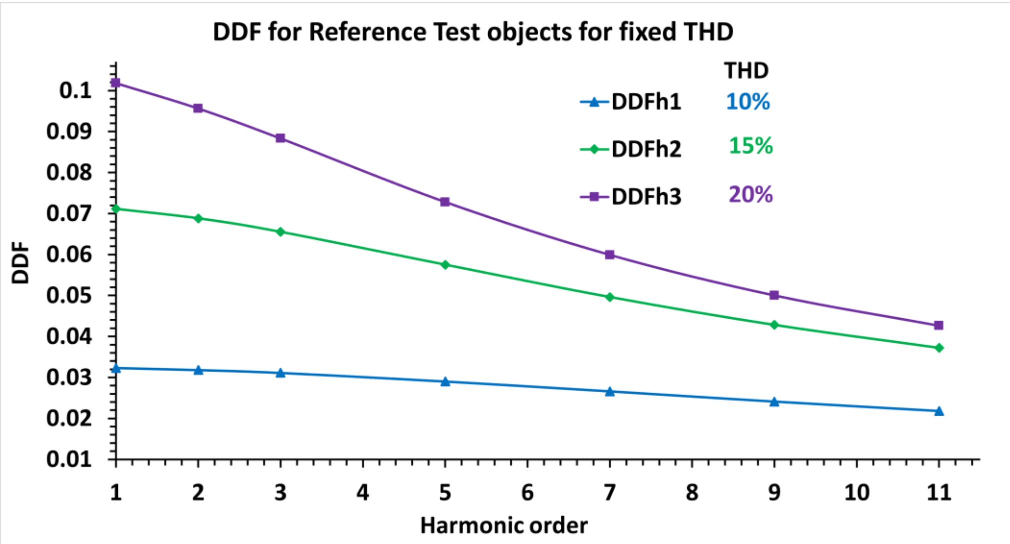

(b)

Fig 3.9 (a) DDF_h vs THD plot for fixed harmonic order (b) DDF_h vs harmonic order plot for fixed THD for different test objects.

Figure 3.9(a) plots the dielectric dissipation factor for harmonically distorted excitation versus the change in THD for a fixed harmonic order. Here, the blue trace is obtained for the case of test object S-1 and the excitation voltage contains the third harmonic only. The green trace is obtained for the case of test object S-2 and the excitation voltage contains the fifth harmonic only. The purple trace is obtained for the case of test object S-3 and the excitation voltage contains the seventh harmonic only. The 0% THD corresponds to the pure sinusoidal case, and the DDF is maximum: 0.0323 for S-1, 0.0711 for S-2, and 0.1018 for S-3. With the increase in the THD, DDF_h decreases following a non-linear trend. Each curve provides evidence that with the increase in percentage harmonics, the DDF goes down in value and the slope is steeper for higher THD.

Figure 3.9(b) plots the dielectric dissipation factor for harmonically distorted excitation versus the change in harmonic order for a fixed THD value. Here, the blue trace is obtained for the case of test object S-1 and the excitation voltage has one harmonic of THD 10%. The green trace is obtained for the case of test object S-2 and the excitation voltage has one harmonic of THD 15%. The purple trace is obtained for the case of test object S-3 and the excitation voltage has one harmonic of THD 20%. Note that harmonic order 1 corresponds to the case of pure sinusoidal excitation, and the DDF is maximum, same starting values as in Figure 3.9(a). All test objects have the same capacitance so the larger the resistance the smaller the DDF. With increasing harmonic order, DDF_h goes down in value following a non-linear trend. Comparing the curves, the slope of the graph is steeper for higher THD. With the increase in THD and the harmonic order, the value of DDF decreases significantly.

(e) Data processing:

The data obtained from the simulation circuit is processed using the MATLAB computer program and plotted. The process is given in Figure 3.10.

The data processing starts with the generation of a distorted waveform and a corresponding plot of the waveform along with the FFT. The distorted excitation and the corresponding distorted current are generated in the beginning. The energy parameters are calculated from the voltage and current. The distortion factor is a function of the harmonic distortion and the harmonic order. The plots are made considering the change in THD and harmonic order on the correction factor and the dielectric dissipation factor.

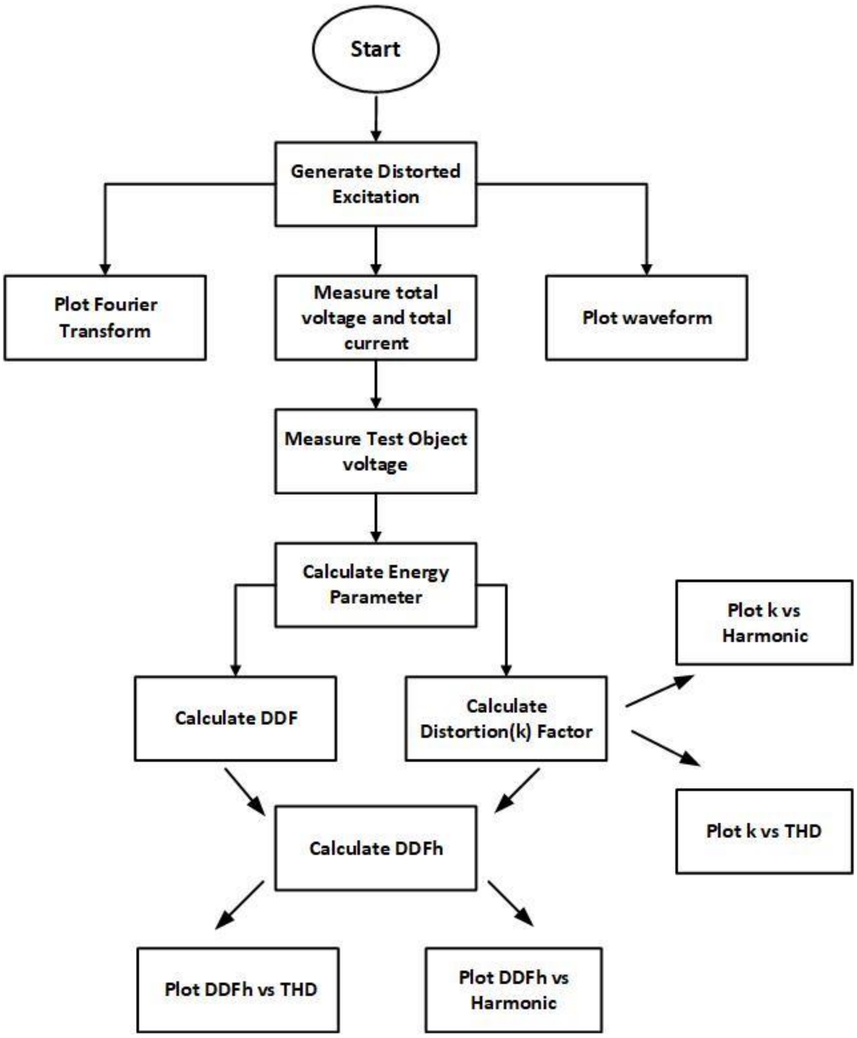

Fig 3.10 Schematic diagram of data processing

3.5 Chapter conclusion

The chapter contains an overall conceptual framework of the dielectric dissipation factor measurement. The implication of distorted excitation on the DDF measurement based on numerical methods was investigated. The voltage supply is implemented to provide distorted excitation to three reference RC test objects of ideal properties. The DDF for pure sinusoidal voltage was calculated first, and the distortion factor and the corresponding DDF are calculated as well. Theoretical calculations and MATLAB numerical computations are in alignment. It is observed that with the increase in harmonic content and total harmonic distortion the slope of the correction factor and the DDF change dramatically.

With the increase in the harmonic order, the correction factor decreases. The decreasing trend is non-linear. The presence of multiple harmonics in the system reduces the correction factor as well. However, the trends are different, and the relative gap increases with an increase in the percentage components. This suggests that with the increase in the relative percentage of the THD and harmonic order, the traditional DDF measurement becomes erroneous. The measurement based on the power ratio is a better approach as it is universal - applicable for both non-distorted and distorted excitations.

Some of the works described in this chapter have been published in:

Pratic A Muntakim, Shubin Zhang, Junyang Zhang, B.T. Phung, "Insulation Assessment Based on Dielectric Dissipation Factor Measurement under Non-sinusoidal Excitation"*, 2021 IEEE 5th International Conference on Condition Assessment Techniques in Electrical Systems (CATCON),* Kerala, India, 3rd -5th December 2021.

Chapter 4
DDF Measurement Under Non-sinusoidal Excitation Voltage

4.1 Background

The degradation of insulation in high voltage equipment during the operating life is inevitable as there is multi-factor ageing caused by electrical, thermal, mechanical, and environmental stresses [114]. These stresses make the insulation degrade, eventually causing breakdowns in the power system. With the evolution of technologies, more and more devices are getting integrated into the system. The deployment of non-linear devices causes the voltages and currents to become non-sinusoidal. Thus, the insulation is subjected to electrical stress from applied voltage not limited to the power frequency (50/60Hz) but also having high-order harmonics [115].

The dielectric dissipation factor or tan-delta is an important parameter for assessing the insulation health [116]. The energy dissipation in a dielectric is related to the loss index or DDF. To date, most research is based on condition assessment of insulation tested under the normal operation frequency (pure sinusoidal 50/60Hz voltage).

This chapter investigates the impact of harmonics on DDF measurement by conducting laboratory experiments using reference test objects of known RC values. The analysis utilised the work developed in the previous chapter.

4.2 Design motivation

The task is the practical implementation for measuring the DDF under non-sinusoidal voltage. The reason for using a parallel RC of known values as the test object is so that the experimental measurements can be compared with the expected results based on the theoretical formula and also MATLAB Simulink computer simulations developed for calculating the DDF under distorted excitation.

4.3 Experimental setup

The experimental setup consists of a reference test object comprising a resistor with negligible inductance/capacitance and a loss-free capacitor. A low-voltage signal generator is connected to an amplifier to produce high voltage excitation. To measure the current through the test object, a resistor is connected in series.

Figure 4.1(a) shows the excitation generator used in the experiment and the digital oscilloscope to record all the waveforms. The resistor for current measurement is shown in Figure 4.1(b). Figure 4.1(c) shows the laboratory setup with the reference test objects. The experiments were carried out in the laboratory under ambient conditions with temperatures typically varying in the range of 20-25 ^{o}C.

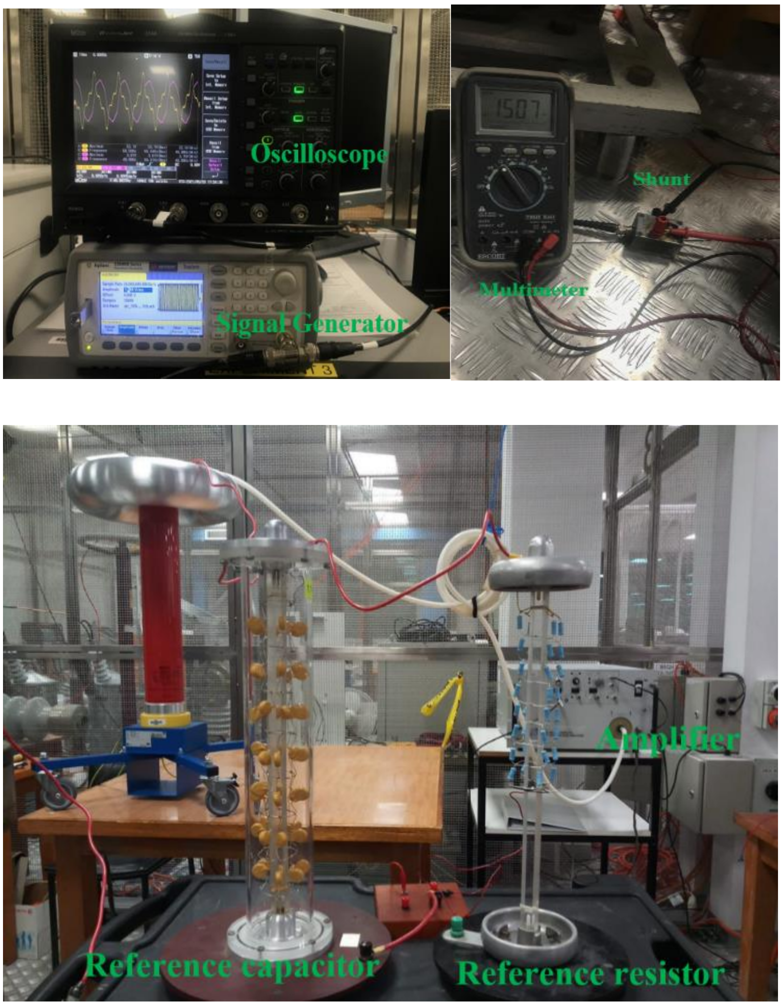

Fig 4.1 (a) Excitation generator (b) Current measuring resistor (c) Laboratory setup

4.4 Distorted excitation parameters

The distorted excitation voltage is generated using an Agilent 33500B programmable arbitrary waveform generator. For the experiment, the excitation waveform is synthesised using the Keysight BenchLink Waveform Builder software. The waveforms are mathematically constructed and generated using this software. An example of this software user interface is shown in Figure 4.2.

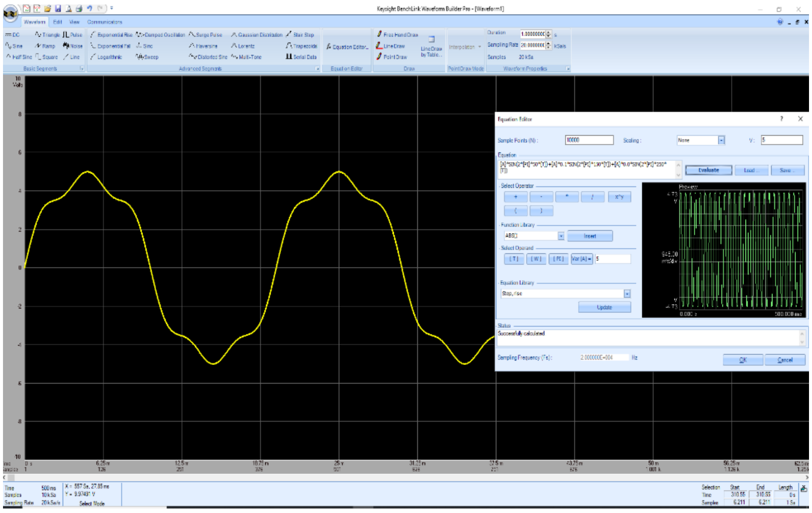

Fig 4.2 User interface of Agilent 33500B programmable arbitrary waveform generator

The generated waveforms contain the fundamental power frequency with the additional harmonic components simulating the grid distorted excitation. The voltage magnitude can be varied and adjusted. The waveform generator can produce low voltage output of up to 10Vpp. The signal is recorded using a LeCroy 314-A digital storage oscilloscope. For generating high voltage, the low voltage signal is fed to a TREK 20/20 high voltage linear amplifier (Figure 4.3) which has a voltage gain of 2000. The specifications for the voltage waveforms used in the experiment are provided in Table 4.1.

Fig 4.3 Trek 20/20 high voltage amplifier

Table 4.1 Voltage excitation parameters

Type	Voltage Level	Harmonic Order
Pure-Sinusoidal	0kV~12kV	-
Non-Sinusoidal	8kV, 10kV	3rd, 5th & combined
Harmonic with phase shift	8kV, 10kV	5th (0º~360º)

4.5 Reference test object

The test object used in the experiment is constructed using a parallel combination of a resistor and a capacitor with very low loss to imitate a dielectric. The capacitor has very low loss relative to the Ohmic loss of the resistor and so the resistor represents the total dielectric loss. The values of the capacitor and resistor are known. Thus, one can predict the dielectric loss and compare it with the actual measurement results. Figure 4.4 shows the reference test object structure.

Fig 4.4 Reference test object setup

In the experiment, the reference test object is subjected to high voltage. The reference capacitor was constructed in-house, using low-loss 1nF/10kV rating capacitors. They are connected in series to form a string that can withstand high voltage applied (up to 70kV) and also in parallel to achieve the total nominal equivalent capacitance of 1nF. The actual value measured is 1.05nF.

For the reference resistor, three different resistors were used and combined, one at a time, with the reference capacitor to form three reference test objects, named S-1, S-2, and S-3. Their parameters were provided in Table 3.1 and used for computer simulations in the previous Chapter. Figure 4.5 show two of the reference resistors: one is a resistor string constructed in-house using non-inductive low-voltage rating resistors whereas the other is an off-the-shelf high-voltage resistor.

Fig 4.5 Reference resistors

4.6 Measurement circuit

The circuit connection for DDF measurement is shown in Figure 4.6. It consists of a signal generator (SG), its output feeding into a high voltage linear amplifier (HV). The signal generator is an Agilent 33500B programmable arbitrary waveform generator, and the amplifier is a TREK 20/20C. The low voltage signal is stepped up with the amplifier and the output is applied to the test object (To), i.e., the reference RC parallel combination.

As the voltage gain of the amplifier is known and fixed, the magnitude and waveform of the high voltage output can be indirectly obtained from the SG low voltage signal. The high voltage output can also be measured using an HV probe or a 1000:1 resistive divider.

The total current through the reference test object is monitored with a resistor R_S connected in series; its value (1.5kΩ) was chosen such that to maximise the measurement sensitivity of its voltage taking into account the impedance of the test object and the input voltage limit of the digital storage oscilloscope (DSO).

The DSO is a LeCroy 314-A, its two input channels Ch-1 and Ch-2 are utilised to capture the voltage signals of SG and R_S. This corresponds to a sampling rate of 10kHz and a Nyquist frequency of 5kHz. The digital data are transferred to a PC and processed using MATLAB which includes an algorithm developed to filter out any noise.

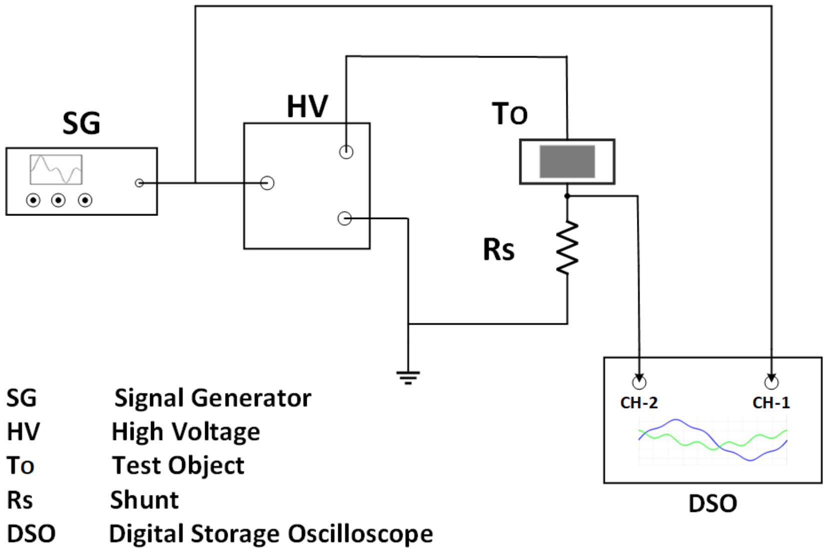

Fig. 4.6 DDF measurement circuit diagram [21]

4.7 Experimental procedure

The experiment consists of testing the parallel RC model for three different excitation voltage waveforms as shown in Table 4.1

Pure sine wave: for the first part of the experiment, a pure 50Hz sinusoidal excitation is applied to the test object and the corresponding voltage is increased with an increment of 2kV from 2kV to 12kV. At each step, the voltage and current waveforms are digitised and used for calculating the DDF.

Harmonic excitation: in the second part of the testing, the distorted 50Hz excitation is applied to the test object. The measurements are carried out for two different applied voltages of fixed values 8kV and 10kV (RMS). The 3rd and 5th order harmonic components are selected as these are mostly present in real power systems. These harmonics are added with the first harmonic (50Hz fundamental) separately, i.e., 1st and 3rd or 1st and 5th, and as a combination, i.e., 1st and 3rd and 5th. The overall RMS value of the combined voltage is kept the same although the percentage magnitudes of the harmonic mix are varied.

Phase shift: Equations 3.9 and 3.10 developed suggest that there is no influence of the phase angle α_i's on the dielectric dissipation factor. The final part of the experiment is to validate this point. The test involves applying a distorted voltage using only one harmonic component (5th) and setting its phase angle α_5 to different values (0 °, 30 °, 60 °, 120 °, 180 ° and 270°).

4.8 Data processing

The experiment data is processed using MATLAB after transferring it from the digital storage oscilloscope. The flow chart is shown in Figure 4.7.

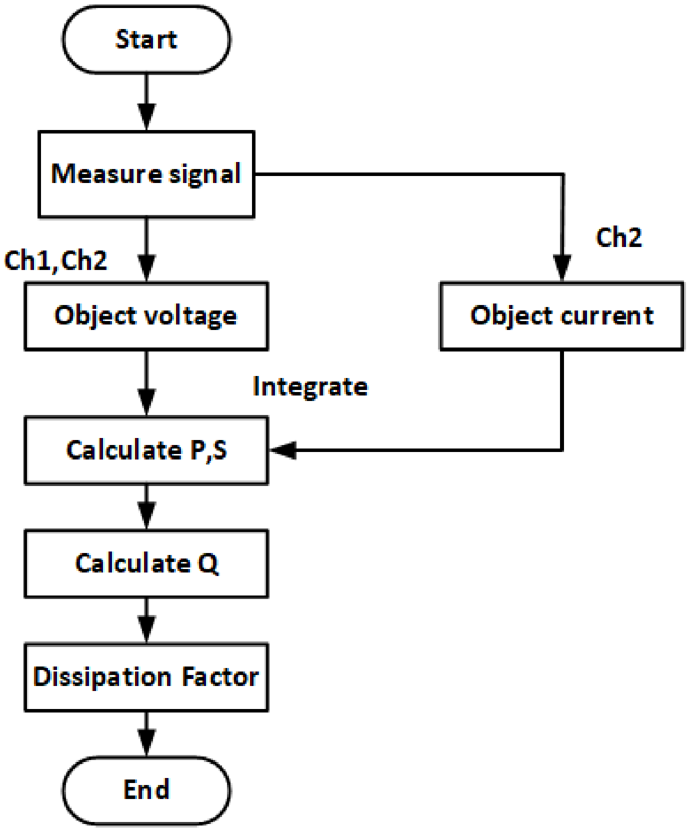

Fig. 4.7 Data processing flow chart

The voltage across the test object is calculated from the difference between the Ch1 and Ch2 voltage measurements. The current through the test object is Ch2/Rs. The apparent power S is calculated using Equation 3.6. The active power P is calculated using the current and the corresponding voltage as per Equation 3.5. Then the reactive power Q is calculated based on Equation 3.7 and the DDF is obtained as the ratio of the active and reactive power, i.e., Equation 3.8.

4.9 Computer simulations

For simulating the DDF measurements, MATLAB Simulink is used to model the circuit as shown in Figure 4.8. The voltage source in the simulation implements the different waveforms defined in Table 4.1. The reference test object is composed of a capacitor and a resistor in parallel and the parameters are given in Table 3.1. The data obtained from the voltage and current measurement blocks are exported to MATLAB and it is numerically processed with an algorithm to output the DDF values. The simulation is based on ideal conditions (no noise or interference as encountered in practice).

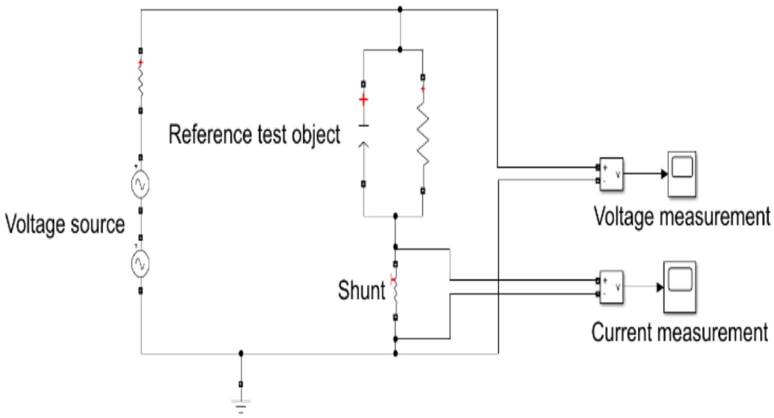

Fig 4.8 DDF measurement simulation circuit diagram

4.10 Results and discussion

The whole experiment can be divided into three parts based on the changing variables and the same testing in each part was carried out on the three test objects. The results follow the same trend so only the case of the S-1 test object is presented below for discussion.

Pure Sine: Figure 4.9 shows the results for the S-1 test object under pure sinusoidal excitation voltage. A comparison is made between the results obtained from the physical experiment, MATLAB Simulink, and the mathematical formula.

From the plots, the MATLAB Simulink results are in perfect alignment with the analytical calculation which is expected. However, the experimental results are consistently slightly higher. This could be attributed to some other real power losses incurred in the experimental setup. Real power losses can incur due to the resistance in the wiring and at the connection points (contact resistance). The wiring is necessary to connect the circuit components. Thus, these losses cannot be separated out. However, attempts were made to minimize such losses by using copper conductors with large cross sections and connection junctions tightly secured with large contact areas. Their impact is expected to be small, and the dominant source is most likely the polarisation loss from the reference capacitor itself. Nevertheless, the maximum percentage difference is only 3.4%. Also observed in the experimental results is a slowly rising trend with the increase in the voltage applied.

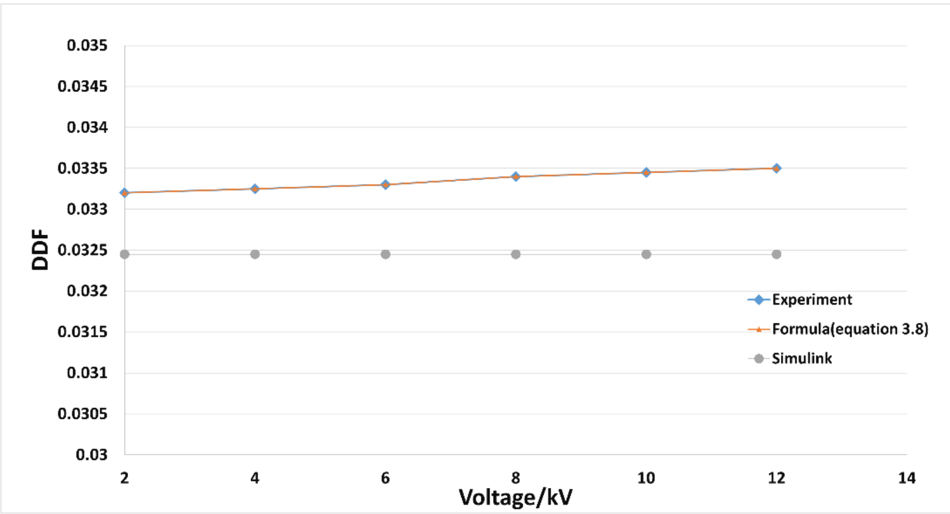

Fig. 4.9 DDF vs applied voltage level (S-1 test object, pure-sine wave)

Distorted excitation: Figure 4.10 plots results for the S-1 test object under distorted excitation voltage at 10kV RMS total with different percentages of the third harmonic from 1% to 10%. Again, the results obtained from the experiment, Simulink, and formula are compared. All three traces follow the same trend, i.e., the DDF value decreases with the increase in the harmonic percentage level. The higher the harmonic content, the higher the rate of change in the DDF value. The simulation (grey) trace closely follows the formula (orange) trace. On the other hand, the experimental results are slightly higher, but the difference is less than 2%.

Other factors could also contribute to the difference between the results. Measurement inaccuracies can be due to the quantization error associated with the limited vertical resolution (8-bit) of the DSO used in the experiment. The number of sample points in the experiment (200 per AC cycle) is less than that in Simulink (2000 per period).

Further testing with the 5th harmonic shows the same trend as compared to the case discussed above. The DDF values are comparatively lower.

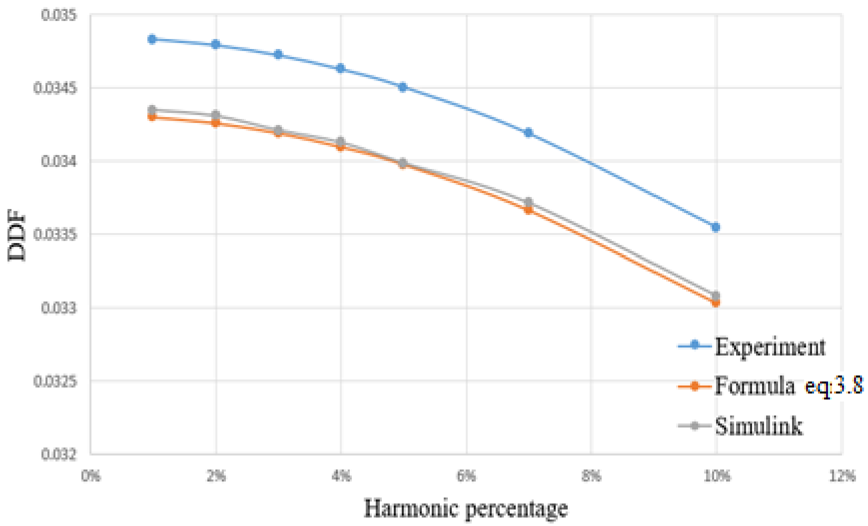

Fig. 4.10 DDF vs harmonic percentage (S-1 test object, 3rd harmonic, 10kV)

Table 4.2 provides the DDF values for test object S-1 with multiple harmonics in the excitation, using a voltage waveform comprising 7% of the 3rd harmonic plus 10% of the 5th harmonic and 8% of the 7th harmonic. The percentage difference between the experiment and formula calculations is around 1%. Table 4.2 shows the DDF values under different test voltages.

Table 4.2 Reference test object DDF values

Applied Voltage	Experiment	Formula
8kV RMS	0.02689	0.02709
10kV RMS	0.02720	0.02750

Phase shift: Generally, there would be some phase shifts between the harmonic components of the distorted voltage in real power grids. Therefore, it is of interest to investigate whether the phase difference between the fundamental component and the harmonics has any influence on the DDF values. The experiment was conducted for the case of 5% of the 5th harmonic. The results are shown in Figure 4.11 which confirms the DDF is not influenced by the phase angle.

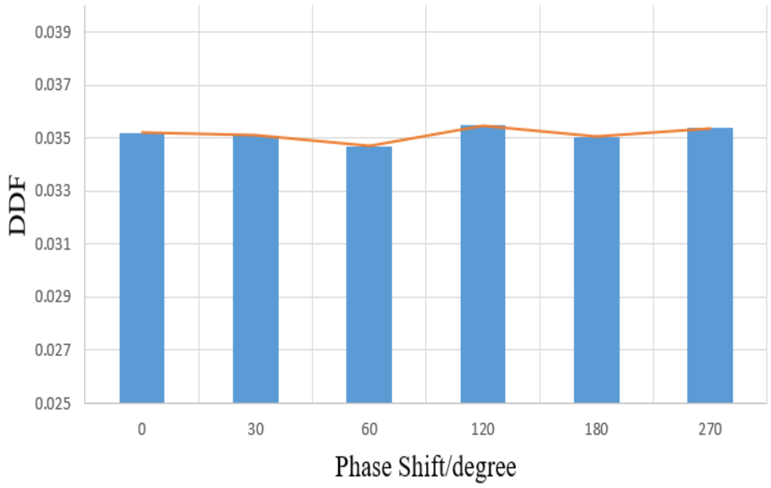

Fig. 4.11 DDF vs phase shift (S-1 test object, 5% 5th harmonic at 10kV)

To conclude, adding harmonics will result in a decrease in the measured values of the DDF as reflected in Equation 3.12. Moreover, the phase shift of the harmonic has no influence on the DDF values. The experiment is repeated several times to check for consistency. Although there are slight variations, all the tests give results that are similar in trends.

4.11 Chapter conclusion

The chapter provides an experimental study of the DDF measurement under sinusoidal and non-sinusoidal voltage excitations with a fundamental frequency of 50Hz. The test objects were constructed using a parallel resistor/capacitor combination of known values to imitate a dielectric. From the measured data, the DDF is calculated based on the mathematical expression developed in Chapter 3 and the Appendix. Validation was demonstrated through theory (mathematical derivation) and computer simulation, based on a linear circuit of R and C to model the dielectric. Validation was also attempted through laboratory experiments with a physical test object equivalent to the model using real RC components. The experimental results (Figs. 4.9, 4.10) show very close agreement with the theoretical/simulation predictions; the error is probably due mostly to the tolerance and non-ideal circuit components, particularly the inherent dielectric loss from the capacitor itself. It is shown that given a fixed RMS voltage, the dielectric dissipation will decrease with increasing harmonic content in terms of the total harmonic distortion, the number of harmonics and the harmonic order. The simulations and experimental trends are in alignment. This provides a practical solution for the measurement of the DDF.

Some of the works described in this chapter have been published in:

Pratic A Muntakim, Shubin Zhang, Junyang Zhang, B.T. Phung," Insulation Assessment Based on Dielectric Dissipation Factor Measurement under Non-sinusoidal Excitation"*, 2021 IEEE 5th International Conference on Condition Assessment Techniques in Electrical Systems (CATCON),* Kerala, India, 3rd -5th December 2021.

Chapter 5

DDF Measurement of Real HV Components

5.1 Background

No insulation material is perfect. With time the insulation in high voltage equipment and components will gradually deteriorate. Traditionally, the dielectric response based on the dielectric dissipation factor at the power frequency (50/60Hz) is an important parameter for the insulation assessment [16]. Knowledge of the DDF and accurate diagnostic interpretation of its measurement is valuable for equipment maintenance [118]. With the presence of non-linear loads and devices in the power systems, the AC grid voltage nowadays is no longer a pure sinusoid [119]. If the applied voltage contains multiple harmonics, the DDF measurement will be affected [78]. Hence, the DDF measurement of high-voltage equipment under non-sinusoidal excitation is an area needing more research [50].

Following the previous chapter which reports the laboratory experiments on the reference test objects of known RC values, this chapter reports the implementation of the dielectric dissipation factor measurement for some real high voltage components under the application of distorted excitation voltage.

5.2 Measurement implementation

After the development of a mathematical and theoretical model of the dielectric dissipation factor with a reference test object, the question was whether a practical measurement process can be implemented for a real test object. Finding out the answer to this question is the motivation behind this research. The dielectric structure is more complex than a simplified parallel *RC* structure. Keeping the losses and complexity of the dielectric in perspective, the simplified circuit model is further extended to account for those losses and a mathematical formula is derived expressing the impact of harmonics on the DDF measurement. A similar laboratory setup is developed for testing current transformers (CTs) under distorted excitation voltage. The theoretical and experimental results are compared with computer simulations using MATLAB Simulink.

5.3 Theoretical modelling

For practical insulation systems, the Debye model of a lossy dielectric as shown in Figure 2.9 is widely used. To simplify, one may assume that only one polarisation mechanism dominates in the frequency range of interest. Figure 5.1 shows a Debye model with only one branch, R_S in series with C_S, representing the polarisation loss along with the basic insulation parameters of R_0 (bulk resistance representing the conduction loss) and C_0 (geometric capacitance). One can convert the polarisation branch R_S in series with C_S into an equivalent of R_P in parallel with C_P as shown in Figure 5.2.

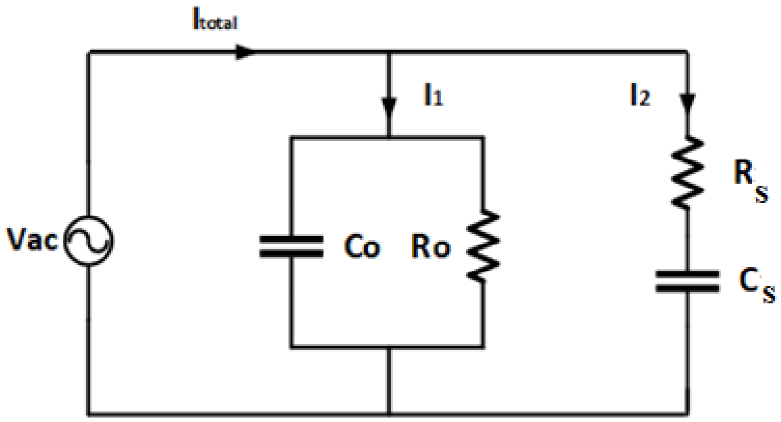

Fig 5.1 Simplified Debye model with one polarisation branch

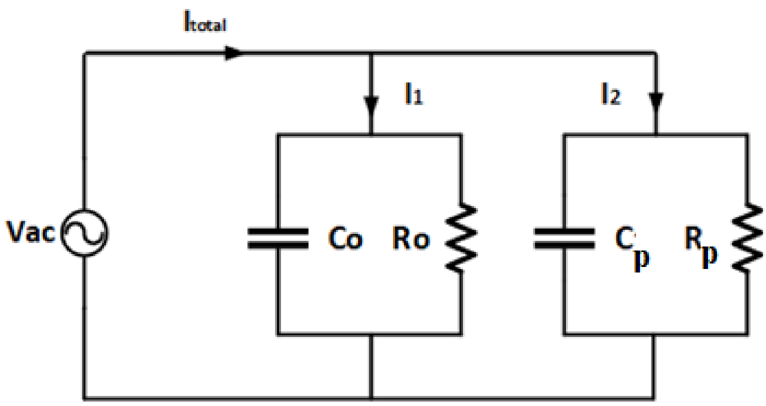

Fig 5.2 Equivalent polarisation branch as a parallel RC

Further, one can combine R_o with R_p as one equivalent resistor R_{eq}, and C_o with C_p as one equivalent capacitance C_{eq}. Thus, the circuit in Figure 5.2 can be simplified as resistor R_{eq} in parallel with capacitor C_{eq}. The equivalent resistance R_{eq} can be considered as the summation of all the real power losses including the bulk insulation conduction losses along with the losses due to polarization.

As discussed in Section 2.6, the dielectric dissipation factor can be defined as the ratio between the active power and the reactive power, i.e.,

$$DDF = \frac{P}{Q} \qquad (5.1).$$

In the case of a pure sinusoidal excitation, Appendix A shows that the DDF given by Equation 5.1 is the same as the tangent of the loss angle between the total current phasor and the capacitor current phasor (Equation 2.12)

$$DDF = \tan\delta = \frac{I_{R_{eq}}}{I_{C_{eq}}} = \frac{1}{\omega R_{eq} C_{eq}} \qquad (5.2).$$

In the presence of harmonics, the phasor approach of DDF modelling becomes ambiguous because of the additional harmonic voltage and current phasors rotating at different angular velocities. When multiple harmonics are considered in the system, one has to revert back to Equation 5.1.

The idea is to determine the dielectric dissipation factor when the distorted excitation is applied. The assumption is that the instantaneous voltage $v(t)$ across the test object and the corresponding instantaneous current $i(t)$ flowing through the test object can be measured. Also, another assumption is that the equivalent capacitance C_{eq} can be measured separately, and its value changes very little over the range of harmonic frequencies considered.

The mathematical development to determine the DDF based on the ratio between the active power and the reactive power is detailed in Appendix A, only the salient points are presented here. The RMS value of the current $i(t)$ is [114]:

$$I_{RMS}^2 = \frac{1}{T}\int_o^T i^2(t)\,dt \qquad (5.3).$$

Here, T is the time period of integration based on the fundamental frequency. The RMS voltage can be expressed in terms of the total harmonic distortion and the fundamental voltage magnitude:

$$V_{RMS}^2 = \frac{V_1^2}{2}\left(1 + THD_h^2\right) \tag{5.4}$$

The apparent power (S) is the product of the voltage and current:

$$S = V_{RMS} \cdot I_{RMS} \tag{5.5}$$

The current through the capacitor C_{eq} is obtained by differentiating the voltage waveform as given in Equation 5.6. It then can be utilized to extract the resistor current from the total current waveform as given in Equation 5.7. Next, the active power can be found as given by Equation 5.8:

$$i_{C_{eq}}(t) = C_{eq}\frac{dv(t)}{dt} \tag{5.6}$$

$$i_{R_{eq}}(t) = i(t) - i_{C_{eq}}(t) \tag{5.7}$$

$$P = \frac{1}{T}\int v(t)\, i_{R_{eq}}(t)dt \tag{5.8}$$

Here, $i_{R_{eq}}(t)$ and $i_{C_{eq}}(t)$ is the time-dependent lossy current and capacitive current. The reactive power is given in Equation 5.9:

$$Q = \sqrt{S^2 - P^2} \tag{5.9}$$

Finally, combining all the equations above, the DDF can be expressed as:

$$DDF_h = k \times \frac{1}{\omega R_{eq} C_{eq}} \tag{5.10}$$

where *k* is defined as the distortion factor or correction factor:

$$k = \sqrt{\frac{1 + THD_h^2}{1 + \sum_{i=2}^{n}\left(i\ell_i\right)^2}} \tag{5.11}$$

It can be seen from Equation 5.11 that $0<k\leq 1$. Thus, the DDF value under distortion is reduced as compared to the case of a pure sinusoid. With increasing harmonic distortion THD_h, the distortion factor k will get smaller and so is the DDF value.

In practice, the insulation system of high-voltage equipment is much more complex than a simplified parallel RC model. The presence of an additional RC branch is an improvement. However, in reality, the parallel branching model is only an approximation. The model can be further modified and needs further extension with multiple branches to account for different polarisation mechanisms occurring in the insulation. Provided the total equivalent capacitance is known, the DDF under non-sinusoidal excitation voltage can be determined by working out the active power P and reactive power Q.

It should be emphasised that the above-mentioned modifications on the model improve the approximation but still imperfect. They do not take into account other effects such as ageing condition, geometry and moisture content. Insulation parameters such as resistivity and capacitance are sensitive to these factors.

5.4 Experimental setup

The experimental setup consists of two separate parts. For the measurement of the DDF, exactly the same setup as used in Chapter 4 is adopted. The only change is the test objects, so an additional part is to measure the dielectric parameters of these real HV components. These parameters are obtained using the Omicron DIRANA (Dielectric Response Analyser). The experiment was conducted in the laboratory under ambient conditions of temperature, humidity, and pressure. The measurement setup is shown in Figure 5.3.

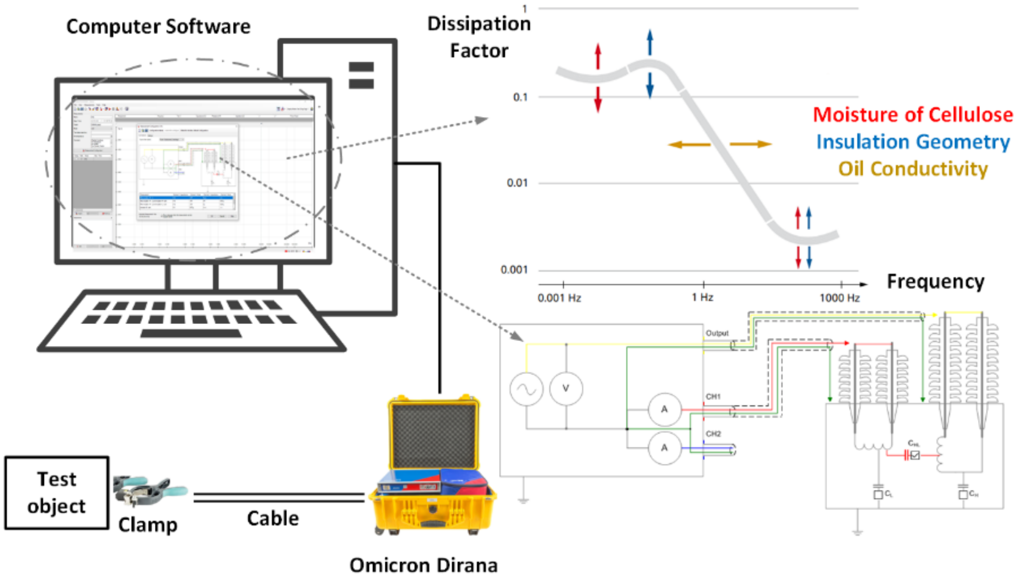

Fig. 5.3 Omicron DIRANA measurement setup

The computer interface provides support for controlling and operating the DIRANA in the PDC (polarization depolarization current) mode or FDS (frequency domain spectroscopy) mode. The DC bulk resistance R_o can be obtained by running the Dirana in the PDC mode. The clamps are connected to the test object, and a DC voltage of 200V is applied. Then the conduction current can be obtained from the difference between the polarisation current and the depolarisation current when reaching their steady state, i.e., stabilized after a long charging and discharging time [53].

In the FDS mode, the equivalent resistance R_{eq} and capacitance C_{eq} of the test object can be obtained over a frequency range 1Hz – 1kHz. Here, the power frequency (50Hz) is selected for measurement and then the geometric capacitance C_o can also be calculated from the complex permittivity obtained in the FDS mode.

Note that although the FDS done by the DIRANA can measure the DDF over different frequencies, it cannot measure the DDF when there are multiple frequency components simultaneously present in the excitation waveform. Thus, the proposed method can be supplementary to the DIRANA, especially in practice when the voltage supply is harmonically polluted. In the context of insulation condition assessment, the applied test voltage level in the proposed method can be at the actual operating voltage of the HV component (but not possible with the DIRANA) so the results obtained are more realistic.

5.5 Test objects

The test objects used in the experiment are three 33kV dry-type current transformers as shown in Figure 5.4. They are of similar design, using epoxy resin for insulation but possibly with different filler materials. For reference, they are designated as CT-1, CT-2 and CT-3. As seen from the photos, the cast resin surface of CT1 appears rougher as compared to CT2 and CT3. This is evident when comparing their dielectric parameters, measured using the DIRANA and shown in Table 5.1.

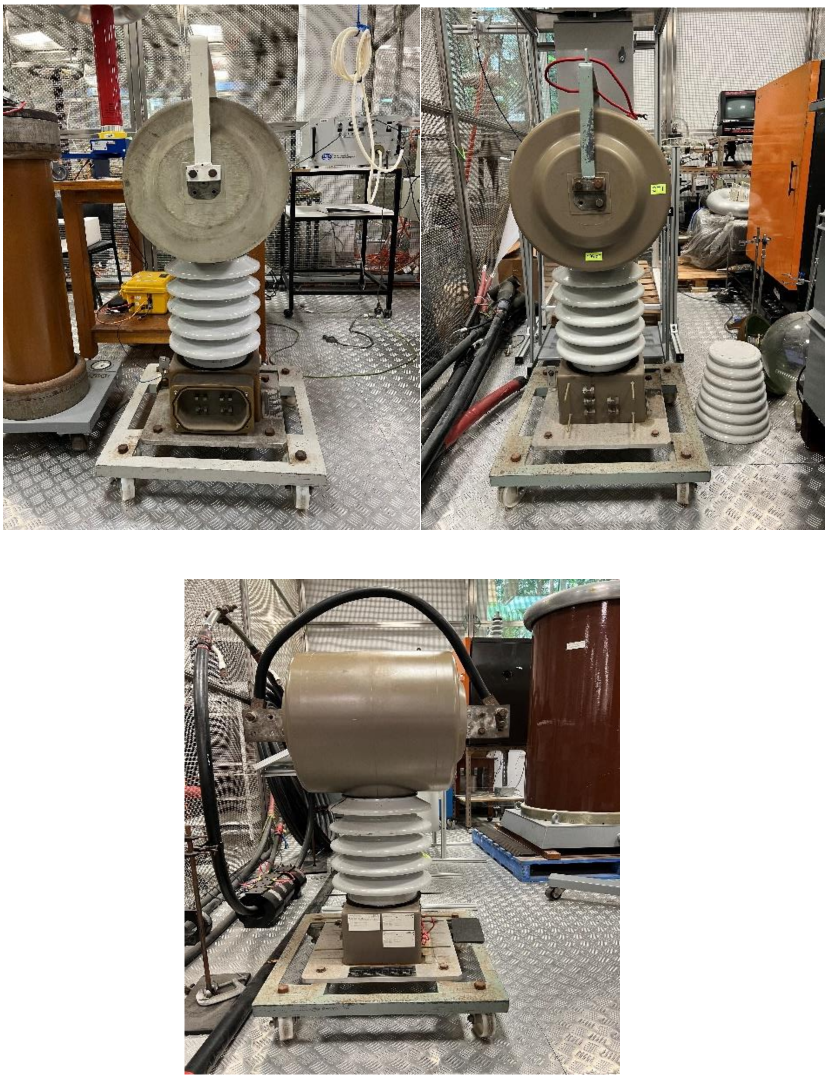

Fig. 5.4 Three different current transformers used as test objects

Table 5.1 Test object insulation parameters

Test object	Geometric Capacitance (pF)	Bulk Resistance (MΩ)
CT-1	901	157.1
CT-2	136	3979
CT-3	130	2196

5.6 Circuit connection

The circuit connection for DDF measurement is shown in Figure 5.5 which is exactly the same as that used in Chapter 4 and the explanations have been provided in Section 4.6. The voltage excitations in the experiments are given in Table 5.2.

To check for partial discharge, measurements were performed on the three CTs using an Omicron Mtronix MPD600 PD measuring system. The inception voltage is well above those test voltage levels considered in Table 5.2 so there should be no real power loss associated with partial discharge in the DDF measurement experiment.

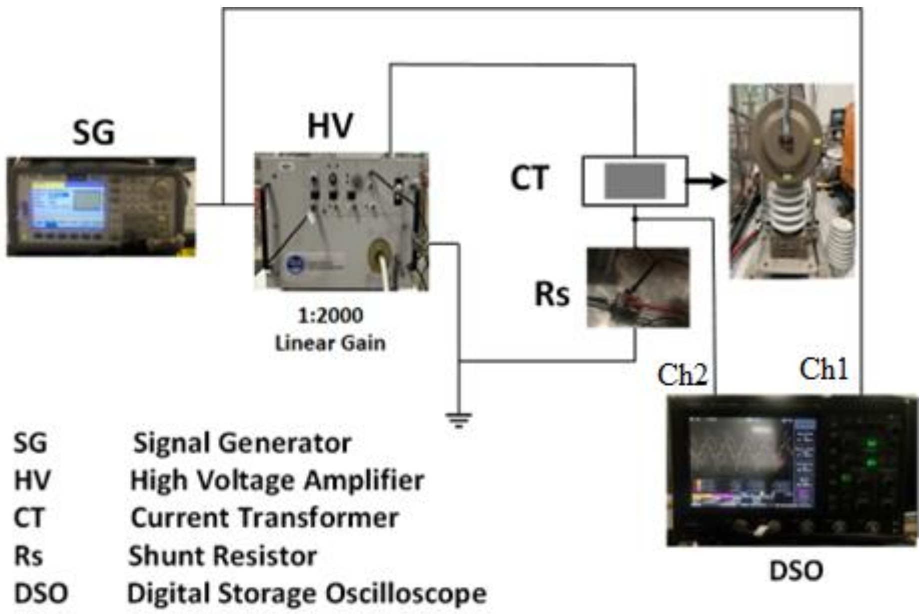

Fig 5.5 DDF measurement circuit diagram

Table 5.2 Voltage excitation parameters

Excitation	Table Column Head		
	Type	***Voltage Level***	***Harmonic Order***
(a)	Pure-Sinusoidal	2kV~12kV	-
(b)	Non-Sinusoidal	2kV~12kV	3^{rd}, 5^{th} (0~10)%
(c)	Harmonic combinations	10kV	5% 5^{th} +(4~10) % 3^{rd}
(d)	Harmonic + phase shift	10kV	5^{th} (0^{o}~360^{o})

The first part of the DDF experiment involves testing the CTs with pure 50Hz sine wave excitation (a). The excitation voltage is raised from 2kV to 12kV with a 2kV increment between steps. The second part of the experiment involves testing the CTs with distorted excitations. As the grid contains mostly the 3^{rd} and 5^{th} order harmonics in the system, testing is done with a single harmonic added (3^{rd} or 5^{th}) and up to 10% THD, i.e., excitation (b). Next, testing is done with both harmonics present in various proportions, i.e., excitation (c). Finally, excitation (d) is applied to investigate the influence of the harmonic phase shift on the DDF.

5.7 Data Processing

The data processing in MATLAB is described using a flow chart in Figure 5.6. The total voltage and current through of the test object can be obtained from the recorded voltage signals in Ch1 and Ch2. The total current through the test object is Ch2/R_s. The total voltage is Ch1 scaled up by the amplifier gain, and then the voltage across the test object can be found by subtracting the voltage across R_s. For obtaining the capacitor current $I_{c_{eq}}$, the voltage signal of Ch1 is differentiated and multiplied by the equivalent capacitance of the test object as per Equation 5.6. Next, the resistor current $I_{R_{eq}}$ can be calculated after subtracting from the total current as per Equation 5.7. The apparent, active and reactive powers can be calculated using Equations 5.5, 5.8, and 5.9 respectively. Finally, the DDF can be calculated as per Equation 5.1.

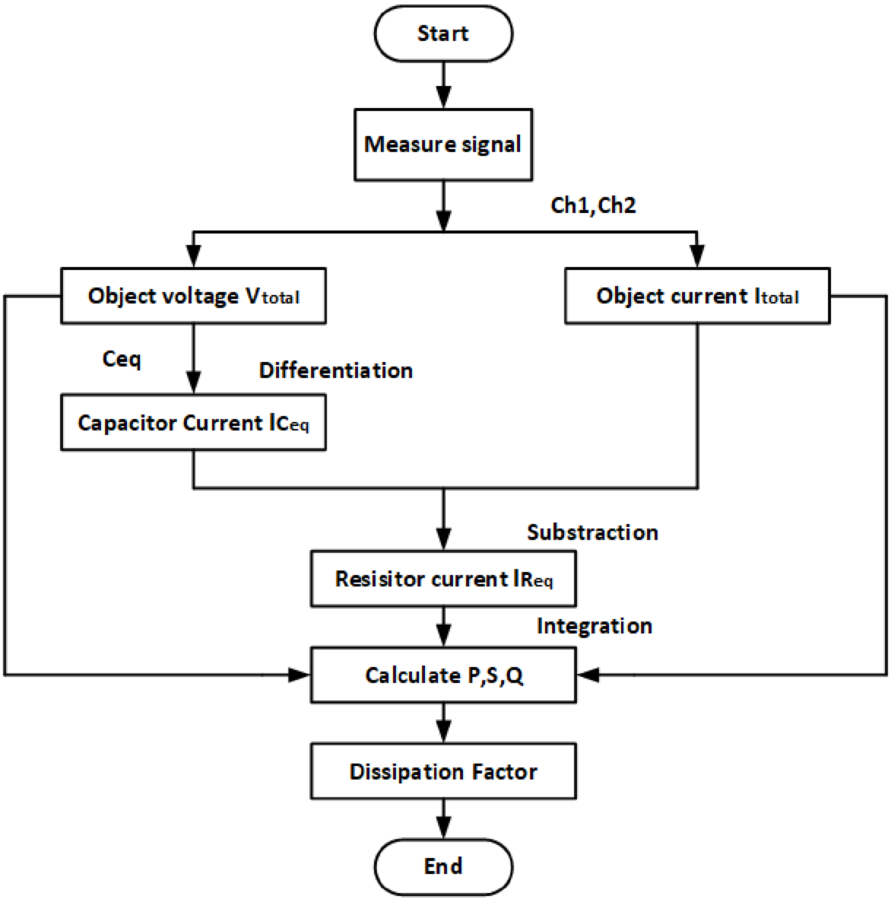

Fig 5.6 Schematic diagram for data processing

Computer simulations are also carried out for comparison. The MATLAB Simulink schematic diagram for the implementation of the DDF measurement circuit is provided in Figure 5.7.

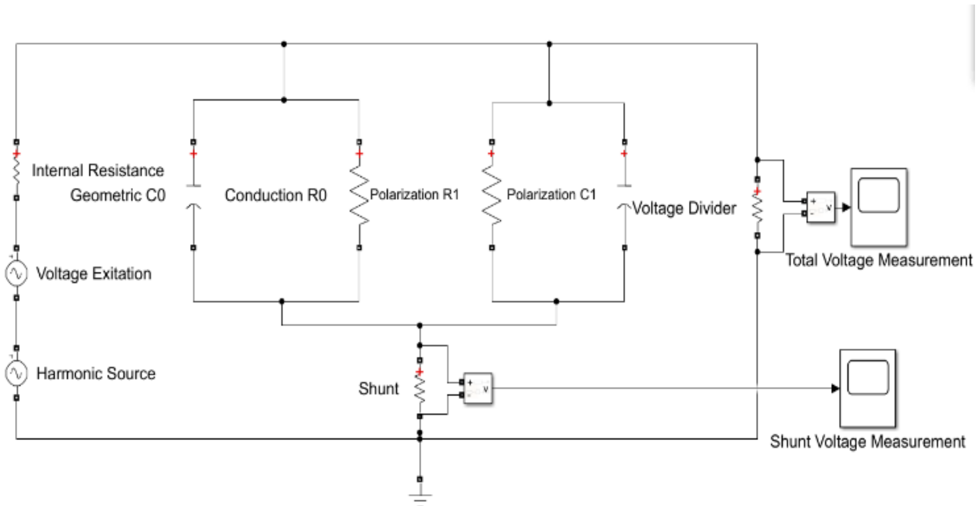

Fig 5.7 DDF measurement simulation diagram

The CT parameters are measured using the DIRANA. Measurements in the FDS mode at 50Hz provide R_{eq}, C_{eq} and also the permittivity from which C_0 can be calculated. The conduction resistance R_0 can be obtained from measurement in the PDC mode. R_1 and C_1 then can be calculated. These values of R and C are added to the simulation model.

The harmonic voltage source is in series with the fundamental voltage source to produce four different types of distorted waveforms as specified in Table 5.2. The simulation results of the two voltage measurement blocks are imported into the MATLAB workspace for the calculation and processing of the test object DDF values. To get precision in measurement, the sampling time for the signal processing is selected to be 1ns and the sampling is in discrete mode.

5.8 Results and Discussion

The testing results for CT-1 for different excitations are presented in Figure 5.8. Note that the applied voltage is kept the same at 10kV RMS for all the cases.

For comparison, the results obtained from the laboratory experiment are plotted together with those calculated using the mathematical formulas along with the numerical simulations using MATLAB Simulink. They are shown in Figure 5.8. The results of the analytical calculation (in blue) match the numerical simulation (in orange) confirming the mathematical derivations. The experimental DDF values (in grey) are lower than the theoretical values.

Figure 5.8(a) shows the changing trend of the DDF in the presence of various levels of the 5th harmonics. In all cases (analytical, numerical, experimental), the DDF value decreases monotonically with the increase in the harmonic percentage in the voltage excitation. There are more variations in the rate of change of the experimental results. The previous chapter describes the decreasing trend of DDF change with the increase in the harmonic level and it is also observed that the variation in the rate of change of the experimental result closely follows the analytical calculation. This implies that the polarisation characteristics in real high voltage components are more complex than expected. The assumption that the equivalent capacitance does not change much with frequency may contribute to discrepancies in the experimental results.

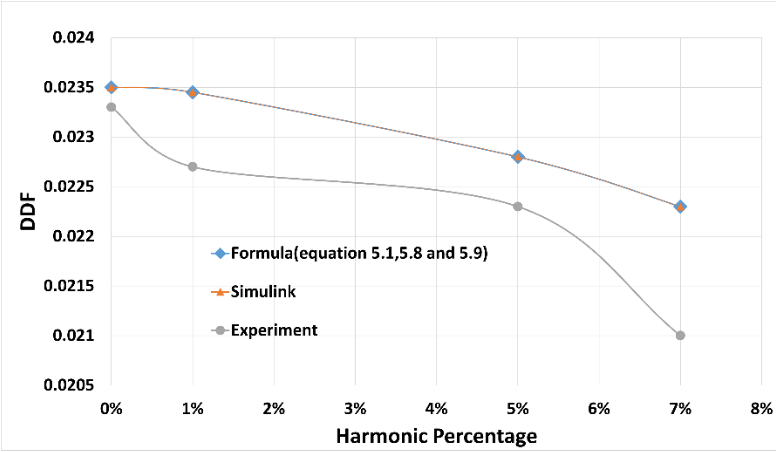

(a)

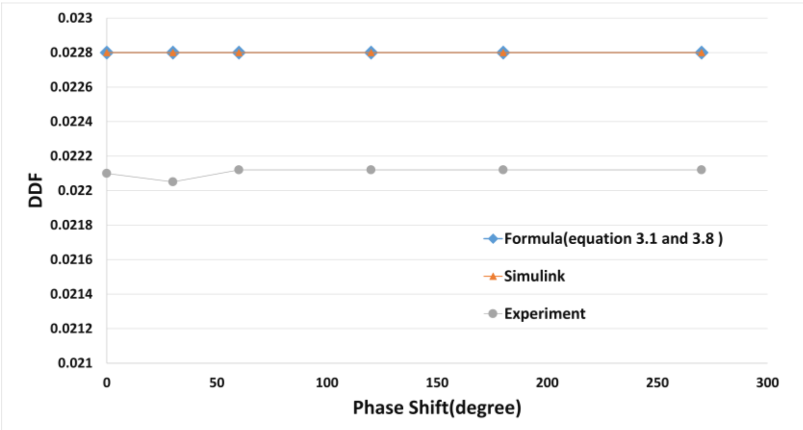

(b)

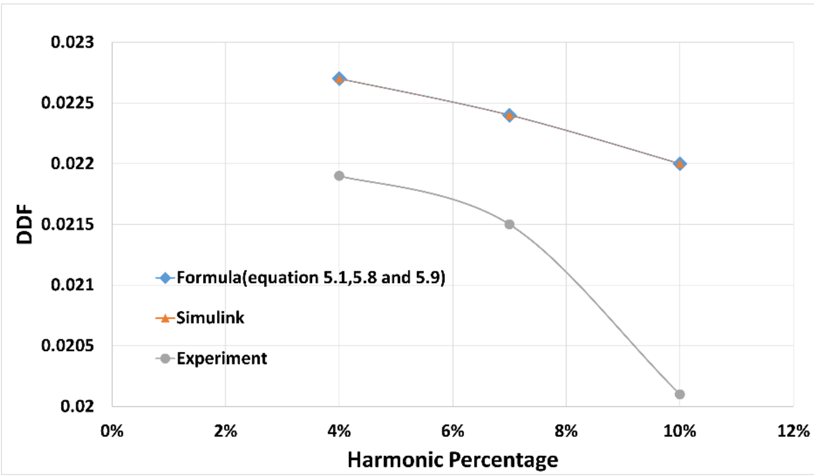

(c)

Fig 5.8 DDF value vs (a) 5^{th} harmonics percentage; (b) 5% 5^{th} harmonic with phase shift in degree; (c) Combined harmonics 5% of 5^{th} + (4~10) % of 3^{rd} [21]

Figure 5.8(b) shows the variation of the DDF in the presence of 5% of the 5th harmonic with respect to the phase shift (between the fundamental and the harmonic components). The DDF value remains almost unchanged irrespective of the phase shift.

Figure 5.8(c) shows the variation of the DDF in the presence of a fixed 5% of the 5th harmonic and a varying amount of the 3rd harmonic from 4% to 10%. The general trend is similar to that in Figure 5.8(a), i.e., the DDF values decrease with the increasing harmonic percentage in a monotonic pattern. Again, the Simulink and the mathematical formula results are aligned. The percentage difference with the experimental results increases with increasing harmonic percentage, from around 3% to 9%.

Figures 5.9 plot the DDF results versus the harmonic percentage for CT-3 under different distorted excitations: having the third harmonic only, (b) having the fifth harmonic only, and (c) having both harmonics with the same percentage. And the comparison is made between the experiment and the theoretical DDF results. There are no consistent patterns, the experimental results fluctuate with different distorted excitations. The difference exceeds 25% for some points, much larger as compared to CT-1 results. Some curve fitting was also applied to smooth out the variation but for the 3 excitations tested, only one shows a very slight reduction in the DDF value at a high harmonic percentage. Like CT-3, the trend of the experimental results for CT-2 is also inconclusive, showing large variations.

On reflection, it is speculated that possible errors in the current measurement sensitivity caused the problem. The measured current amplitude is in the order of mA or less. Comparatively, the measured current for the case of CT-2 and CT-3 is much smaller than that of CT-1 by an order of magnitude. The DSO has only an 8-bit vertical resolution and the vertical gain setting was kept the same in all measurements. The result is a better accuracy for CT-1 measurement at the expense of CT-2 and CT-3.

The Omicron DIRANA was used in the FDS mode to measure the DDF at individual frequencies. For all 3 CTs, the DDF decreases monotonously over the frequency range of interest, i.e., fundamental to the seventh harmonic. This tends to support, at least for distorted excitations involving harmonics in this frequency range, the argument put forward in this research that for the same total RMS voltage, the DDF decreases with increasing distortion.

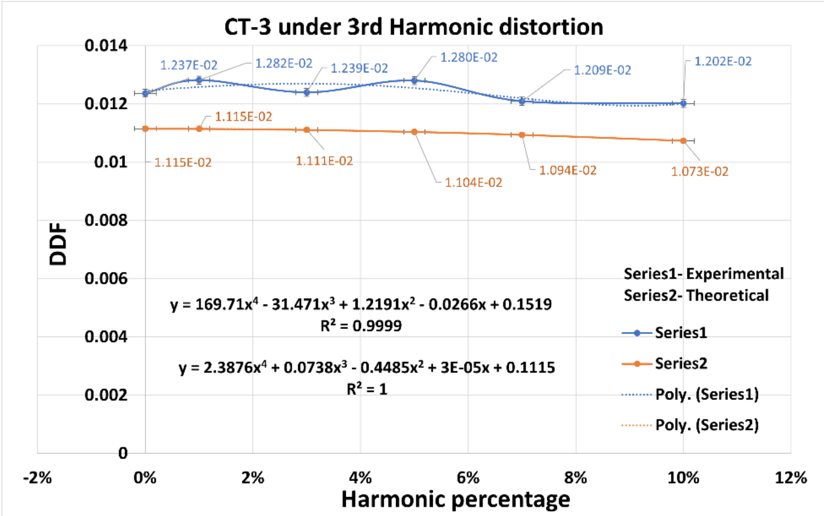

(a)

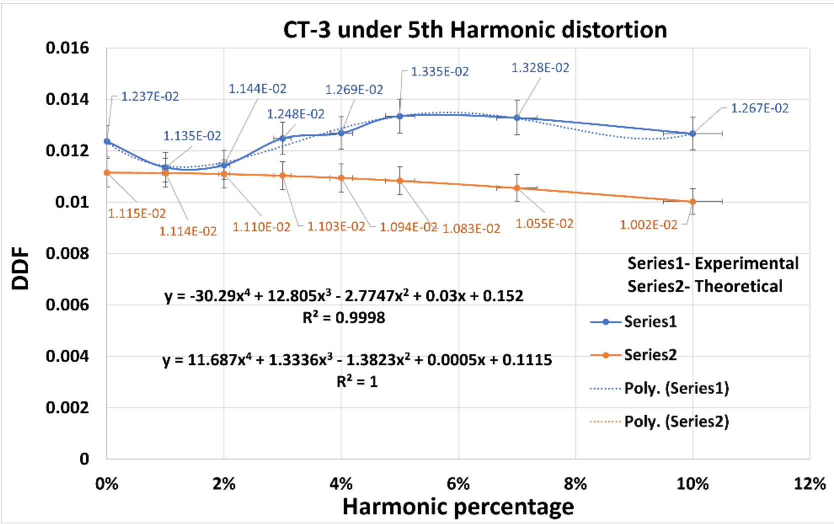

(b)

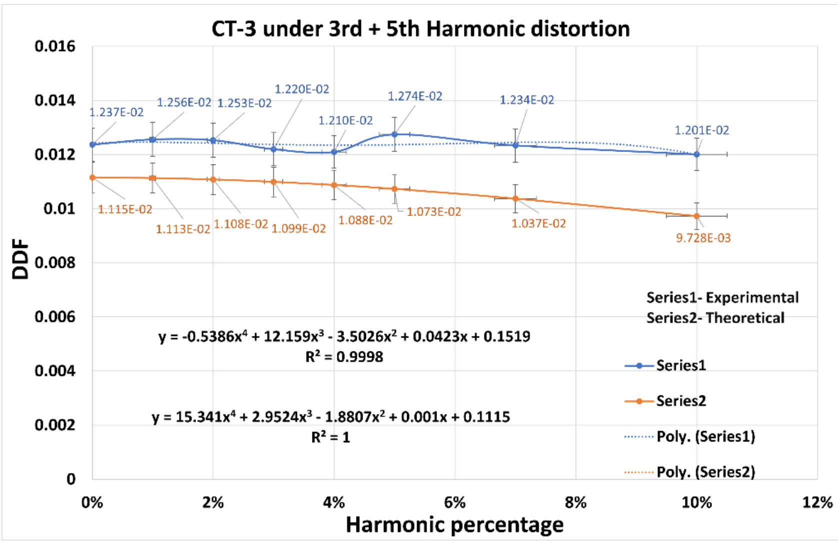

(c)

Fig 5.9 Current transformer 3 under different distorted excitations

5.9 Chapter summary

The work in this chapter attempts to validate the hypothesis by testing dielectrics of components used in real HV power networks, namely three 33kV resin-impregnated current transformers of the same design but with different insulation fillers. Here, a slightly more complex model (Debye model with one polarisation branch) was employed. It is still a linear circuit of RC components, but the conduction loss and the polarisation loss are separately represented in the model. Overall, the experimental results seem inconclusive. For CT-1, the trends follow the prediction, i.e., the DDF value decreases with increasing harmonic distortion. The largest difference between the experimental result and the prediction is within 10%. However, for the other two CTs, there are no clear trends. The difference exceeds 25% for some points. The results in Fig. 5.8 show similar trending between the experimental and analytical/simulation results but deviate from that observed when tested using RC components. The discrepancy may be due to several factors. Firstly, it was assumed that there is only one dominant polarisation mechanism (others are negligible and so can be ignored). A more accurate model calls for multiple polarisation branches. Secondly, modelling the dielectric as a linear RC circuit may be inappropriate for this particular case, i.e., the dielectric is non-linear.

Some of the works described in this chapter have been published in:

Pratic A Muntakim, Junyang Zhang, Shubin Zhang, B.T. Phung," Dielectric Dissipation Factor Measurement of Power Equipment under Distorted Excitation Voltage*", 2021 International Conference on Smart-Green Technology in Electrical and Information Systems (ICSGTEIS),* Bali, Indonesia, 28th -30th October 2021

Chapter 6
Conclusions

6.1 Conclusions

High voltage power system equipment is one of the most essential components of the electricity supply infrastructure. Thus, to ensure supply reliability, regular condition monitoring of the equipment insulation is needed. To this end, the dielectric response based on DDF measurement at the power frequency is a diagnostic indicator for assessing the health of the insulation. The DDF value reflects the dielectric loss in the insulation.

It is established that the supply voltage in the grid is not purely sinusoidal but often distorted with multiple harmonics components. This poses a challenge to the measurement of the DDF, traditionally based on a pure sinusoidal excitation voltage at the standard power frequency (50/60Hz). The existing commercial DDF measuring systems operate on this basis - from the classic bridge-based configuration to the modern approach of measuring the phase angle δ between the measuring current and the reference capacitive current.

In the presence of multiple harmonics, the impedance of the bridge elements changes with frequency. Balancing the bridge simultaneously for multiple frequencies is not possible. Also, the phase angle δ is no longer unique but changes for each harmonic. Thus, the DDF measurement under distorted excitation will be inaccurate if it is measured based on the traditional process. It is necessary to develop a DDF measurement system that can accommodate a distorted excitation voltage, reflecting the grid supply voltage in practice.

To solve this problem, this research follows the approach of measuring the DDF as the ratio of the real power to the reactive power as per Equation 3.8. This approach is more universal. Under pure sinusoidal excitation, it gives the same answer as the traditional method. For practical applications, the new method involves simultaneous measurement of the voltage across the test object and the current through the test object. From these data, the real and reactive power can be found and the DDF can be calculated. The process is described in Section 3.2.

Through this research, it is found that the DDF under distorted excitation is reduced as compared to the case of no distortion by the correction factor k where $0 < k \leq 1$. as per Equation 3.12. This is the key finding of this research which is supported by mathematical derivations based on the lumped parallel RC model of the dielectric, computer simulations and experimental measurements.

As per Equation 3.12, the correction factor k is a function of the harmonic components: their harmonic order and relative amplitude with respect to the fundamental component. On the other hand, the total harmonic distortion (THD) as per Equation 3.11 is often used as a parameter to quantify the overall distortion. The larger the THD, the smaller k will become and the DDF will reduce accordingly by the factor k. The relationship is non-linear, the rate of reduction in the DDF value increases with the THD and the harmonic order. Also from Equation 3.12, another conclusion is that the phase angle of the harmonic components or their phase shift with respect to the reference fundamental component has no influence on the DDF results.

The proposed DDF measurement scheme was implemented for testing in the laboratory. To begin, parallel RC models were constructed from discrete resistors and capacitors of known values to imitate a lossy dielectric. In the experiments, they were used as reference test objects, energised to different excitation voltage waveforms (pure sinusoidal, distorted with different harmonics) and then the measurement results obtained are compared with the theoretical prediction for validation. The findings presented in Chapter 4 confirm the alignment. The trends between the experiment, simulation, and formula are consistent. The discrepancy is within a few percent.

Subsequent experiments involved testing with real high voltage components: three 33kV cast resin current transformers of the same design but different insulation fillers. Overall, the experimental results seem inconclusive. For CT-1, the trends follow the prediction, i.e., the DDF value decreases with increasing harmonic distortion. The largest difference between the experimental result and the prediction is within 10%. However, for the other two CTs, there are no clear trends. The difference exceeds 25% for some points.

6.2 Future research scope

There is scope for this research to be further expanded. Whilst the method to measure the DDF based on the power ratio is universal (applicable for any forms of distorted but periodic voltage waveforms), practical implementation will require improved instrumentation for accurate measurement of the voltage and current.

The dielectric losses under distorted excitation can be further studied for different insulation materials including linear and nonlinear dielectrics.

Different distorted excitation voltages with different harmonic components can be implemented for experimental investigations. For example, renewable energy sources (PV, wind etc) are rapidly entering and penetrating the grid. The distorted voltage conditions imposed by such types of voltages can be implemented to investigate their impacts on the DDF for different HV components, e.g., HV cable insulation. The variable speed drives for motor control employ fast rise time high-frequency pulse width modulation (PWM) voltage, the switching frequency is typically around a few kHz. The insulation of the motor windings as well as the connecting cable is subjected to such a voltage waveform which is severely distorted. This presents another interesting area for DDF investigation.

The test voltage used in this research had been kept well below the partial discharge inception voltage of the test objects. This is to avoid the contribution of the PD loss to the measured dielectric loss. The focus of this research was on the conduction loss and the polarization loss. It is anticipated that the DDF will increase in the presence of PDs due to the real power loss incurred during the breakdown. The effective capacitance would change during the PD event as well so the overall effect on the DDF is complicated under the presence of distorted excitation. This is an interesting challenge for future investigation.

Appendix A

DDF as a ratio of P and Q

Consider a voltage source applied to a parallel *RC* network (assuming the resistance and capacitance are fixed) as shown in Figure A.1. This *RC* combination represents a simple model for a lossy dielectric as discussed in Section 2.6.1. In the following, the DDF will be derived from the ratio of the real power and the reactive power.

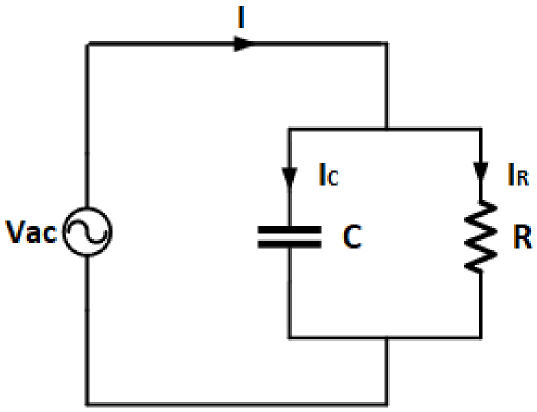

Fig A.1 Distorted voltage applied to a parallel RC branch

A periodic, non-sinusoidal function that is integrable can be resolved into a trigonometric series known as the Fourier series. Hence a periodic, non-sinusoidal voltage source of instantaneous value *v(t)* can be written as:

$$v(t) = V_{d.c.} + V_1 \sin(\omega t + \alpha_1) + V_2 \sin(2\omega t + \alpha_2) + \ldots + V_n \sin(n\omega t + \alpha_n) \quad \text{(A.1).}$$

Here, $V_{d.c}$ denotes the DC voltage component. For the *n*-th harmonic voltage component, its amplitude is V_n, and the corresponding RMS value is $V_n/\sqrt{2}$, and α_n denotes the phase angle. ω denotes the angular frequency. For AC only, the DC component can be discarded and so:

$$v(t) = V_1 \sin(\omega t + \alpha_1) + \ldots + V_i \sin(i\omega t + \alpha_i) + \ldots + V_n \sin(n\omega t + \alpha_n)$$

$$= V_1\left[\sin(\omega t+\alpha_1)+\ldots+\ell_i\sin(i\omega t+\alpha_i)+\ldots+\ell_n\sin(n\omega t+\alpha_n)\right] \quad \text{(A.2),}$$

where, $\ell_i = V_i/V_1$, denotes the amplitude of the *i*-th harmonic as a fraction of the fundamental component. Here, all the sine functions are orthogonal functions, and therefore, the RMS of the total voltage can be expressed as [112]:

$$V_{RMS} = \sqrt{V_{1_{RMS}}^2 + V_{2_{RMS}}^2 + \ldots + V_{n_{RMS}}^2} \quad \text{(A.3),}$$

$$V_{RMS}^2 = \left(\frac{V_1}{\sqrt{2}}\right)^2\left(1+\ell_2^2+\ell_3^2+\ldots+\ell_n^2\right) \quad \text{(A.4).}$$

The corresponding response current in the system can be written as:

$$i(t) = I_1\sin(\omega t+\alpha_1+\psi_1)+I_2\sin(2\omega t+\alpha_2+\psi_2)+\ldots+I_n\sin(n\omega t+\alpha_n+\psi_n) \quad \text{(A.5).}$$

Here, ψ is added phase shift in the current, and I_n is the n-th harmonic amplitude. Similarly, the RMS current can be written as:

$$I_{RMS} = \sqrt{I_{1_{RMS}}^2 + I_{2_{RMS}}^2 + \ldots + I_{n_{RMS}}^2} \quad \text{(A.6).}$$

If *Z* represents the impedance of the parallel *RC*, and *Y* denotes its admittance:

$$Y = \frac{1}{Z} \;\Rightarrow\; |Y_1| = \sqrt{\left(\frac{1}{R}\right)^2 + (\omega C)^2} \;;\; |Y_i| = \sqrt{\left(\frac{1}{R}\right)^2 + (i\omega C)^2} \quad \text{(A.7).}$$

Similar to Equation A.4, the RMS current can be written as:

$$I_{RMS}^2 = \left(\frac{V_1}{\sqrt{2}}\right)^2\left(Y_1^2+\ell_2^2Y_2^2+\ell_3^2Y_3^2+\ell_4^2Y_4^2+\ldots\right) \quad \text{(A.8).}$$

The real power dissipated P is:

$$P = \frac{V_{RMS}^2}{R} \quad \text{(A.9),}$$

$$P = \left(\frac{1}{R}\right)\left(\frac{V_1}{\sqrt{2}}\right)^2\left(1+\ell_2^2+\ell_3^2+\ldots+\ell_n^2\right) \quad \text{(A.10).}$$

The Volt-Amperes or apparent power *S* can be written as [126]:

$$S^2 = V_{RMS}^2 I_{RMS}^2$$

$$= \left(\frac{V_1}{\sqrt{2}}\right)^2 \left(1+\ell_2^2+\ell_3^2+\ldots+\ell_n^2\right)\times\left(\frac{V_1}{\sqrt{2}}\right)^2 \left(Y_1^2+\ell_2^2Y_2^2+\ell_3^2Y_3^2+\ldots+\ell_n^2Y_n^2\right)$$

$$= \left(\left(\frac{V_1}{\sqrt{2}}\right)^2\right)^2 \left(1+\ell_2^2+\ell_3^2+\ldots+\ell_n^2\right)\times\left(Y_1^2+\ell_2^2Y_2^2+\ell_3^2Y_3^2+\ldots+\ell_n^2Y_n^2\right) \quad \text{(A.11).}$$

And the reactive power Q can be written as:

$$Q = \sqrt{S^2 - P^2}$$

$$= \left(\frac{V_1}{\sqrt{2}}\right)^2 \sqrt{B}\sqrt{C-D}$$

$$= \left(\frac{V_1}{\sqrt{2}}\right)^2 \sqrt{B}\sqrt{E} \quad \text{(A.12),}$$

where,

$$B = 1+\ell_2^2+\ell_3^2+\ldots+\ell_n^2 \quad \text{(A.13),}$$

$$C = Y_1^2+\ell_2^2Y_2^2+\ell_3^2Y_3^2+\ldots+\ell_n^2Y_n^2 \quad \text{(A.14),}$$

$$D = \left(\frac{1}{R}\right)^2 \left(1+\ell_2^2+\ell_3^2+\ldots+\ell_n^2\right) \quad \text{(A.15),}$$

$$E = \left(\omega C\right)^2 + \ell_2^2\left(2\omega C\right)^2 + \ell_3^2\left(3\omega C\right)^2 + \ldots + \ell_n^2\left(n\omega C\right)^2 \quad \text{(A.16).}$$

A more general approach for determining the dielectric dissipation factor is based on the ratio of the real power *P* (dielectric loss) and the reactive power *Q*. It can be defined as [112]:

$$DDF = \frac{\text{Real Power}}{\text{Reactive Power}} = \frac{P}{Q} \quad \text{(A.17).}$$

From Equations A.10 - A.17, we can write:

$$DDF = \frac{\left(\frac{1}{R}\right)\left(\frac{V_1}{\sqrt{2}}\right)^2 B}{\left(\frac{V_1}{\sqrt{2}}\right)^2 \sqrt{B}\sqrt{E}} \quad \text{(A.18).}$$

After simplifying we get,

$$DDF = \frac{1}{\omega RC}\frac{\sqrt{1+\ell_2^2+\ell_3^2+\ldots+\ell_n^2}}{\sqrt{1+(2\ell_2)^2+(3\ell_3)^2+\ldots+(n\ell_n)^2}} \quad \text{(A.19),}$$

$$DDF = k\times\frac{1}{\omega RC} \quad \text{(A.20),}$$

where k denotes the correction factor:

$$k = \frac{\sqrt{1+\ell_2^2+\ell_3^2+\ldots+\ell_n^2}}{\sqrt{1+(2\ell_2)^2+(3\ell_3)^2+\ldots+(n\ell_n)^2}} \quad \text{(A.21).}$$

If THD_h denotes the total harmonic distortion and is defined as:

$$THD_h = \sqrt{\sum_{i=2}^{n}(\ell_i)^2} \quad \text{(A.22),}$$

then Equation A.21 can be written as

$$k = \sqrt{\frac{1+THD_h^2}{1+\sum_{i=2}^{n}(i\ell_i)^2}} \quad \text{(A.23).}$$

It can be seen that when there are no higher-order harmonics, i.e., only the fundamental component of the voltage and corresponding current present, $k=1$. Thus, the DDF for a pure sinusoidal excitation voltage as given by equation A.20 becomes:

$$DDF = \frac{1}{\omega RC} \quad \text{(A.24).}$$

References

[1] G. W. Massey, "Estimation methods for power system harmonic effects on power distribution transformers," *IEEE Trans. Ind. Appl.*, vol. 30, no. 2, pp. 485–489, 1994.

[2] R. Singh and A. Singh, "Energy loss due to harmonics in residential campus — A case study," in *45th International Universities Power Engineering Conference UPEC2010*, 2010, pp. 1–6.

[3] D. Kumar and F. Zare, "Harmonic Analysis of Grid Connected Power Electronic Systems in Low Voltage Distribution Networks," *IEEE J. Emerg. Sel. Top. Power Electron.*, vol. 4, no. 1, pp. 70–79, 2016, doi: 10.1109/JESTPE.2015.2454537.

[4] M. Florkowski, B. Florkowska, J. Furgał, and P. Zydron, "Impact of high voltage harmonics on interpretation of partial discharge patterns," *IEEE Trans. Dielectr. Electr. Insul.*, vol. 20, no. 6, pp. 2009–2016, 2013.

[5] T. W. Dakin, H. M. Philofsky, and W. C. Divens, "Effect of electric discharges on the breakdown of solid insulation," *Trans. Am. Inst. Electr. Eng. Part I Commun. Electron.*, vol. 73, no. 2, pp. 155–162, 1954.

[6] D. Kumar and F. Zare, "Analysis of harmonic mitigations using hybrid passive filters," in *2014 16th International Power Electronics and Motion Control Conference and Exposition*, 2014, pp. 945–951.

[7] T. D. Kefalas and A. G. Kladas, "Harmonic impact on distribution transformer no-load loss," *IEEE Trans. Ind. Electron.*, vol. 57, no. 1, pp. 193–200, 2009.

[8] R. Singh and A. Singh, "Aging of distribution transformers due to harmonics," in Proceedings of 14th International Conference on Harmonics and Quality of Power-ICHQP 2010, 2010, pp. 1–8.

[9] Y. Shirasaka, H. Murase, S. Okabe, and H. Okubo, "Cross-sectional comparison of insulation degradation mechanisms and lifetime evaluation of power transmission equipment," *IEEE Trans. Dielectr. Electr. Insul.*, vol. 16, no. 2, pp. 560–573, 2009.

[10] P. Caramia, G. Carpinelli, P. Verde, G. Mazzanti, A. Cavallini, and G. C. Montanari, "An approach to life estimation of electrical plant components in the presence of harmonic distortion," in *Ninth International Conference on Harmonics and Quality of Power.*

Proceedings (Cat. No. 00EX441), 2000, vol. 3, pp. 887–892.

[11] A. Cavallini, D. Fabiani, and G. C. Montanari, “Power electronics and electrical insulation systems-part 2: life modeling for insulation design,” *IEEE Electr. Insul. Mag.*, vol. 26, no. 4, pp. 33–39, 2010.

[12] D. Fabiani and G. C. Montanari, “The effect of voltage distortion on ageing acceleration of insulation systems under partial discharge activity,” *IEEE Electr. Insul. Mag.*, vol. 17, no. 3, pp. 24–33, 2001.

[13] B. D. Malpure and K. Baburao, “Failure analysis & diagnostics of power transformer using dielectric dissipation factor,” in *2008 International Conference on Condition Monitoring and Diagnosis*, 2008, pp. 497–501.

[14] S. Morsalin and B. T. Phung, “Modeling of dielectric dissipation factor measurement from very low to power frequency,” in *2018 IEEE 2nd International Conference on Dielectrics (ICD)*, 2018, pp. 1–4.

[15] A. Banik, “Condition assessment of high voltage insulators in different environments with non-sinusoidal excitation,” PhD thesis, Queensland University of Technology, 2020.

[16] A. K. Pradhan, S. Chatterjee, A. Banik, S. Dalai, and B. Chatterjee, “Condition assessment of outdoor porcelain insulator based on dielectric dissipation factor evaluated from non-linear equivalent circuit,” *IET Sci. Meas. Technol.*, vol. 10, no. 8, pp. 866–873, 2016.

[17] D. Zhang *et al.*, “Study on FDS characteristics of oil-immersed paper insulation bushing under non-uniform moisture content,” *IET Sci. Meas. Technol.*, vol. 12, no. 5, pp. 691–697, 2018.

[18] R. Sarathi, K. H. Oza, C. L. G. P. Kumar, and T. Tanaka, “Electrical treeing in XLPE cable insulation under harmonic AC voltages,” *IEEE Trans. Dielectr. Electr. Insul.*, vol. 22, no. 6, pp. 3177–3185, 2015.

[19] S. Morsalin and B. T. Phung, “A comparative study of dielectric dissipation factor measurement under very low and power frequencies,” in *2017 3rd International Conference on Condition Assessment Techniques in Electrical Systems (CATCON)*, 2017, pp. 10–14, doi: 10.1109/CATCON.2017.8280175.

[20] S. Morsalin, B. T. Phung, and A. Cavallini, “Measurement and modeling of partial discharge arising from different cavity geometries at very low frequency,” *IEEE Trans.*

Dielectr. Electr. Insul., vol. 27, no. 4, pp. 1110–1118, 2020.

[21] P. A. Muntakim, J. Zhang, S. Zhang, and B. T. Phung, "Dielectric Dissipation Factor Measurement of Power Equipment under Distorted Excitation Voltage," in *2021 International Conference on Smart-Green Technology in Electrical and Information Systems (ICSGTEIS)*, 2021, pp. 91–95.

[22] M. Abou-Dakka, A. Bulinski, and S. S. Bamji, "On-site diagnostic technique for smart maintenance of power cables," in *2011 IEEE Power and Energy Society General Meeting*, 2011, pp. 1–5, doi: 10.1109/PES.2011.6039394.

[23] W. Hauschild, "Critical review of voltages applied for quality-acceptance and diagnostic field tests on high-voltage and extra-high-voltage cable systems," *IEEE Electrical Insulation Magazine*, vol. 29, no. 2. IEEE, pp. 16–25, 2013, doi: 10.1109/MEI.2013.6457596.

[24] S. Hvidsten, B. Holmgren, L. Adeen, and J. Wetterstrom, "Condition assessment of 12- and 24-kV XLPE cables installed during the 80s. Results from a joint Norwegian/Swedish research project," *IEEE Electr. Insul. Mag.*, vol. 21, no. 6, pp. 17–23, 2005, doi: 10.1109/MEI.2005.1541485.

[25] S. Rengarajan, M. D. Agrawal, and R. S. Nema, "Behavior of High Voltage Miachine Insulation System in the Presence of Thermal and Electrical Stresses," *IEEE Trans. Electr. Insul.*, no. 1, pp. 104–110, 1985.

[26] J. C. Fothergill, S. J. Dodd, L. A. Dissado, T. Liu, and U. H. Nilsson, "The measurement of very low conductivity and dielectric loss in XLPE cables: a possible method to detect degradation due to thermal aging," *IEEE Trans. Dielectr. Electr. Insul.*, vol. 18, no. 5, pp. 1544–1553, 2011.

[27] W. Deng, Z. Zheng, L. Ruan, Y. Shen, Q. Xie, and H. Wang, "Power apparatus insulation diagnosis through partial discharge in a smarter grid," in *2010 IEEE International Symposium on Electrical Insulation*, 2010, pp. 1–4, doi: 10.1109/ELINSL.2010.5549838.

[28] J. Liu, D. Zhang, C. Bin, L. Huang, Y. Gao, and X. Li, "A New method of aging assessment for XLPE cable insulation based on dielectric response," in *2015 IEEE 11th International Conference on the Properties and Applications of Dielectric Materials (ICPADM)*, 2015, pp. 560–563, doi: 10.1109/ICPADM.2015.7295333.

[29] C. Chou and C. Chen, "Measurement and analysis of partial discharge of high and medium voltage power equipment," in *2018 7th International Symposium on Next*

Generation Electronics (ISNE), 2018, pp. 1–4, doi: 10.1109/ISNE.2018.8394749.

[30] L. Yang, J. Chen, J. Gao, H. Zheng, and Y. Li, "Accelerating frequency domain dielectric spectroscopy measurements on insulation of transformers through system identification," *IET Sci. Meas. Technol.*, vol. 12, no. 2, pp. 247–254, 2018, doi: 10.1049/iet-smt.2017.0253.

[31] T. K. Saha, R. Middleton, and A. Thomas, "Understanding frequency & time domain polarisation methods for the insulation condition assessment of power transformers," in *2009 IEEE Power & Energy Society General Meeting*, 2009, pp. 1–8.

[32] X. Yang, S. Nielsen, and G. Ledwich, "Experimental investigations of improved dielectric condition monitoring methods on transformer oil-paper insulation system," in *2014 IEEE 18th International Conference on Dielectric Liquids (ICDL)*, 2014, pp. 1–4, doi: 10.1109/ICDL.2014.6893101.

[33] G. Liang, Y. Jing, Z. Li, X. Liu, and L. Ma, "Modelling of frequency characteristics of the oil-paper compound insulation based on the fractional calculus," *IET Sci. Meas. Technol.*, vol. 11, no. 5, pp. 646–654, 2017.

[34] E. Gockenbach and W. Hauschild, "The selection of the frequency range for high-voltage on-site testing of extruded insulation cable systems," *IEEE Electr. Insul. Mag.*, vol. 16, no. 6, pp. 11–16, 2000.

[35] W. S. Zaengl, "Dielectric spectroscopy in time and frequency domain for HV power equipment. I. Theoretical considerations," *IEEE Electr. Insul. Mag.*, vol. 19, no. 5, pp. 5–19, 2003, doi: 10.1109/MEI.2003.1238713.

[36] H. M. Ryan, *High voltage engineering and testing*, no. 32. Iet, 2001.

[37] S. M. Barr and A. Zee, "Electric dipole moment of the electron and of the neutron," *Phys. Rev. Lett.*, vol. 65, no. 1, p. 21, 1990.

[38] W. S. Zaengl, "Applications of dielectric spectroscopy in time and frequency domain for HV power equipment," *IEEE Electr. Insul. Mag.*, vol. 19, no. 6, pp. 9–22, 2003, doi: 10.1109/MEI.2003.1266348.

[39] Y. Grabovsky and N. Hovsepyan, "On feasibility of extrapolation of the complex electromagnetic permittivity function using Kramer-Kronig relations," *arXiv Prepr. arXiv2009.12441*, 2020.

[40] P. Agarwal, M. E. Orazem, and L. H. Garcia-Rubio, "Application of Measurement Models

to Impedance Spectroscopy: III. Evaluation of Consistency with the Kramers-Kronig Relations," *J. Electrochem. Soc.*, vol. 142, no. 12, p. 4159, 1995.

[41] H. Fröhlich, "Theoretical Aspects of Superconductivity: Crystal Structure and Superconductivity," *Nature*, vol. 168, no. 4268, p. 280, 1951.

[42] S. Morsalin and B. T. Phung, "Modeling of dielectric dissipation factor measurement for XLPE cable based on Davidson-Cole model," *IEEE Trans. Dielectr. Electr. Insul.*, vol. 26, no. 3, pp. 1018–1026, 2019.

[43] S. Morsalin and T. Phung, "Electrical field distribution on the cross-linked polyethylene insulation surface under partial discharge testing," *Polym. Test.*, vol. 82, p. 106311, 2020.

[44] H. V. P. Nguyen, B. T. Phung, and S. Morsalin, "Modelling partial discharges in an insulation material at very low frequency," in *2017 International Conference on High Voltage Engineering and Power Systems (ICHVEPS)*, 2017, pp. 451–454.

[45] C. Pan, G. Chen, J. Tang, and K. Wu, "Numerical modelling of partial discharges in a solid dielectric-bounded cavity: A review," *IEEE Trans. Dielectr. Electr. Insul.*, vol. 26, no. 3, pp. 981–1000, 2019.

[46] A. V Sopilnik and J. C. L. Van Peppen, "Representation of imperfect dielectric materials by an equivalent circuit," *Electron. Lett.*, vol. 16, no. 10, pp. 368–370, 1980.

[47] R. Färber, "Endurance of Polymeric Insulation under Mixed-Frequency Medium-Voltage Stress." ETH Zurich, 2019.

[48] T. Linde and K. Backhaus, "Comparison of Dielectric Loss Measuring Methods on Epoxy Samples under Harmonic Distorted Voltages," in *VDE High Voltage Technology 2020; ETG-Symposium*, 2020, pp. 1–6.

[49] M. D. Ingram, "Conduction and Dielectric Loss Mechanisms in β-Alumina and Glass: A Discussion Based on the Paired Interstitialcy Model," *J. Am. Ceram. Soc.*, vol. 63, no. 5-6, pp. 248–253, 1980.

[50] L. Donzel and J. Schuderer, "Nonlinear resistive electric field control for power electronic modules," *IEEE Trans. Dielectr. Electr. Insul.*, vol. 19, no. 3, pp. 955–959, 2012.

[51] A. Küchler, *High Voltage Engineering: Fundamentals - Technology - Applications*. Springer Berlin Heidelberg, 2017.

[52] J. G. Kirkwood, “On the theory of dielectric polarisation,” *J. Chem. Phys.*, vol. 4, no. 9, pp. 592–601, 1936.

[53] S. Morsalin and B. T. Phung, “Dielectric response study of service-aged XLPE cable based on polarisation and depolarisation current method,” *IEEE Trans. Dielectr. Electr. Insul.*, vol. 27, no. 1, pp. 58–66, 2020.

[54] S. Abbasian and T. Johnson, “RF current mode class-D power amplifiers under periodic and non-periodic switching conditions,” in *2013 IEEE International Symposium on Circuits and Systems (ISCAS)*, 2013, pp. 610–613.

[55] S. S. Kelkar, L. L. Grigsby, and J. Langsner, “An extension of Parseval’s theorem and its use in calculating transient energy in the frequency domain,” *IEEE Trans. Ind. Electron.*, no. 1, pp. 42–45, 1983.

[56] R. Xia, “Characteristic Analysis and Measurement of Dielectric Loss in Non-linear Insulating Materials,” in *Advanced Materials Research*, 2014, vol. 986, pp. 1471–1476.

[57] R. Xia, H. Xv, and Z. Li, “Dielectric Parameters of Non-linear Insulating Materials and Their Measurements,” in *2006 IEEE 8th International Conference on Properties & applications of Dielectric Materials*, 2006, pp. 984–988.

[58] H. H. Kordkheili, H. Abravesh, M. Tabasi, M. Dakhem, and M. M. Abravesh, “Determining the probability of flashover occurrence in composite insulators by using leakage current harmonic components,” *IEEE Trans. Dielectr. Electr. Insul.*, vol. 17, no. 2, pp. 502–512, 2010.

[59] N. Bashir and H. Ahmad, “Odd harmonics and third to fifth harmonic ratios of leakage currents as diagnostic tools to study the ageing of glass insulators,” *IEEE Trans. Dielectr. Electr. Insul.*, vol. 17, no. 3, pp. 819–832, 2010.

[60] J. Y. Zhou and S. A. Boggs, “Measurement of nonlinear dielectric properties-effect of dielectric dispersion,” in *2001 Annual Report Conference on Electrical Insulation and Dielectric Phenomena (Cat. No. 01CH37225)*, 2001, pp. 153–156.

[61] A. Baral and S. Chakravorti, “Condition assessment of cellulosic part in power transformer insulation using transfer function zero of modified debye model,” *IEEE Trans. Dielectr. Electr. Insul.*, vol. 21, no. 5, pp. 2028–2036, 2014, doi: 10.1109/TDEI.2014.004517.

[62] D. Zhang *et al.*, “Insulation condition diagnosis of oil-immersed paper insulation based on the non-linear frequency-domain dielectric response,” *IEEE Trans. Dielectr. Electr.*

Insul., vol. 25, no. 5, pp. 1980–1988, 2018.

[63] M. Krüger, M. Koch, A. Kraetge, K. Rethmeier, O. Energy, and A. A. Dierks, “Diagnostic measurements on power transformers,” *Energetyka*, vol. 5, pp. 299–305, 2009.

[64] X. Qi, Z. Zheng, and S. Boggs, “Engineering with nonlinear dielectrics,” *IEEE Electr. Insul. Mag.*, vol. 20, no. 6, pp. 27–34, 2004.

[65] M. Schultze *et al.*, “Controlling dielectrics with the electric field of light,” *Nature*, vol. 493, no. 7430, pp. 75–78, 2013.

[66] E. J. G. Santos and E. Kaxiras, “Electric-field dependence of the effective dielectric constant in graphene,” *Nano Lett.*, vol. 13, no. 3, pp. 898–902, 2013.

[67] J. Krupka, K. Derzakowski, B. Riddle, and J. Baker-Jarvis, “A dielectric resonator for measurements of complex permittivity of low loss dielectric materials as a function of temperature,” *Meas. Sci. Technol.*, vol. 9, no. 10, p. 1751, 1998.

[68] T. Christen, R. Kochetov, and L. Almquist, “High-voltage low-frequency dielectric-spectroscopy used for characterization of nonlinear insulation materials,” in *2016 IEEE International Conference on Dielectrics (ICD)*, 2016, vol. 2, pp. 848–851.

[69] A. Banik, A. Mukherjee, and S. Dalai, “Development of a pollution flashover model for 11 kV porcelain and silicon rubber insulator by using COMSOL multiphysics,” *Electr. Eng.*, vol. 100, no. 2, pp. 533–541, 2018.

[70] I. Safi and P. Joyez, “Time-dependent theory of nonlinear response and current fluctuations,” *Phys. Rev. B*, vol. 84, no. 20, p. 205129, 2011.

[71] L. Almquist, “Nonlinear Impedance Spectroscopy,” *Using High. Harmon. response Differ. impedance Electr. Charact. DC Insul. Mater. Master’s thesis, Chalmers Univ. Technol. Gothenburg, Sweden*, 2015.

[72] R. Lu and A. Lu, “Applications of the superposition theorem to nonlinear resistive circuits,” in *APCCAS 2006-2006 IEEE Asia Pacific Conference on Circuits and Systems*, 2006, pp. 1333–1336.

[73] A. Banik, S. Nielsen, and G. Nourbakhsh, “Impact of voltage harmonics on condition assessment of polluted insulator through a simulation model,” in *2018 Condition Monitoring and Diagnosis (CMD)*, 2018, pp. 1–5.

[74] C. Xie, Y. Wang, X. Shao, and Y. Jin, “The application research of very low-frequency diagnostic methods in acceptance tests on new cable systems of medium voltage,” in *2018 China International Conference on Electricity Distribution (CICED)*, 2018, pp. 47–

53.

[75] A. J. Adebomi, H. T. Putter, and P. Legler, “Contemporary Techniques and Case Studies in Offline Condition Assessment of MV Underground Power Cables,” in *2018 IEEE International Conference on High Voltage Engineering and Application (ICHVE)*, 2018, pp. 1–6.

[76] R. J. Duffin and A. C. Schaeffer, “A class of non-harmonic Fourier series,” *Trans. Am. Math. Soc.*, vol. 72, no. 2, pp. 341–366, 1952.

[77] H. Helson, *Harmonic analysis*. London, 1983.

[78] D. Shmilovitz, “On the definition of total harmonic distortion and its effect on measurement interpretation,” *IEEE Trans. Power Deliv.*, vol. 20, no. 1, pp. 526–528, 2005.

[79] M. McGranaghan and G. Beaulieu, “Update on iec 61000-3-6: Harmonic emission limits for customers connected to mv, hv, and ehv,” in *Transmission and Distribution Conference and Exhibition*, 2006, pp. 1158–1161.

[80] C. K. Duffey and R. P. Stratford, “Update of harmonic standard IEEE-519: IEEE recommended practices and requirements for harmonic control in electric power systems,” *IEEE Trans. Ind. Appl.*, vol. 25, no. 6, pp. 1025–1034, 1989.

[81] S. J. B. Ong and Y. J. Cheng, “An overview of international harmonics standards and guidelines (IEEE, IEC, EN, ER and STC) for low voltage system,” in *2007 International Power Engineering Conference (IPEC 2007)*, 2007, pp. 602–607.

[82] C. Masetti, “Revision of European Standard EN 50160 on power quality: Reasons and solutions,” in *Proceedings of 14th International Conference on Harmonics and Quality of Power-ICHQP 2010*, 2010, pp. 1–7.

[83] D. M. Joseph, P. Haigh, and J. McCullagh, “Ensuring grid code harmonic compliance of wind farms,” in *10th IET International Conference on AC and DC Power Transmission (ACDC 2012)*, 2012, pp. 1–6.

[84] B. W. Jaekel, “Description and classification of electromagnetic environments-revision of IEC 61000-2-5,” in *2008 IEEE International Symposium on Electromagnetic Compatibility*, 2008, pp. 1–4.

[85] J. Kuffel and P. Kuffel, *High voltage engineering fundamentals*. Elsevier, 2000.

[86] E. Taslak, O. Arikan, C. F. Kumru, and O. Kalenderli, “Analyses of the insulating characteristics of mineral oil at operating conditions,” *Electr. Eng.*, vol. 100, no. 1, pp.

321–331, 2018.

[87] P. Cichecki, "Testing and Diagnosis of High Voltage and Extra High Voltage Power Cables with Damped AC Voltages," 2018.

[88] W. Hauschild and E. Lemke, "Measurement of Dielectric Properties," in *High-Voltage Test and Measuring Techniques*, Springer, 2019, pp. 253–270.

[89] W. Hauschild and E. Lemke, *High-voltage test and measuring techniques*, vol. 1. Springer, 2014.

[90] S. Morsalin, T. B. Phung, M. Danikas, and D. Mawad, "Diagnostic challenges in dielectric loss assessment and interpretation: a review," *IET Sci. Meas. Technol.*, vol. 13, no. 6, pp. 767–782, 2019.

[91] S. C. Bera and S. Chattopadhyay, "A modified Schering bridge for measurement of the dielectric parameters of a material and the capacitance of a capacitive transducer," *Measurement*, vol. 33, no. 1, pp. 3–7, 2003.

[92] N. L. Kusters and O. Petersons, "A transformer-ratio-arm bridge for high-voltage capacitance measurements," *IEEE Trans. Commun. Electron.*, vol. 82, no. 5, pp. 606–611, 1963.

[93] M. P. MacMartin and N. L. Kusters, "A direct-current-comparator ratio bridge for four-terminal resistance measurements," *IEEE Trans. Instrum. Meas.*, vol. 15, no. 4, pp. 212–220, 1966.

[94] W. H. P. Leslie, "Choosing transformer ratio-arm bridges," *Proc. IEE-Part B Electron. Commun. Eng.*, vol. 108, no. 41, pp. 539–545, 1961.

[95] R. Leupers, W. Sheng, and J. Castrillon, "Software compilation techniques for MPSoCs," in *Handbook of Signal Processing Systems*, Springer, 2010, pp. 639–678.

[96] S. Morsalin, "Diagnostic Measurement and Modelling of Electrical Insulation Based on Very Low Frequency High Voltage Excitation." UNSW Sydney, 2020.

[97] J. Lukić, S. Teslić, Đ. Jovanović, S. Milosavljević, and D. Kovačević, "Power Transformers Condition Based Assessment Derived From Paper/Oil Analysis."

[98] P. Wang, M. R. Raghuveer, W. McDermid, and J. C. Bromley, "A digital technique for the on-line measurement of dissipation factor and capacitance," *IEEE Trans. Dielectr. Electr. Insul.*, vol. 8, no. 2, pp. 228–232, 2001.

[99] A. Küchler, *High Voltage Engineering: Fundamentals - Technology - Applications*.

Springer Berlin Heidelberg, 2017.

[100] A. Davies, *Handbook of condition monitoring: techniques and methodology*. Springer Science & Business Media, 2012.

[101] S. Svensson, *Power measurement techniques for nonsinusoidal conditions. The significance of harmonics for the measurement of power and other AC quantities*. Chalmers University of Technology, 1999.

[102] J. Zhao, S. You, H. Yin, J. Tan, and Y. Liu, “Data quality analysis and solutions for distribution-level PMUs,” in *2019 IEEE Power & Energy Society General Meeting (PESGM)*, 2019, pp. 1–5.

[103] K. Dartawan and A. M. Najafabadi, “Case study: Applying IEEE Std. 519-2014 for harmonic distortion analysis of a 180 MW solar farm,” in *2017 IEEE Power & Energy Society General Meeting*, 2017, pp. 1–5.

[104] T. C. Shuter, H. T. Vollkommer, and T. L. Kirkpatrick, “Survey of harmonic levels on the American electric power distribution system,” *IEEE Trans. power Deliv.*, vol. 4, no. 4, pp. 2204–2213, 1989.

[105] N. Dhahbi-Megriche and A. Beroual, “Time-frequency analyses of leakage current waveforms of high voltage insulators in uniform and non-uniform polluted conditions,” *IET Sci. Meas. Technol.*, vol. 9, no. 8, pp. 945–954, 2015.

[106] S. Elphick, V. Smith, V. Gosbell, and R. Barr, “The Australian long term power quality survey project update,” in *Proceedings of 14th International Conference on Harmonics and Quality of Power-ICHQP 2010*, 2010, pp. 1–7.

[107] V. J. Gosbell, D. Mannix, D. A. Robinson, and S. Perera, “Harmonic survey of an MV distribution system,” 2001.

[108] N. Yousefpoor, S. H. Fathi, N. Farokhnia, and H. A. Abyaneh, “THD minimization applied directly on the line-to-line voltage of multilevel inverters,” *IEEE Trans. Ind. Electron.*, vol. 59, no. 1, pp. 373–380, 2011.

[109] V. Komornik and P. Loreti, *Fourier series in control theory*. Springer Science & Business Media, 2005.

[110] W. Cao, K. J. Bradley, and A. Ferrah, “Development of a high-precision calorimeter for measuring power loss in electrical machines,” *IEEE Trans. Instrum. Meas.*, vol. 58, no. 3, pp. 570–577, 2008.

[111] A. Pinkus and S. Zafrany, *Fourier series and integral transforms*. Cambridge University Press, 1997.

[112] W. D. Shepherd and P. Zand, “Energy flow and power factor in nonsinusoidal circuits,” 1979.

[113] P. A. Muntakim, S. Zhang, J. Zhang, and B. T. Phung, “Insulation Assessment Based on Dielectric Dissipation Factor Measurement under Non-sinusoidal Excitation,” in *2021 IEEE 5th International Conference on Condition Assessment Techniques in Electrical Systems (CATCON)*, 2021, pp. 242–246.

[114] D. P. Kothari and I. J. Nagrath, *Modern power system analysis*. Tata McGraw-Hill Education, 2003.

[115] R. Arora and W. Mosch, *High voltage and electrical insulation engineering*, vol. 69. John Wiley & Sons, 2011.

[116] W. S. Zaengl, “Applications of dielectric spectroscopy in time and frequency domain for HV power equipment,” *IEEE Electr. Insul. Mag.*, vol. 19, no. 6, pp. 9–22, 2003.

[117] R. R. Nigmatullin and Y. E. Ryabov, “Cole-Davidson dielectric relaxation as a self-similar relaxation process,” *Phys. Solid State*, vol. 39, no. 1, pp. 87–90, 1997.

[118] T. Gonen, *Modern power system analysis*. CRC Press, 2013.

[119] T. Linde, J. T. Loh, S. Kornhuber, K. Backhaus, S. Schlegel, and S. Großmann, “Implications of Nonlinear Material Parameters on the Dielectric Loss under Harmonic Distorted Voltages,” *Energies*, vol. 14, no. 3, p. 663, 2021.

[120] G. G. Raju, *Dielectrics in electric fields*. CRC Press, 2016.

[121] G. C. Montanari, G. Mazzanti, F. Palmieri, A. Motori, G. Perego, and S. Serra, “Space-charge trapping and conduction in LDPE, HDPE and XLPE,” *J. Phys. D. Appl. Phys.*, vol. 34, no. 18, p. 2902, 2001.

[122] C. K. Alexander and M. N. O. Sadiku, *Fundamentals of electric circuits*. McGraw-Hill Education, 2000.

[123] C. L. Wadhwa, *High voltage engineering*. New Age International, 2006.

[124] Y. Han and Y. H. Song, “Condition monitoring techniques for electrical equipment-a literature survey,” *IEEE Trans. Power Deliv.*, vol. 18, no. 1, pp. 4–13, 2003.

[125] F. De La Rosa, *Harmonics and power systems*. CRC Press Boca Raton, 2006.

[126] R. L. Boylestad, *Electronic devices and circuit theory*. Pearson Education India, 2009.